UNIVERSITY OF CALIFORNIA
RIVERSIDE

Power Scheduling for Multi-Hop Wireless Networks

A Dissertation submitted in partial satisfaction
of the requirements for the degree of

Doctor of Philosophy

in

Electrical Engineering

by

Yuan Yu

December 2009

Dissertation Committee:

Professor Yingbo Hua, Chairperson
Professor Illya Dumer
Professor Sheldon Tan

The Dissertation of Yuan Yu is approved:

Committee Chairperson

University of California, Riverside

Acknowledgments

I would like to take this opportunity to express my greatest appreciation to my thesis advisor, Professor Yingbo Hua, for his continuous guidance, help and support. Without his suggestion, encouragement, patience and conscientiousness, it is impossible for me to complete this thesis.

I would also like to thank Prof. Ilya Dumer and Prof. Sheldon Tan for serving on my committee.

I would express my appreciation to all the members in Laboratory of Signals, Systems and Networks, past and present, from whom I learned a great deal and with whom I shared my laughs. Thanks to Dr. Bin Zhao, Dr. Yue Rong for their helpful discussion. Thanks to Dr. Yan Mei, Dr. Zheng Fang, Dr Kezhu Hong, Yi Huang, Ting Kong, Jie Liang, Shengyang Xu, Xiang Dong and Haitao Liu for their help and friendship.

Finally, I dedicate this thesis to my parents and my brother. They provide a constant source of motivation in my life. Thanks to Meng Wang, my girlfriend, for her sincere support.

The materials shown in this thesis are partially contained in the published and submitted papers [39, 40, 68].

To my parents.

ABSTRACT OF THE DISSERTATION

Power Scheduling for Multi-Hop Wireless Networks

by

Yuan Yu

Doctor of Philosophy, Graduate Program in Electrical Engineering
University of California, Riverside, December 2009
Professor Yingbo Hua, Chairperson

Multi-hop wireless networks remain an important research frontier of wireless communications. Multi-hop wireless networks are rapidly deployable to extend the coverage of the Internet, which can be an economical alternative to building new base stations. Multi-hop wireless networks are particularly useful for first responders for disaster relief, and military operations in battlefields. In this thesis, we study power scheduling issues for multi-hop wireless networks. Power scheduling, also known as medium access control consisting of link scheduling, power control and source beamforming, fundamentally governs the capacity of multi-hop wireless networks.

In the first part of this thesis, the achievable network throughput of large-scale multi-hop wireless networks is evaluated under a power scheduling scheme called opportunistic synchronous array method (O-SAM). Under O-SAM, a large network is partitioned into many small subnets, and within each subnet, the link with best channel gain is scheduled for transmission. We examine the impact of traffic load, network topology and multiple antennas on the achievable network throughput. Compared with slotted ALOHA, the throughput

of O-SAM is significantly higher. In addition to O-SAM, a distributed synchronous array method (D-SAM) is proposed, and its performance is also evaluated.

In the second part of this thesis, we focus on the power scheduling problem for multi-input multi-output (MIMO) relay networks. A generalized water filling (GWF) theorem is established for link rate maximization with multiple power constraints. The corresponding GWF algorithm is a fast solution to an important class of convex optimization problems. The GWF algorithm is a useful building block for joint source and relay optimization for a multiuser MIMO relay network. We study the power scheduling problems for both uplink and down- link cases of the multiuser MIMO relay network. A number of computational strategies are proposed to maximize the sum rate subject to power constraints or to minimize the sum power subject to rate constraints.

Contents

List of Figures

List of Tables

Chapter 1

Introduction

1.1 Background

Wireless communication changes people's life significantly. Nowadays, there are over 3 billion people across more than 212 countries and territories using cell phones[2]. The Global System for Mobile communications (GSM) standard is successful to support voice service and low speed data transmission; however, people are expecting more services offered, such as video calls via cell phone, browsing websites and downloading videos. All these data applications demand a new generation wireless network to provide much higher data rates and more reliable connections.

Wireless networks can be categorized into single-hop and multi-hop networks. In a single-hop network, packets are transmitted directly from source to destination. In a multi-hop network, packets hop from one node to another to reach the destination, where the intermediate nodes are called relays. A multi-hop network is also referred as a relay

network.

A wireless mesh network can be seen as a special type of wireless multi-hop network. It is often assumed that all nodes in a wireless mesh network are static and do not experience mobility. In a mesh network, a node can send and receive messages, and functions as a router to relay messages for its neighbors. A wireless mesh network can be set up easily to provide reliable communication. A mesh network can have thousands of nodes. Such a multi-hop wireless network is particularly useful for first responders for disaster relief, and military operations in battlefields.

The relay concept can also be applied to cellular networks where the one end of the signal path is a base station. The base station and relays maintain a stable topology while the users can move randomly. Wireless relays can be used to combat the shadowing, interference, multi-path fading and long-distance path loss of wireless channel. A typical scenario is the so-called "dead zone" in cellular network, in which the direct link from user to base station is too poor to provide the desired quality of service. This zone may be located at the edge of the cell or blocked by buildings or interfered by other radio waves. Another example is the underground parking lot. In these situations, wireless relays are useful to improve the quality of service.

Compared with the single-hop network, the multi-hop network has advantage in both data rate and connection reliability. Usually, in multi-hop network, communication happens between neighboring nodes. A long distance hop is partitioned into several short hops. This makes links more reliable without increasing transmission power consumed by individual nodes. Another advantage of multi-hop network is that if one data path fails,

there can be other backup paths available.

For a wireless mesh network or a cellular network with relays, there is typically a relatively fixed topology where the routing task is quite simple. The routes can be determined once the system is set up.

Related standards and protocols about mesh network include IEEE 802.11 [3], IEEE 802.15 [4] and IEEE 802.16 [5]. The relay schemes in cellular networks have been proposed for 3GPP LTE [6] and IEEE 802.16 [5].

In this thesis, a throughput analysis is provided for a medium access control scheme for wireless mesh network. A joint source and relay design for a mulituser MIMO relay system is also investigated. The next section reviews the current research progress in these two areas.

1.2 Paper Survey

1.2.1 Medium Access Control in MESH Network

We consider large-scale wireless mesh networks of low mobility within a time interval. Depending on applications, this time interval can be on a time scale of minutes, hours, days or even longer. Such networks include many types of rapidly deployable wireless networks. There are two types of traffic in ad hoc networks. One is inter-network traffic where traffic flows through one or more gateways (also known as access points) to or from a backbone network. The other is intra-network traffic where traffic stays within the ad hoc network. For inter-network traffic, the aggregated network throughput is obviously

upper bounded by the capacity of the gateways. By either throughput or capacity, we mean spectral efficiency in terms of bits/s/Hz (bits per second per Hertz). We will also use two variations of bits/s/Hz. We will not further consider the inter-network traffic in this paper.

For intra-network traffic, the achievable network throughput has been a topic of research by information theorists for many years. A well known result on this subject is the scaling law shown in [7]. This is also a subject reviewed in [1]. It is arguable that if a network is large in terms of the number of nodes relative to the logarithm of the available transmission power from each node, the network throughput in bits-hop/s/Hz/node is upper bounded [1]. Here, bits-hop means the number of bits transported from one node to any of its adjacent nodes. This measure of throughput is also a per-link network throughput. If the network node density is denoted by ρ, then the distance per hop is in the order of $1/\rho$ for 1-D network, $1/\rho^{1/2}$ for 2-D network, and $1/\rho^{1/3}$ for 3-D network. If we denote the upper bound of the per-link network throughput by c, then the distance weighted network throughput in bits-meter/s/Hz/node is upper bounded by c/ρ for 1-D network, $c/\rho^{1/2}$ for 2-D network, and $c/\rho^{1/3}$ for 3-D network. Here, bits-meter means the number of bits transported over one meter distance. In this thesis, we will only consider 2-D networks. The above expression $c/\rho^{1/2}$ for 2-D network is equivalent to the capacity scaling law shown in [7] for a 2-D network of arbitrary topology where total n nodes are inside a unit-area disk and hence $\rho = n$. It is further shown in [7] that if the network topology is random, then the averaged network throughput has an extra penalty factor in the form of $1/\sqrt{\log n}$. Since [7], there have been new findings on the capacity scaling laws of large-scale ad hoc networks in various alternative settings [8], [9], [10], [11], [12], [13] and [14]. It should be

noted that although representing a theoretical challenge to the above stated scaling law, a result shown in [15] requires extremely-large-scale virtual multiple-input-multiple-output (MIMO) channels and is highly infeasible according to our analysis.

The capacity scaling laws as discussed above only reveal the effect of the network size. The exact throughput of a large network depends on a wide range of factors. Among them, medium access control (MAC) is critically important. Most of the existing MAC schemes for ad hoc networks are variations of the two basic forms: ALOHA [16][17] and CSMA (carrier sense multiple access)[3]. With CSMA, a node can transmit a packet only when there is no other concurrent co-channel transmission within a large radius. The per link throughput of CSMA diminishes to zero as quickly as the inverse of the number of nodes within the carrier sensing radius. It is useful to note however that CSMA is adopted in IEEE 802.11 standards [3] for small networks. With ALOHA, each node initiates a packet transmission randomly. This packet can be received successfully if the intended receiver is ready and the interference is not too high. Because concurrent co-channel transmissions are allowed by ALOHA, the per link throughput of ALOHA does not reduce to zero as the node density increases. In other words, with ALOHA, the capacity scaling law $c/\rho^{1/2}$ in bits-meter/s/Hz/node holds for networks of regular topologies. A throughput analysis of ALOHA for large network is available in [18]. The throughput shown in [18] was not maximized over the target SINR ξ. As shown in [19], ξ affects the network throughput significantly and can be optimized in practice. In this thesis, we distinguish between SINR (signal to interference and noise ratio) and SNR (signal to noise ratio).

For many potential applications, ad hoc networks have low mobility during opera-

tions, which allows cooperations that are not exploited by ALOHA. In [1], the synchronous array method (SAM) was proposed. The essence of SAM is to partition all links in the network into multiple interleaved subsets of links where each subset of links with desired spacing between them corresponds to a set of concurrent co-channel transmissions. As an example, Figure 1.1 illustrates the impact of the spacing between concurrent co-channel transmissions on the network throughput. For this figure, all nodes are on the square grid. For square topology, the spacing or sparseness is measured by p and q which are the vertical and horizontal spacing units between concurrent co-channel transmitters [1]. Also for this figure, the target SINR ξ (i.e., the required SINR value for a packet to be received successfully) is optimized for each pair of p and q, the channels are non-fading, and single omnidirectional antenna is used on each node. We see that the impact of the sparseness is significant. For regular topologies such as square, triangle and hexagon, the sparseness can also be measured by the ratio f_s of the total number of nodes in the network over the number of nodes that are receiving (or transmitting) in each time-frequency slot. In Figure 1.1, $p = 2$ and $q = 3$ are optimal. The corresponding f_s is six. Depending on network topology, antenna properties and channel fading characteristics, the optimal value of f_s varies. But for regular topologies and omnidirectional antennas, the optimal value of f_s has been found mostly in the range of four, five and six [19].

The analysis in [19] shows that the throughput of SAM is significantly (about two times) higher than that of ALOHA. In [20], an opportunistic SAM (O-SAM) was proposed that allows concurrent co-channel transmissions to be locally adaptive to channel gain variations. This idea is similar to one used in a channel-state dependent ALOHA [21] for a single-hop network. But the context for O-SAM is a multi-hop network rather than a single-hop network. Since the strongest channel gain within each local area is exploited each time, the throughput of O-SAM is much improved. The effect of using multiple antennas is also considered in [22]. However, all of the existing throughput analyses of ALOHA, SAM and O-SAM are under a full loading condition where each node always has a packet waiting to be transmitted at any time.

1.2.2 MIMO Relay

It has been found that multiple antennas at transmitter and receiver can improve the wireless network performance significantly. Some of the fundamental techniques, such as space time coding, beamforming, multiplexing, are available in such textbooks [23, 24, 25].

Recently, wireless relay attracts more and more research efforts because of its usefulness for improving network throughput and extending transmission range.

Based on the ways how the relay processes the received signal, wireless relay can be categorized into: decode and forward (DF), compress and forward (CF), amplify and forward (AF). DF means that the relay decodes the original information and retransmit that information to destination. CF compresses (or quantizes) the received signal and then transmits the compressed signal. AF amplifies and forwards the received signal. Obviously,

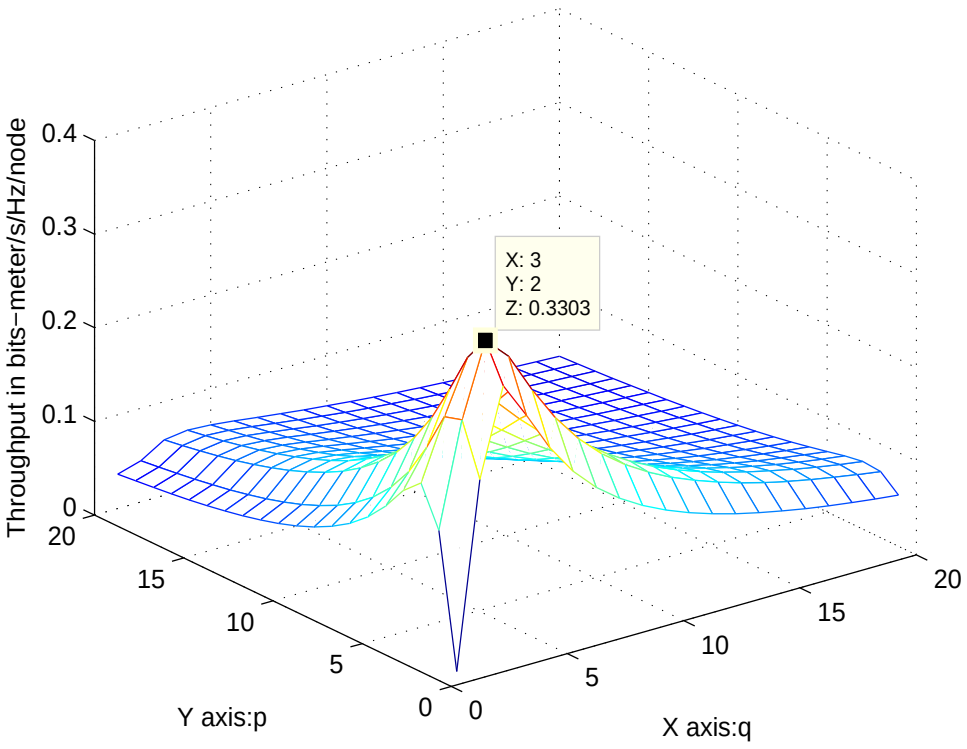

Figure 1.1: The throughput in bits-meter/s/Hz/node of a large network of 245 nodes on square grid versus p and q in the SAM protocol [1]. The node density is one. The SNR at each receiver is 40dB. The channel coefficients are constant.

the DF and CF are more complex than AF.

This thesis discusses a source and relay design for a multi-hop network where there is a single relay between the base station and multiple users. The relay is a multi-antenna AF relay..

A special MIMO relay network includes three terminals: source node, destination node and relay node. This type of MIMO relay network has been studied in [26, 27, 28, 29]. All these works assumes that the direct link from source to destination is negligible. The relay works in a half-duplex mode, in other words, the relay receives signals from source then transmits the amplified version of received signal in different times or frequencies.

A large number of works aim to improve the system capacity or decrease the outage probability. The authors in [26] derived the optimal MIMO relay structure under power constraint assuming the source covariance matrix is isotropic. This optimal design is based on the Singular Value Decomposition (SVD) of the MIMO channel. It can be proved that the optimal relay has to diagonalize the channel from source to relay and the channel from relay to destination, i.e. the equivalent MIMO channel is translated into a bunch of parallel SISO subchannels. Furthermore, the relay also permutes the two stage subchannels so that these subchannels are matched in a certain pattern. After the subchannel matching, the optimal power allocation among different subchannels is performed by a waterfilling-like algorithm. The authors in [27] extend [26]'s work to the joint source and relay design. The optimal structure of source and relay is the same as that in [26] to diagonalize the channel. An iterative algorithm is proposed on power allocation to maximize the system capacity. The authors in [28] derived the same result as in [26] in a different way. The

optimal relay is designed by diagonalizing the cascade channel. Also, the source is assumed to be white and with same power on each data stream. From the point of view of signal estimation, the authors in [29] address the problem of linear transceiver design in this type of MIMO relay system to minimize the mean-squared error (MSE). Based on this MMSE criterion, the relay is designed to diagonalizing the cascade channel as well like [26]. This result is not that surprising since the MMSE has the same expression as the point-point channel capacity. The authors in [30] compare several MIMO relay designs to maximize system capacity. It includes scalar amplification, channel diagonalization ([26, 27, 28]) and decoding then forward scheme. (DF is the best, then channel diagonalization degrades slightly, scalar amplification is the worst).

Multiple MIMO relays network with single pair of source and destination are also considered in [30, 31]. In [30], the proposed relay selection scheme exploits the spatial diversity. In [31], the authors first study the relays design without power constraints. Two problems are addressed in this scenario: minimization of MMSE given the SNR constraint and maximization of SNR subject to ZF; later, the power constraint is included at the receiver and these two problems are also studied. Finally, the transmission rate maximization problem under power constraint at the receiver is studied. Notice that the power constraint at receiver has similar expression as that at relay. The author in [32] proposes a suboptimal relay, which utilizes the QR decomposition to translate the equivalent source-relay-destination channel to a lower triangular channel. At the destination node, successive interference cancellation (SIC) is performed to separate the data streams.

Another type of the MIMO relay network is the point-to-multipoint (P2MP) relay

network (multiuser network). Typical P2MP relay network is the two-hop broadcast channel with a MIMO relay assisted in wireless cellular network. The multiuser independent downlink signals from base station are transmitted to the wireless relay then amplified and forward to each independent user. The base station and the relay are equipped with multiple antennas, while each user on has a single antenna on it. The relay is also working in a half-duplex mode.

In [33], the authors derive an achievable sum rate for this MISO-BC relay network by assuming ZF-DPC is used by base station. After a high SNR approximation, the joint optimization of linear relay and precoding matrix are proposed utilizing geometric programming.

In [34], the authors identify the dualilty relationships in AF relay networks. A general duality result for multihop multiple access and broadcast channels where each hop may consist of parallel AF relays and the relays may be equipped with multiple antennas. For the two hop case, it is shown that multiple access channel with total transmit power of all users equal to P and total relay transmit power P_r is the dual of the BC obtained when the destination becomes the transmitter and the transmitters become the receivers, and the powers are switched as well, i.e. in the dual BC, the transmit power is Pr and the total relay power is P. the capacity region of SISO-BC relay network and MISO-BC relay network are investigated respectively via uplink-downlink duality, the optimal DPC is assumed in base station.

In [35], the same system model is studied. The problem of joint beamforming and power allocation at base station and relay to minimize transmitting power under SNR

constraint is investigated. The basic idea is to fix the beamforming matrix at base station and optimize over beamforming at relay, then fix relay to optimize over beamforming base station. These two subproblems are solved by the second-order cone programming. In fact, the maximum sum rate under power constraint in [33] and minimum power consumption under QoS constraint in [35] both utilize the idea in [26, 28] based on SVD, although the optimality of this type relay is still not clear. The simulation suggests that this channel-diagonalization relay is best so far.

A more complicated relay network is the multi-point to multi-point relay network. The MIMO relay receives signals from multiple source nodes then amplify and forward to multiple destination nodes. Each user is equipped with single antenna.

The authors in [36] investigate robust relay design in such a system. The proposed robust method is to minimize the maximum transmit power at relay by keeping the minimum SNR above a certain threshold. Usually, such a problem is not convex, but it can be relaxed to a convex problem by semidefinite relaxation technique.

In [37], the authors derive optimal SNR-based transmit antenna selection rules at the source and relay for the nonregenerative half-duplex MIMO relay channel. In [38], the transmitting antenna selection scheme is studied in multi-hop MIMO relay scenario. Both these two result study the outage probability of the relay systems.

1.3 Thesis Overview

This thesis consists of two main parts: medium access control for a the large scale mesh network and power allocation for a cellular network with MIMO relay.

In the first part, the throughput of O-SAM scheme is analyzed under different conditions, such as traffic load, network topology and the number of antennas. We also present how the transmission distance affects the over all network throughput, which can be fairly compared by distance-weighted throughput in bits-meter/s/Hz/node. This O-SAM needs a central node to partition the large scale network to small subnets. A SAM based distributed MAC scheme (D-SAM) is also presented. The throughput of Slotted ALOHA is studied to compare with the O-SAM and D-SAM.

The power allocation in multiuser MIMO relay system is studied in the second part. A generalized water-filling algorithm (GWF) is designed to find the optimal source covariance matrix to maximize the point to point MIMO channel capacity with multiple weighted power constraints. This result can be applied to many practical problems. Then we study the power allocation at source and relay in multiuser MIMO relay system. In this thesis, the relay is constraint to be in AF fashion. The uplink case and downlink case are both considered. The several strategies are presented for each case. The use of multiple carriers is also discussed.

Opportunistic SAM is analyzed in Chapter 2. The throughput of O-SAM is studied under different conditions. The traffic load is formulated in a probability variable and is consider in throughput analysis. The throughput is given by $bits/s/Hz/node$ with triangle, square and hexagon topology under fading channel. Moreover, throughput in $bits-meters/s/Hz/node$ is compared for the O-SAM on these regular grids. Slotted ALOHA is also studied in this chapter.

Chapter 3 investigates a distributed MAC scheme: D-SAM. The protocol is given

and the throughput is evaluated by simulations. In regular topology, D-SAM is compared with ALOHA and O-SAM. Single antenna and multiple antennas are both included in simulations. The throughput of D-SAM in random topology is also provided.

In chapter 4, a generalized water filling (GWF) theorem is presented. For this convex optimization problem, an analytical solution is proved to be the global optimal. The algorithm is based on the Newton method. All the information needed in the algorithm is provided in appendix.

In chapter 5, we examine the joint source and relay design problem in multiuser system. Both uplink and downlink cases are considered. Two strategies are investigated in both cases; maximize sum rate with power constraint and minimize total power with rate constraint. It is also shown that our algorithms can be easily extended to the multicarrier scenario.

Chapter 6 summarizes the contributions of the Ph.D. work.

Chapter 2

Opportunistic Synchronous Array Method: O-SAM

A further development of the synchronous array method (SAM) as a medium access control scheme for large-scale ad hoc wireless networks is presented in this chapter. Under SAM, all transmissions of data packets between adjacent nodes are synchronized on a frame-by-frame basis, and the spacing between concurrent co-channel transmissions is properly controlled. An opportunistic SAM (O-SAM) is presented that allows concurrent co-channel transmissions to be locally adaptive to channel gain variations. For networks of low mobility, the control overhead required by SAM can be made much smaller than the payload.

The content of this chapter is partially contained in [39, 40].

2.1 Introduction

In this chapter, three main contributions will be presented. The first is describe the O-SAM protocol under a more general loading condition. This condition is modeled as the probability ζ that each node has a packet for transmission at any given time. We will reveal that the (ξ optimized) throughput of ALOHA is lower than that of O-SAM unless ζ is small (e.g., less than 10%). The second is a comparison of longer-distance transmission versus shortest-distance transmission in terms of the distance-weighted throughput in bits-meter/s/Hz/node, which shows that the former is worse than the latter unless ζ is very small (e.g., less than 1%). The third is an analysis of O-SAM for the case of multiple antennas on each node, which is an extension of that in [20] and [22].

We will measure network throughput by bits-meter/s/Hz/node. All numerical examples to be shown are useful fundamental benchmarks for large networks.

The reminder of this chapter is organized as follows. In Section 2.2, we extend O-SAM presented in [22] by taking into account the loading probability ζ. In Section 2.3, we analyze the network throughput of O-SAM, where the single-input-single-output (SISO), single-input-multiple-output (SIMO) and multiple-input-multiple-output (MIMO) channels are all considered. In Section 2.4, we revisit the slotted ALOHA with consideration of the loading probability ζ. By a distance weighted throughput, a comparison of long distance transmission versus short distance transmission is also presented.

2.2 Opportunistic SAM

2.2.1 Subnet partitions

As mentioned before, the essence of SAM proposed in [1] is to partition all links in the network into multiple interleaved subsets of links where each subset of links with desired spacing between them corresponds to a set of concurrent co-channel transmissions. An equivalent description of SAM is that in any given time-frequency slot, the entire network is partitioned into contiguous subnets and each subnet consists of a receiving node, a transmitting node and possibly several idle nodes. In different time-frequency slots, the corresponding partitions of subnets are relatively shifted from each other.

Fig. 2.1 illustrates the partitions of subsets for square, triangle and hexagonal topologies. For opportunistic SAM (O-SAM), each receiving node is chosen to be at the center of each subnet, and the transmitting node in each subnet is opportunistically selected from other nodes in the subnet. This is different from SAM in [1] which will also be referred to as centralized SAM (C-SAM) where both receiving and transmitting nodes in each subnet are pre-determined.

For the O-SAM protocol shown next and the Gaussian fading channels, the subnet partitions shown in Fig. 2.1 have been found to be optimal among other possible partitions. It is useful to note that except for the hexagonal topology, the subnet partitions shown in this figure are not exactly the same as the optimal ones for C-SAM as shown in [19]. But the fact that the optimal subnet partition for the hexagonal topology is the same for both C-SAM and O-SAM makes the hexagonal topology more interesting. This is because the throughput gain by O-SAM via opportunistic selection of transmitters is no longer compromised by altering the subnet partition from the optimal one determined by C-SAM. This advantage will be illustrated numerically later.

2.2.2 The protocol

The O-SAM protocol is described next. Without loss of generality, we can focus on a single time-frequency frame. For a large network, almost all subnets can be treated like a subnet in the center of the network. We will refer to such a subnet as subnet 0 and any other subnet as subnet j with $j = 1, 2, ..., S$. We let I_0 denote the set of the indices of all potential transmitting nodes that have packets to transmit to the receiver in subnet

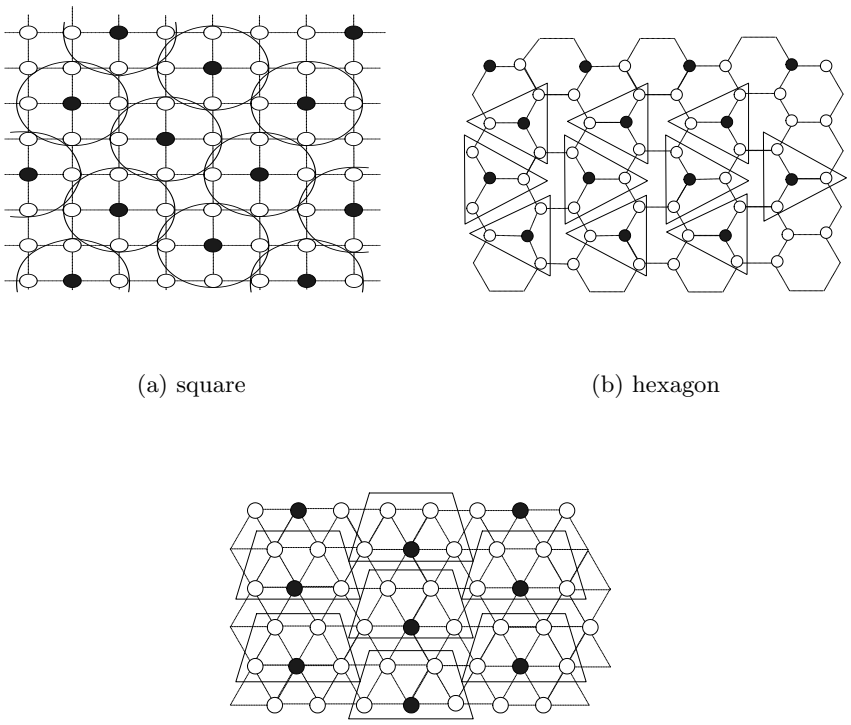

(a) square

(b) hexagon

(c) triangle

Figure 2.1: Optimal subnet partitions of large networks on regular topologies for O-SAM: the upper left is square, the upper right is hexagon, and the lower is triangle. The sparseness factor f_s is five for the square and triangle topologies and four for the hexagonal topology. The black nodes are concurrent co-channel receivers. One of the blank nodes in each subnet can be a transmitter in that subnet.

0. We let n_0 be the total number of nodes, other than the receiver, in subnet 0. Since ζ is the probability that a node has a packet to transmit to another node, the probability that I_0 contains k nodes is $\zeta^k(1-\zeta)^{n_0-k}$. Note that the set I_0 is a random set in each time-frequency frame.

SISO channels

If the channel between every two nodes is modelled as SISO channel, the channel coefficient from the ith node in I_0 to its receiver is denoted by $h_{0,0}(i)$. The corresponding channel gain is $v_{0,0}(i) = |h_{0,0}(i)|^2$. The index of the node with the strongest gain in subnet 0 is denoted by $i_{0,max} = \arg\max_{i \in I_0} v_{0,0}(i)$. The index of the node selected for transmission in subnet 0 is

$$k_0 = \begin{cases} i_{0,max}, & \text{if } v_{0,0}(i_{0,max}) \geq \theta \\ \{\emptyset\}, & \text{otherwise} \end{cases} \tag{2.1}$$

Here, no node is selected for transmission in subnet 0 if the gain of the node with the strongest gain in the subnet is less than a pre-specified threshold θ. The reason behind the use of θ is that if the strongest gain in a subnet is too small, abandoning packet transmission in this subnet causes little loss of information in this subnet and at the same time reduces interference to other subnets. Clearly, the choice of θ affects the network throughput.

The O-SAM protocol (2.1) requires each subnet to know the channel gains of all potential transmitting nodes in the subnet. This requires channel estimation and associated exchanges of control packets. This task is feasible if the channel coherence time is relatively long. In fact, for networks of low mobility, the channel coherence time can be very large (e.g., many mini-seconds). In this case, only a small fraction (e.g., a few micro seconds)

of the channel coherence time needs to be spent for channel estimation. Clearly, the more coordinated is the channel estimation in all subnets, the less time is needed. We will not further address the implementation issues of channel estimation for O-SAM.

On the other hand, if the channel gains do not change over time, there is no opportunity to be exploited by O-SAM and the protocol (2.1) is not meaningful. But random changes in channel gains can be induced artificially if they are not present naturally. To induce random channel gains, one can use multiple transmit (or receive) antennas on each node and choose a transmit (or receive) beam vector for each node randomly from frame to frame. This technique also applies to the SIMO and MIMO cases discussed below. The key is to compress the dimension of the channel responses randomly at the receiver side and/or the transmitter side.

SIMO channels

If each transmitting node uses one antenna and each receiving node uses multiple antennas, we have a SIMO channel between each transmitter and its receiver. In this case, we define the O-SAM protocol as (2.1) except that we use $v_{0,0}(i) = \|\mathbf{h}_{0,0}(i)\|^2$ where $\mathbf{h}_{0,0}(i)$ is the channel response vector between the ith node in I_0 and its receiver.

We will skip the MISO case since it is similar to the SIMO case.

MIMO channels

If each node has multiple transmit antennas and multiple receive antennas, we have a MIMO channel between each transmitter and its receiver. In this case, we define the

O-SAM protocol as (2.1) except that $v_{0,0}(i) = \lambda_{max}\left(\mathbf{H}_{0,0}(i)\mathbf{H}_{0,0}^{H}(i)\right)$ where λ_{max} denote the largest eigenvalue and $\mathbf{H}_{0,0}(i)$ is the channel response matrix between the ith node in I_0 and its receiver. The use of λ_{max} implies that the principal stream of each MIMO channel is used but all other streams are ignored. Because of the interference between concurrent co-channel transmissions, the inclusion of the non-principal streams of each MIMO channel into the O-SAM protocol would make the throughput analysis intractable to us at this stage. For this reason, we only consider the principal stream of each MIMO channel.

2.3 Throughput Analysis of Opportunistic SAM

For throughput analysis, we assume that all elements in channel coefficients, channel response vectors and channel response matrices are independent and identically distributed (i.i.d.) complex Gaussian random variables. This implies in particular that the channel coefficient between any receive antenna and any transmit antenna is independent of all other channel coefficients.

2.3.1 SISO channels

For SISO channels, the signal y_0 received by the receiving node in subnet 0 can be written as

$$y_0 = h_{0,0}x_0 + \sum_{j>0} h_{0,j}x_j + w_0 \tag{2.2}$$

where x_j is the transmitted signal from the transmitter in subnet j, $h_{0,j}$ is the channel coefficient between the transmitter in subnet j and the receiver in subnet 0, and w_0 is white

Gaussian noise with zero mean and variance σ^2. We assume that $h_{0,j}$ is complex Gaussian random variable (from frame to frame) with zero mean and variance $E|h_{0,j}|^2 = d_{0,j}^{-\alpha}$. Here, α is the path loss exponent and $d_{0,j}$ is the distance between the transmitter and the receiver. For convenience of analysis, we assume that all nodes transmit with the same power P, i.e. $E|x_j|^2 = P$. Hence, the instantaneous SINR at the receiver in subnet 0 is

$$SINR = \frac{v_{0,0}P}{\sum_{j>0} v_{0,j}P + \sigma^2} \tag{2.3}$$

where $v_{0,0} = |h_{0,0}|^2$ and $v_{0,j} = |h_{0,j}|^2$. We assume that the instantaneous SINR at each receiver is not known to the desired transmitter, which is due to random transmissions from other subnets. We also assume that for a large network, almost all the subnets are statistically equivalent to each other. Then, the network throughput in bits-meter/s/Hz/node can be expressed as:

$$C_{O-SAM} = \frac{\beta}{L\sqrt{\rho}} R_\xi P_d \tag{2.4}$$

where $R_\xi = \log_2(1+\xi)$ is the packet spectral efficiency, and $P_d = \Pr\{SINR \geq \xi\}$ is the probability of a successful packet detection. Also, L is the node population in each subnet. As illustrated in Fig. 2.1, $L = 5$ for the square and triangle topologies, and $L = 4$ for the hexagonal topology. Finally, β is a conversion factor from bits/hop/s/Hz/node to bits-meter/s/Hz/node. As shown in [19], we have $\beta = 0.785$ for square topology, $\beta = 0.689$ for hexagonal topology, and $\beta = 0.975$ for triangle topology.

From the O-SAM protocol, it is clear that the instantaneous SINR in each time-frequency frame is a random variable that depends on θ and ζ, and hence the network throughput is effected by ξ, θ and ζ.

In order to evaluate the network throughput (2.4), we need a more explicit form of P_d, which is derived next:

$$\begin{aligned} P_d &= Pr\{SINR \geq \xi, v_{0,0} \geq \theta\} \\ &= Pr\left\{ v_{0,0} \geq \xi(\sigma^2/P + \sum_{j>0} v_{0,j}), v_{0,0} \geq \theta \right\} \\ &= Pr\left\{ \sum_{j>0} v_{0,j} \leq \frac{v_{0,0}}{\xi} - \frac{\sigma^2}{P}, v_{0,0} \geq \theta \right\} \\ &= \int_{\max(\frac{\xi\sigma^2}{P},\theta)}^{\infty} \left(\int_0^{\frac{y}{\xi}-\frac{\sigma^2}{P}} f_{v_I}(x)dx \right) f_{v_{0,0}}(y)dy \end{aligned} \tag{2.5}$$

where $f_{v_{0,0}}(y)$ is the pdf (probability density function) of $v_{0,0}$, and $f_{v_I}(x)$ is the pdf of $v_I = \sum_{j>0} v_{0,j}$.

In order to evaluate P_d shown in (2.5), we need to obtain the expressions of the two pdf functions $f_{v_{0,0}}(y)$ and $f_{v_I}(x)$. We start with $f_{v_{0,0}}(y)$. Since $|h_{0,0}(m)|^2$ is exponentially distributed with the mean $D_{0,0}(m) = d_{0,0}^{-\alpha}(m)$, where $d_{0,0}(m)$ is the distance between the transmitter and receiver in subnet 0 and α is the path loss exponent, it follows that

$$Pr\{v_{0,0} \leq y\} = \prod_{m \in I_0} Pr\{v_{0,0}(m) \leq y\} = \prod_{m \in I_0} (1 - \exp\{-y/D_{0,0}(m)\})U(y) \tag{2.6}$$

where $U(y)$ is the unit step function. The above expression is not ready to use since I_0 is a random set. Alternatively and equivalently, we can think of a node that has no packet to transmit as if it is a node that has zero channel gain with respect to the receiver. Following this thinking, we can write

$$\begin{aligned} Pr\{v_{0,0} \leq y\} &= \prod_{m=1}^{n_0} \{(1 - \exp\{-y/D_{0,0}(m)\})\zeta + (1-\zeta)\} U(y) \\ &= \prod_{m=1}^{n_0} (1 - \zeta \exp\{-y/D_{0,0}(m)\})U(y) \end{aligned} \tag{2.7}$$

where n_0 is the number of potential transmitters in subnet 0. The pdf $f_{v_{0,0}}(y)$ follows readily from the derivative of $Pr\{v_{0,0} \leq y\}$ shown in (2.7), i.e.,

$$f_{v_{0,0}}(y) = \sum_{k=1}^{n_0} \left(\delta(y) + \zeta \frac{1}{D_{0,0}(k)} \exp\{-y/D_{0,0}(k)\} \right) \prod_{m=1, m\neq k}^{n_0} (1 - \zeta \exp\{-y/D_{0,0}(m)\}) U(y) \quad (2.8)$$

where $\delta(y)$ is the Dirac's delta function.

To derive the pdf $f_{v_I}(x)$ where $v_I = \sum_{j>0} v_{0,j}$, we start with the following:

$$\begin{aligned} Pr\{v_{0,j} \leq x\} &= \left\{ \overline{P_j} + \sum_{l=1}^{n_j} P_{j,l} Pr\{|h_{0,j}(l)|^2 \leq x\} \right\} U(x) \\ &= \left\{ \overline{P_j} + \sum_{l=1}^{n_j} P_{j,l} \left(1 - \exp\{-x/D_{0,j}(l)\}\right) \right\} U(x) \end{aligned} \quad (2.9)$$

where $\overline{P_j}$ is the probability that there is no transmission in subnet j, and $P_{j,l}$ is the probability that the lth node in subnet j transmits. We have used n_j to denote the number of potential transmitters in subnet j. In (2.9), we also used the property that $|h_{0,j}(l)|^2$ is exponentially distributed with the mean $D_{0,j}(l) = d_{0,j}^{-\alpha}(l)$, where $d_{0,j}(l)$ is the distance between the lth transmitter in subnet j and the receiver in subnet 0. It follows that

$$\overline{P_j} = 1 - \sum_l P_{j,l} \quad (2.10)$$

$$\begin{aligned} P_{j,l} &= \zeta \cdot Pr\left\{ v_{j,j}(l) \geq \theta, \max_{k\neq l, k\in I_j} v_{j,j}(k) \leq v_{j,j}(l) \right\} \\ &= \zeta \int_\theta^\infty \frac{1}{D_{j,j}(l)} e^{-\frac{x}{D_{j,j}(l)}} \prod_{k\neq l, k\in\{1,2,\ldots,n_j\}} (1 - \zeta e^{-x/D_{j,j}(k)}) dx \end{aligned} \quad (2.11)$$

where we have used the technique used for (2.7). Then, the pdf $f_{v_{0,j}}(x)$ follows readily from the derivative of (2.9), which is a superimposed-exponential, i.e.,

$$f_{v_{0,j}}(x) = \overline{P_j}\delta(x) + \sum_{l=1}^{n_j} P_{j,l} \frac{1}{D_{0,j}(l)} e^{\frac{-x}{D_{0,j}(l)}} U(x) \quad (2.12)$$

Since v_I is the sum of the independent random variables $v_{0,j}$ for all $j > 0$, the pdf of $f_{v_I}(x)$ is the convolution of $f_{v_{0,j}}(x)$ for all $j > 0$. Assume that $f_{v_I}(x)$ is negligible for $x \geq T$. We can write the Fourier series expansion of $f_{v_I}(x)$ as follows:

$$f_{v_I}(x) = \sum_{k=-K}^{K} g_k \exp(\upsilon \frac{2\pi k}{T} x) \tag{2.13}$$

where $\upsilon = \sqrt{-1}$ and

$$\begin{aligned} g_k &= \frac{1}{T} \int_0^T f_{v_I}(t) \exp(-\upsilon \frac{2\pi k}{T} t) dt \\ &= \frac{1}{T} \prod_{j>0} (\overline{P_j} + \sum_{l=1}^{n_j} \frac{P_j^l}{1 + \upsilon \frac{2\pi k}{T} D_{0,j}(l)}) \end{aligned} \tag{2.14}$$

We will assume that g_k is negligible for $k > K$.

With $f_{v_{0,0}}(x)$ and $f_{v_I}(x)$ as shown above, P_d in (2.5) can be readily computed.

2.3.2 SIMO channels

For SIMO channels where there are n_r receiving antennas at each node, the signal received by the receiver in subnet 0 has the following expression:

$$\mathbf{y}_0 = \mathbf{h}_{0,0} x_0 + \sum_{j>0} \mathbf{h}_{0,j} x_j + \mathbf{w}_0 \tag{2.15}$$

Here, x_i denotes the signal transmitted from subnet i. $\mathbf{h}_{i,j} \in \mathbb{C}^{n_r \times 1}$ is the channel coefficient vector between the transmitter in subnet j and the receiver in subnet i. The entries in $\mathbf{h}_{i,j}$ are assumed to be independent and identically distributed complex Gaussian random variables with zero mean and variance $d_{i,j}^{-\alpha}(k_j)$ where k_j is given by (2.16) and $d_{i,j}(k_j)$ is the distance between the transmitter in subnet j and the receiver in subnet i, α is the path loss exponent. $\mathbf{w}_i$ is the complex noise vector at the receiver in subnet i, and assumed to

have zero mean and the covariance matrix $E\{\mathbf{w}_i^H \mathbf{w}_i\} = \sigma^2 \mathbf{I}_{n_r}$ where $\mathbf{I}_{n_r}$ denotes the $n_r \times n_r$ identity matrix. We also assume that all the nodes in the network transmit with the same power P, i.e. $E\{x_i^H x_i\} = P$.

It is important to note that based on the O-SAM protocol, $\mathbf{h}_{i,j} = \mathbf{h}_{i,j}(k_j)$ where

$$k_j = \arg\left(\max_{k \in I_j, \|\mathbf{h}_{j,j}(k)\|^2 \geq \theta} \|\mathbf{h}_{j,j}(k)\|^2 \right). \tag{2.16}$$

Also recall that $\mathbf{h}_{i,j}(k)$ is the channel response vector from the kth potential transmitter in subnet j to the receiver in subnet i.

A sufficient statistics of $\mathbf{y}_0$ is given by $r_0 = \mathbf{h}_{0,0}^H \mathbf{y}_0$. The SINR in r_0 is

$$\begin{aligned} SINR &= \frac{\mathbf{h}_{0,0}^H \mathbf{h}_{0,0}}{\sum_{j>0} \frac{|\mathbf{h}_{0,0}^H \mathbf{h}_{0,j}|^2}{\|\mathbf{h}_{0,0}\|^2} + \sigma^2/P} \\ &= \frac{v_{0,0}}{\sum_{j>0} v_{0,j} + \sigma^2/P} \end{aligned} \tag{2.17}$$

where $v_{0,0} = \mathbf{h}_{0,0}^H \mathbf{h}_{0,0}$ and $v_{0,j} = \frac{|\mathbf{h}_{0,0}^H \mathbf{h}_{0,j}|^2}{\|\mathbf{h}_{0,0}\|^2}$.

Given any $\mathbf{h}_{0,0}$, $h_j(l) \doteq \frac{\mathbf{h}_{0,0}^H \mathbf{h}_{0,j}(l)}{\|\mathbf{h}_{0,0}\|}$ is a linear combination of the elements of $\mathbf{h}_{0,j}(l)$ which are i.i.d. complex Gaussian random variable, and hence $h_j(l)$ is a complex Gaussian variable. Each element of $\mathbf{h}_{0,j}(l)$ has zero mean and the variance $D_{0,j}(l) = d_{0,j}^{\alpha}(l)$ where $d_{0,j}(l)$ is the distance between the lth node in subnet j and the receiver in subnet 0. Furthermore, one can verify as in [41] that $h_j(l)$ has zero mean and the variance $D_{0,j}(l)$. It follows that $v_{0,j}(l) = |h_j(l)|^2$ for $j > 0$ is independent of $\mathbf{h}_{0,0}$ and is exponentially distributed with mean $D_{0,j}(l)$, i.e.,

$$f_{v_{0,j}(l)}(y) = \frac{1}{D_{0,j}(l)} \exp(-y/D_{0,j}(l)) U(y), \ j > 0 \tag{2.18}$$

Since $v_{0,j} = v_{0,j}(k_j)$ with k_j given by (2.16), $v_{0,j}$ for $j > 0$ is also independent of $\mathbf{h}_{0,0}$.

Therefore, with the above description of $v_{0,0}$ and $v_{0,j}$, the throughput expression (2.4) and the probability-of-detection expression (2.5) are also valid for the case of SIMO channels except that the expressions of the pdf $f_{v_{0,0}}(y)$ of $v_{0,0}$ and the pdf $f_{v_I}(x)$ of $v_I = \sum_{j>0} v_{0,j}$ need to be revised as follows.

To find $f_{v_{0,0}}(y)$, we first write

$$Pr\{v_{0,0} \le y\} = \prod_{m=1}^{n_0} \left\{\zeta Pr(\|\mathbf{h}_{0,0}(m)\|^2 \le y) + (1-\zeta)\right\} U(y) \tag{2.19}$$

It is known that $\|\mathbf{h}_{0,j}(l)\|^2$ is Chi-square or Gamma distributed with $2n_r$ degrees, i.e.,

$$f_{\|\mathbf{h}_{0,j}(l)\|^2}(x) = \frac{x^{n_r-1}}{(n_r-1)!D_{0,j}^{n_r}(l)} e^{-\frac{x}{D_{0,j}(l)}} U(x) \tag{2.20}$$

Therefore,

$$\begin{aligned} Pr\{v_{0,0} \le y\} &= \prod_{m=1}^{n_0} \left\{ \zeta \int_0^y \frac{x^{n_r-1}}{(n_r-1)!D_{0,0}^{n_r}(m)} e^{-\frac{x}{D_{0,0}(m)}} dx + (1-\zeta) \right\} U(y) \\ &= \prod_{m=1}^{n_0} \left\{ \zeta \left(1 - e^{-\frac{y}{D_{0,0}(m)}} \sum_{k=0}^{n_r-1} \frac{y^k}{D_{0,0}^k(m)k!} \right) + 1 - \zeta \right\} U(y) \\ &= \prod_{m=1}^{n_0} \left\{ 1 - \zeta e^{-\frac{y}{D_{0,0}(m)}} g\left(\frac{y}{D_{0,0}(m)}\right) \right\} U(y) \end{aligned} \tag{2.21}$$

where $g(y) = \sum_{k=0}^{n_r-1} \frac{y^k}{k!}$. The pdf $f_{v_{0,0}}(y)$ is simply given by the derivative of (2.21). If all potential transmitters in each subnet have the same distance to the receiver in the same subnet, i.e., $D_{j,j}(m) = D$ for all j and all m, the pdf $f_{v_{0,0}}(y)$ can be shown to be

$$\begin{aligned} f_{v_{0,0}}(y) &= \frac{\partial}{\partial y} Pr\{v_{0,0} \le y\} \\ &= \sum_{\mu=1}^{n_0} \begin{pmatrix} n_0 \\ \mu \end{pmatrix} (-1)^{\mu+1} \zeta^\mu e^{-\frac{\mu}{D}y} g^{\mu-1}(y/D) \frac{\mu y^{n_r-1}}{D^{n_r}(n_r-1)!} U(y) + (1-\zeta)^{n_0}\delta(y) \\ &= n_0[1 - \zeta e^{\frac{-y}{D}} g(\frac{y}{D})]^{n_0-1} \frac{\zeta e^{\frac{-y}{D}} y^{n_r-1}}{D^{n_r}(n_r-1)!} U(y) + (1-\zeta)^{n_0}\delta(y) \end{aligned} \tag{2.22}$$

We now derive the pdf $f_{v_I}(x)$ of $v_I = \sum_{j>0} v_{0,j}$ where $v_{0,j} = \frac{|\mathbf{h}_{0,0}^H \mathbf{h}_{0,j}|^2}{\|\mathbf{h}_{0,0}\|^2}$. Since the pdf of $v_{0,j}(l)$ is the same as that for the SISO channels, all expressions for the pdf $f_{v_I}(x)$ are the same as for the SISO case except that $P_{j,l}$ needs to be revised as follows:

$$\begin{aligned} P_{j,l} &= \zeta \cdot Pr\{\|\mathbf{h}_{j,j}(l)\|^2 \geq \max_{k \neq l} \|\mathbf{h}_{j,j}(k)\|^2, \|\mathbf{h}_{j,j}(l)\|^2 \geq \theta\} \\ &= \zeta \int_\theta^\infty \frac{x^{n_r-1}}{(n_r-1)! D_{j,j}^{n_r}(l)} e^{-\frac{x}{D_{j,j}(l)}} \prod_{k \neq l} \left(1 - \zeta e^{-\frac{x}{D_{j,j}(k)}} \sum_{q=0}^{n_r-1} \frac{x^q}{D_{j,j}(k)^q q!}\right) dx \end{aligned} \quad (2.23)$$

where we have used (2.20). If $D_{j,j}(l) = D$ for all j and all l, then $P_{j,l}$ becomes independent of l, and $P_{j,l}$ can be simplified as:

$$P_{j,l} = \zeta \int_\theta^\infty \frac{x^{n_r-1}}{(n_r-1)! D^{n_r}} e^{-\frac{x}{D}} \left(1 - \zeta e^{-\frac{x}{D}} \sum_{q=0}^{n_r-1} \frac{x^q}{D^q q!}\right)^{n_0-1} dx \quad (2.24)$$

2.3.3 MIMO channels

For MIMO channels, the received signal model in subnet 0 is given by:

$$\mathbf{y}_0 = \mathbf{H}_{0,0}\mathbf{x}_0 + \sum_{i>0} \mathbf{H}_{0,i}\mathbf{x}_i + \mathbf{w}_0 \quad (2.25)$$

where $\mathbf{H}_{i,j} \in \mathbb{C}^{n_r \times n_t}$ is the channel coefficient vector between the transmitter in subnet j and the receiver in subnet i. The entries in $\mathbf{H}_{i,j}$ are assumed to be independent and identically distributed complex Gaussian random variables with zero mean and variance $d_{i,j}^{-\alpha}(k_j)$ with k_j defined by (2.26). $\mathbf{x}_i$ is the complex vector signal transmitted from subnet i. $\mathbf{w}_i$ is the complex noise vector at the receiver in subnet i, and assumed to have zero mean and the covariance matrix $E\{\mathbf{w}_i^H \mathbf{w}_i\} = \sigma^2 I_{n_r}$, where I_{n_r} denotes the $n_r \times n_r$ identity matrix. We also assume that all the nodes in the network transmit with the same power P, i.e. $tr\{E\{\mathbf{x}_i \mathbf{x}_i^H\}\} = P$. We further assume that $n_r = n_t$.

Based on the O-SAM protocol, $\mathbf{H}_{i,j} = \mathbf{H}_{i,j}(k_j)$ where

$$k_j = \arg\left(\max_{k\in I_j, \lambda_{max}(\mathbf{H}_{i,j}(k))\geq\theta} \lambda_{max}(\mathbf{H}_{i,j}(k))\right) \tag{2.26}$$

Denote the singular value decomposition (SVD) of $\mathbf{H}_{i,i}$ as $\mathbf{H}_{i,i} = \mathbf{U}_{i,i}\Lambda_{i,i}^{1/2}\mathbf{V}_{i,i}^H$ where $\Lambda_{i,i}$ is a diagonal matrix of non-negative entries in descending order. Then, we can transform (2.25) to the following:

$$\tilde{\mathbf{y}}_0 = \Lambda_{0,0}^{1/2}\tilde{\mathbf{x}}_0 + \sum_{i>0}\tilde{\mathbf{H}}_{0,i}\tilde{\mathbf{x}}_i + \tilde{\mathbf{w}}_0 \tag{2.27}$$

where $\tilde{\mathbf{y}}_0 = \mathbf{U}_{0,0}^H\mathbf{y}_0$, $\tilde{\mathbf{x}}_i = \mathbf{V}_{i,i}^H\mathbf{x}_i$, $\tilde{\mathbf{H}}_{0,i} = \mathbf{U}_{0,0}^H\mathbf{H}_{0,i}\mathbf{V}_{i,i}$ and $\tilde{\mathbf{w}}_0 = \mathbf{U}_{0,0}^H\mathbf{w}_0$.

Under the O-SAM protocol, we only use the principal stream of each MIMO link. In this case, only the first entry of the vector $\tilde{\mathbf{x}}_i$ is non-zero, which is denoted by x_i. Therefore, a sufficient statistics of the vector $\tilde{\mathbf{y}}_0$ is given by its first element, which is denoted by y_0, and (2.27) is equivalent to the scalar equation:

$$y_0 = \lambda_{max}^{1/2}x_0 + \sum_{j>0}h_{0,j}x_j + w_0 \tag{2.28}$$

where λ_{max} is the largest eigenvalue of $\mathbf{H}_{0,0}\mathbf{H}_{0,0}^H$, and $h_{0,j}$ is the upper-left entry of $\tilde{\mathbf{H}}_{0,j}$ which is complex Gaussian with zero mean and variance $d_{0,j}^{-\alpha}(k_j)$.

The SINR in y_0 is given by

$$SINR \;=\; \frac{v_{0,0}}{\sum_{j>0}v_{0,j} + \sigma^2/P} \tag{2.29}$$

where $v_{0,0} = \lambda_{max}$, and $v_{0,j} = |h_{0,j}|^2$ which is exponentially distributed with the mean $D_{0,j}(k_j) = d_{0,j}^{-\alpha}(k_j)$.

Assuming that $d_{0,0}(m) = 1$ for all $m = 1, 2, ..., n_0$, the cdf (cumulative distribution function) of λ_{max} is known [42] to be

$$F_{\lambda_{max}}(x) = \frac{1}{\prod_{j=1}^{n_r} \Gamma(j)^2} \det |(\gamma_{i+j-2})| \tag{2.30}$$

where (γ_{i+j-2}) is a $n_r \times n_r$ matrix with element $\gamma_{i+j-2} = \int_0^x \omega^{i+j-2} \exp(-\omega) d\omega$ and $\Gamma(j) = (j-1)!$.

The expressions (2.4) and (2.5) still hold for the MIMO case except that $f_{v_I}(x)$ and $f_{v_{0,0}}(y)$ need to be revised as follows.

We know that

$$\begin{aligned} Pr\{v_{0,0} \leq y\} &= \prod_{m=1}^{n_0} \{\zeta F_{\lambda_{max}}(y) + (1-\zeta)\} \\ &= \{\zeta F_{\lambda_{max}}(y) + (1-\zeta)\}^{n_0} \end{aligned} \tag{2.31}$$

Then, $f_{v_{0,0}}(y)$ is given by the derivative of (2.31).

The expressions for $f_{v_I}(x)$ are the same as those for the SISO and SIMO cases except that

$$P_{j,l} = \frac{1}{n_j}(1 - \overline{P_j}) \tag{2.32}$$

$$\overline{P_j} = (1 - \zeta + \zeta F_{\lambda_{max}}(\theta))^{n_j} \tag{2.33}$$

2.4 Loading Adaptive ALOHA

Slotted ALOHA (or ALOHA for short) is a useful benchmark for throughput comparison. The protocol of ALOHA is as follows. In each time slot or frame, if a node A has a packet to deliver to a neighboring node B, then the node A transmits the packet

to the node B with a transmission probability ε. If the node B is not transmitting in the same time slot, the node B attempts to receive the packet from the node A.

The throughput of ALOHA can be shown as follows. Since each node has the probability ζ to have a packet for its neighbor, the effective probability for a node to choose to transmit is $\zeta\varepsilon$. Hence, the throughput of ALOHA in bits-meter/s/Hz/node for networks of regular topologies is given by the following expression [19]:

$$C_{ALOHA} = \frac{\beta}{\sqrt{\rho}}(1-\zeta\varepsilon)\zeta\varepsilon R_\xi P_d \tag{2.34}$$

Here, as defined before, R_ξ is the packet spectral efficiency, and $P_d = Pr\{SINR \geq \xi\}$ is the probability of packet detection. However, the statistics of $SINR$ for ALOHA is different from that for SAM.

For throughput analysis of ALOHA, we will only consider SISO channels. Then, given that a node transmits a packet and one of its neighboring nodes receives the packet, the signal received by the receiving node can be modelled as

$$y_0 = h_0 x_0 + \sum_{j>0} h_j x_j u_j + w_0 \tag{2.35}$$

where x_0 is the desired signal, h_0 is the channel coefficient between the desired transmitter-receiver pair, x_j for $j > 0$ is the interfering signal from node j, h_j for $j > 0$ is the channel coefficient between the interfering node j and the receiving node, and w_0 is the noise. We assume Gaussian fading channels and Gaussian noise. Here, $u_j \in \{0, 1\}$ are i.i.d. binary random variables with $Pr\{u_j = 1\} = \zeta\varepsilon$. Then, the instantaneous SINR in y_0 in each time slot is

$$SINR = \frac{g_0 P}{\sigma^2 + \sum_{j>0} g_j u_j P} \tag{2.36}$$

where P is the transmitted power from each transmitting node, σ^2 is the noise variance, $g_i = \|h_i\|^2$ is an exponentially distributed random variable with the mean $\mu_i = d_i^{-\alpha}$, and d_i is the distance between the node i and the receiver.

Unlike (2.5), we now have

$$\begin{aligned} P_d &= Pr\{SINR \geq \xi\} = Pr\left\{\frac{g_0}{\sigma^2/P + \sum_{j>0} g_j u_j} \geq \xi\right\} \\ &= E_{\{g_i,u_i,i>0\}}\left[\int_{(\sigma^2/P+\sum_{j>0} g_j u_j)\xi}^{\infty} \frac{1}{\mu_0} e^{-\frac{x}{\mu_0}} dx\right] \\ &= E_{\{g_i,u_i,i>0\}} \exp\left\{-\frac{(\sigma^2/P + \sum_{j>0} g_j u_j)\xi}{\mu_0}\right\} \\ &= \exp\left\{-\frac{\sigma^2\xi}{P\mu_0}\right\} \prod_{j>0} E_{g_i,u_i}\left\{\exp\left(-\frac{g_i u_i \xi}{\mu_0}\right)\right\} \\ &= \exp\left\{-\frac{\sigma^2\xi}{P\mu_0}\right\} \prod_{j>0} E_{u_i}\left\{\frac{1}{1 + u_i\mu_i\xi/\mu_0}\right\} \\ &= \exp\left\{-\frac{\sigma^2\xi}{P\mu_0}\right\} \prod_{j>0}\left[\zeta\varepsilon\frac{1}{\xi\mu_j/\mu_0 + 1} + (1 - \zeta\varepsilon)\right] \end{aligned} \tag{2.37}$$

The above analysis is similar to one in [18]. Since ζ and ε always appear in the product form $\zeta\varepsilon$, given that all other parameters are fixed, there is an optimal choice for the product, which is to be denoted by p^*. Assuming that each node knows the traffic loading condition as measured by ζ, then a loading adaptive ALOHA should adopt the following transmission probability:

$$\varepsilon = \begin{cases} 1 & \zeta \leq p^* \\ \frac{p^*}{\zeta} & \zeta > p^* \end{cases} \tag{2.38}$$

For the throughput comparison shown next, we will use the loading adaptive ALOHA.

2.5 Throughput Evaluation

In this section, we will illustrate and compare the throughput of O-SAM, D-SAM and ALOHA. We will use the following list of assumptions. All network topologies to be considered have the unit node density $\rho = 1$. All channel coefficients are independent realizations of complex Gaussian random variables from frame to frame. We choose the path loss exponent $\alpha = 4$ unless specified otherwise. By SIMO, we mean 1×4 SIMO, and by MIMO, we mean 4×4 MIMO. For O-SAM, we will consider a large network of 245 nodes on three regular grids as shown in Figure 2.1. The subnet partitions shown in this figure are already optimized for O-SAM. For the Fourier series expansion (2.13) and (2.14), we choose $K = 500$ and $T = 50$. These values were confirmed to be sufficiently large. For ALOHA, we will only consider the square topology and SISO channels.

Figure 2.2 shows the throughput of O-SAM versus SNR and the traffic load probability ζ. For each pair of SNR and ζ, the throughput was maximized over ξ (the target SINR) and θ (the channel gain threshold). The square topology as shown in Fig. 2.1 was used. The Gaussian SISO channels were considered. This figure is to highlight the fact that the network throughput is saturated to a constant when SNR is large. In the sequel, we will choose $SNR = 10\log_{10}(P/\sigma^2) = 40dB$ unless otherwise specified.

Figure 2.3 compares the throughput of O-SAM and ALOHA versus the traffic load probability ζ. For each ζ, the throughput of O-SAM was maximized over both ξ and θ. The square topology as shown in Figure 2.1 and the Gaussian SISO channels were considered. We see that as long as $\zeta > 10\%$, O-SAM yields higher throughput than ALOHA. In other words, only when the traffic load is low, does ALOHA yield a higher throughput.

Figure 2.4 illustrates the throughput of ALOHA for 1-hop, 2-hop and 3-hop distance transmission. Note that bits-meter/s/Hz/node is a distance-weighted throughput unit. By 2-hop distance transmission, for example, we mean that the transmission distance between the transmitter and the receiver equals two times the shortest distance between two adjacent nodes. For each of the three cases, we adjusted the transmission power P such that the SNR of the received signal is kept at 40dB. This means that the transmission power used for 2-hop distance transmission is 2^α times higher than that for 1-hop distance transmission, and the transmission power used for 3-hop distance transmission is 3^α times higher than that for 1-hop distance transmission. The same square topology as shown in Figure 2.1 and the Gaussian SISO channels were considered. For each ζ, the throughput was maximized over ξ. We see that only when the traffic load is very low (i.e., $\zeta < 1\%$), is the throughput of 2-hop distance transmission better than that of 1-hop distance transmission. In order for 3-hop distance transmission to be better than 2-hop distance transmission, the traffic load probability ζ needs to be less than 0.4%.

In figure 2.5, we show the ratio of the "2-hop distance" throughput over the "1-hop distance" throughput and the ratio of the "3-hop distance" throughput over the "1-hop distance" throughput. These ratios are lower than one unless the traffic load probability ζ is very small. When ζ approaches zero, the two ratios become two and three, respectively.

Figures 2.4 and 2.5 suggest that for peer-to-peer networks, the shortest distance transmission is the most efficient in both spectrum and energy unless the traffic load is extremely low.

Figure 2.6 compares the throughput of O-SAM for each of SISO, SIMO and MIMO

cases. For O-SAM, the throughput was maximized over ξ and θ. The square network was considered. This figure illustrates that multiple antennas can significantly improve the network throughput.

2.6 Summary

We have presented a further development of synchronous array method (SAM) as a medium access control scheme for ad hoc wireless networks. We have focused on intra-network throughput enhancement for a large network where any node can be a source node or a destination node. We have used the distance-weighted throughput measure: bits-meter/s/Hz/node. We have presented and evaluated SAM-based schemes: O-SAM which is a centralized scheme.

With O-SAM, the subnet partition within each time frame needs to be pre-determined. Provided that the channel coherence time is sufficiently long, local channel estimation is feasible which allows opportunistic exploitation of channel gains within each subnet. In order to induce variations of channel gains, multiple antennas can be used at each node.

We have also compared the throughput of O-SAM with the throughput of ALOHA under a varying probability ζ of traffic load. It has been shown that ALOHA yields lower throughput than O-SAM unless ζ is small, e.g., less than 10%. We have further examined the effect of long distance transmission on the distance-weighted throughput. We have found that the shortest distance transmission leads to the highest throughput unless ζ is very small, e.g., less than 1%.

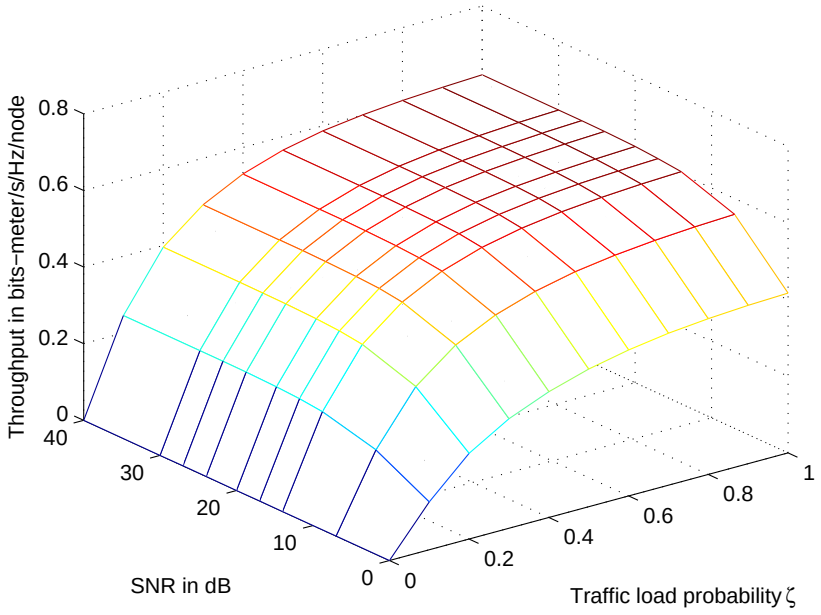

Figure 2.2: Throughput of O-SAM versus load probability ζ and SNR. We used $\rho = 1$, square topology, and SISO channels.

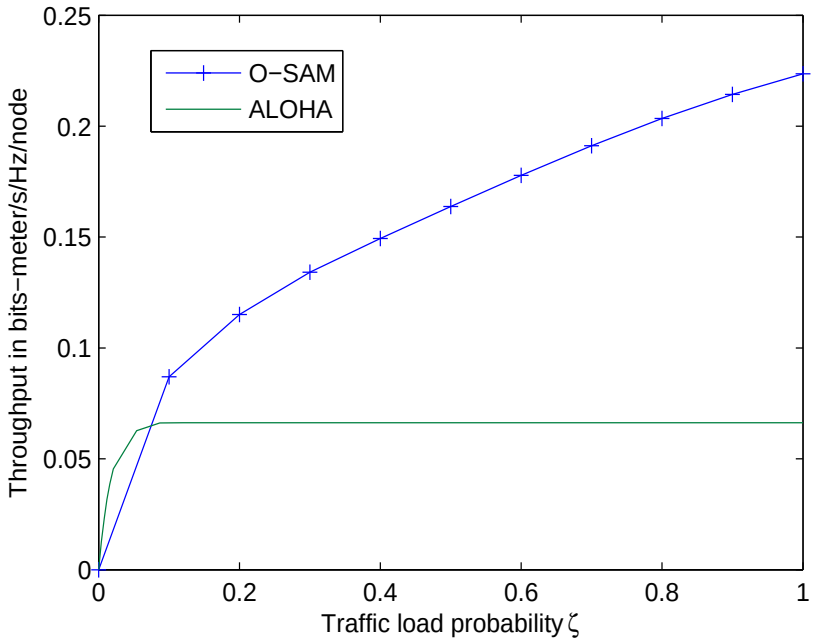

Figure 2.3: Throughput comparison of O-SAM and ALOHA. We used $\rho = 1$, $SNR = 40dB$, square topology, and SISO channels.

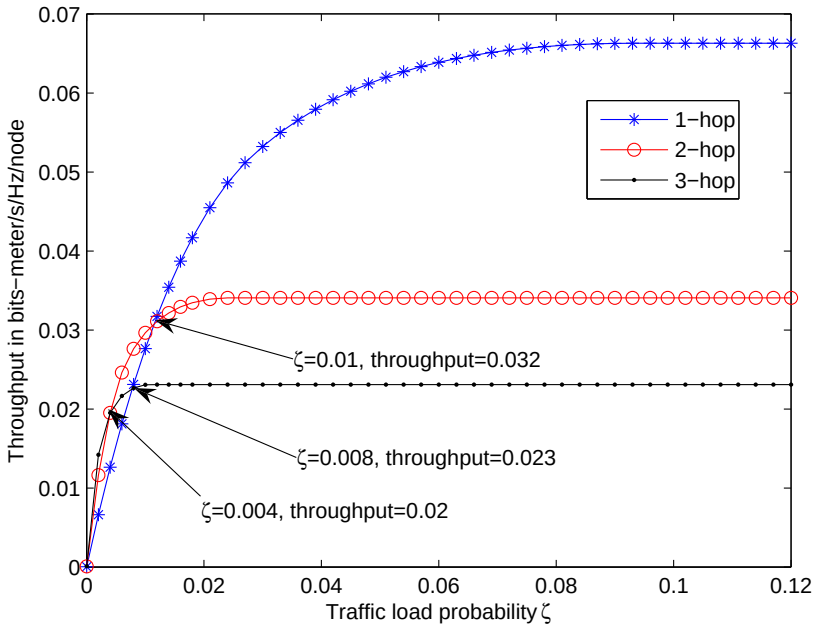

Figure 2.4: Throughput of ALOHA with different transmission ranges: 1-hop, 2-hop and 3-hop ranges . We used $\rho = 1$, square topology, and SISO channels. The transmission power for each of the three cases is adjusted so that the SNR (excluding interference) at every receiver is 40dB.

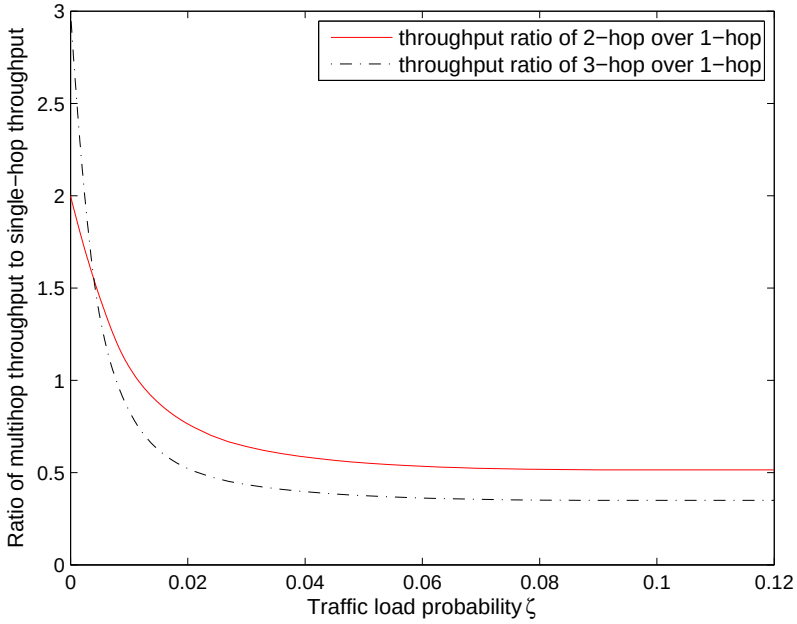

Figure 2.5: Ratios of throughput: 2-hop range over 1-hop range, and 3-hop rang over 1-hop range. All conditions are the same as for Fig. 2.4.

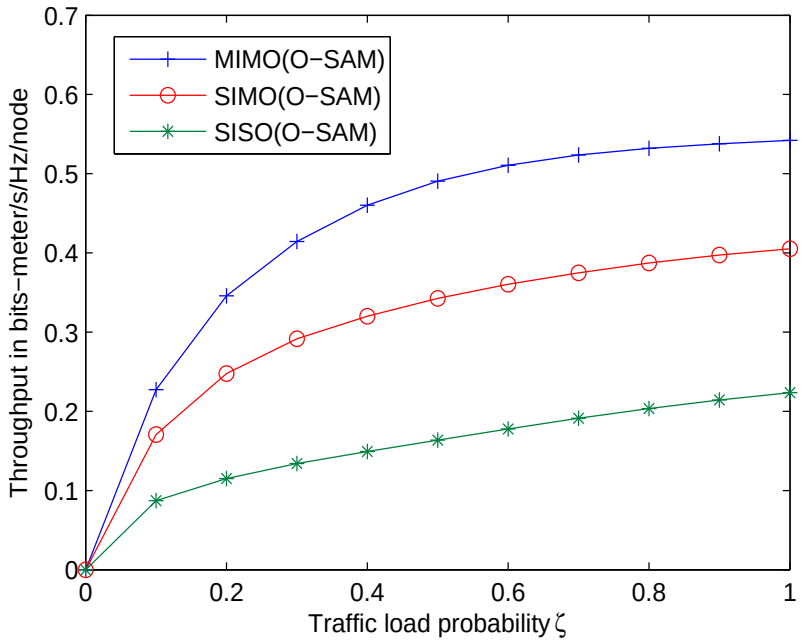

Figure 2.6: Throughput of O-SAM for SISO, SIMO and MIMO channels. We used $\rho = 1$, $SNR = 40dB$, and square topology.

Chapter 3

Distributed Synchronous Array Method: D-SAM

The (centralized) SAM shown in [1] and the opportunistic SAM shown in the section 2.2 all require a subnet partition in a centralized fashion. The dimension of each subnet or the spacing between concurrent co-channel transmissions is critical for network throughput. In this chapter, we present a distributed SAM (D-SAM) that encapsulates an essence of SAM in that all concurrent co-channel transmissions are properly spaced from each other. The distributed SAM (D-SAM) is discussed that schedules all concurrent co-channel transmissions in a distributed fashion. D-SAM forms subnets in each time frame in a distributed and dynamic fashion. D-SAM also works with random network topology.

The essence of D-SAM is similar to that of MSH-DSCH in IEEE 802.16 standards [5]. However, there has been no prior study of the fundamental throughput of MSH-DSCH in large networks. The understanding of D-SAM for large networks can serve this purpose.

The study shown in [43] focuses on the dynamic of control packet exchanges, which as explained later does not reveal the fundamental throughput of a network of low mobility. By simulation, we will show the effect of a cooperative radius R on the throughput of D-SAM. Within the radius R centered at a receiver, only the desired transmitter is allowed to transmit. This study interestingly supports that the two-hop rule adopted in MSH-DSCH (i.e., all interfering transmitters to a receiver are kept two hops away from the receiver) is a good choice for regular or near regular topologies. This study also provides a corresponding guidance for choosing a proper packet spectral efficiency, which is not available in IEEE 802.16.

The principle of D-SAM differs from that of a distributed and cooperative link scheduling (DCLS) algorithm shown in [44]. The former is based on the distance information of neighboring nodes. But the latter is based on local calibration of SINR for each link. For environment where distance does not well reflect signal attenuation, DCLS could be a better alternative. A detailed comparison between D-SAM and DCLS is not yet available.

By analysis in the previous chapter and simulation on D-SAM, the intra-network throughput of O-SAM and D-SAM is evaluated. The effects of traffic load and multiple antennas on the intra-network throughput are studied. The throughput of ALOHA is also compared with that of O-SAM and D-SAM. The study of D-SAM reveals an insight into the MSH-DSCH protocol adopted in IEEE 802.16[5].

The rest of this chapter is organized as follows: in Section 3.1, we present D-SAM in detail. In Section 3.2, we evaluate and compare the network throughput of ALOHA, O-SAM and D-SAM. The content of this chapter is partially contained in [40].

3.1 Distributed Synchronous Array Method

In D-SAM, time is slotted into frames of equal duration as shown in Fig. 3.1. Each frame is further divided into control subframe and data subframe. Assuming that the data subframe is much longer than the control subframe, the network spectral efficiency is dominated by the spectral efficiency in each data subframe. A control subframe is used for each node to compete for data transmission opportunity in a data subframe. Each control subframe consists of a group of M contention slots. For analysis of maximal achievable throughput, we will assume without loss of generality that each data subframe consists of a single data slot.

At the beginning of each frame, D-SAM allows each node to randomly initialize a choice for one of the M contention slots if the node has a packet to transmit to another node. If the node has packets to be transmitted (separately) to multiple neighboring nodes, the node chooses multiple contention slots - one slot for each receiver. During a chosen contention slot, the node contends for the upcoming data subframe by starting a handshaking process with its intended receiving node. The handshaking involves three packets: RTS (request-to-sent), CTS (clear-to-sent), and ACK. If the handshaking is successful, the upcoming data subframe is reserved for data transmission between the transmitter-and-receiver pair. During each contention slot, the handshaking packets are received by neighboring nodes so that these nodes are aware of the reservation status of the upcoming data frame. For each frame and each neighborhood in a predetermined range, the data subframe can only be reserved for one transmitter-and-receiver pair. This means that the first contention slot has the highest priority, the second contention slot has the second pri-

ority, and so on. In the next frame, the contention process repeats without memory of the previous contentions, which ensures fairness.

More details of D-SAM are as follows. We assume that each node k maintains a neighborhood list N_k which contains the identifications of all its neighboring nodes inside a range R. The range R is an important parameter for the performance of D-SAM. The ith node in N_k is indexed by $\mathrm{N}_k(i)$. The neighborhood list at each node can be established at the startup of the network. For networks of low mobility, this startup is feasible. We assume that every node can be set to one of three states for the upcoming data subframe: T, R and S. Here, T stands for transmitting, R for receiving, and S for standby. We denote the state of node k as S_k and the state of $\mathrm{N}_k(i)$ as $\mathrm{S}_{\mathrm{N}_k(i)}$.

1. *Initialization*: At the beginning of each frame, set every node to state S, i.e., $\mathrm{S}_k = S$ for all k. Then, we allow that every node k generates a "contention request vector" $\boldsymbol{v}_k$ that randomly maps each neighboring node in list N_k to one of M contention slots if node k has traffic load intended to those neighbors. Here, we assume M is larger than the size of every neighbor list, i.e., $M \geq |\mathrm{N}_k|$ for all k. The ratio of M over $|\mathrm{N}_k|$ affects the probability of handshaking collisions. The larger is the ratio, the lower is the probability of handshaking collisions. We denote the mth element of $\boldsymbol{v}_k$ as $v_k(m)$, which is

$$v_k(m) = \begin{cases} j, & \text{if node } k \text{ has traffic to node } j, \text{ and } j \text{ is mapped into contention slot } m, \\ 0, & \text{otherwise.} \end{cases} \tag{3.1}$$

   In other words, the value of $v_k(m)$ is the index of the receiving node for which the

transmitting node k wants to contend during the contention slot m for the upcoming data subframe. If $v_k(m) = 0$, it means that, in the mth contention slot, node k will not contend for the upcoming data subframe.

2. *In contention slot* m: each node k will first check its contention request vector. If $v_k(m) = 0$, node k eavesdrops ongoing handshaking within the neighborhood of range R. If node k hears any CTS or ACK packet, it retrieves the information from the packet and resets the states of the nodes in N_k accordingly. If $v_k(m) = j$ where $j > 0$, node k will try to finish the following three-way RTS-CTS-ACK handshaking with node j:

   - RTS

     Node k sends a RTS packet to node j which contains the identity of node k, if the following conditions are satisfied:

     (a) $\mathrm{S}_k = S$.

     (b) $\mathrm{S}_{\mathrm{N}_k(i)} \neq R$ for all i.

   - CTS

     If node j has successfully received the RTS packet from node k and the following conditions are satisfied:

     (a) $\mathrm{S}_j = S$

     (b) $\mathrm{S}_{\mathrm{N}_j(i)} = S$ for all i

     (c) $v_j(m) = 0$

then node j resets $\mathrm{S}_j = R$ and $\mathrm{S}_{\mathrm{N}_j(i_k)} = T$ where i_k is the index for node k in the table N_j, and sends a CTS packet back to node k.

- ACK

  If node k has successfully received the CTS packet from node j, the node k resets $\mathrm{S}_k = T$ and $\mathrm{S}_{\mathrm{N}_k(i_j)} = R$ where i_j is the index of node j in the table N_k, and sends back the ACK packet.

During any contention slot, if there is a collision of control packets, the operation in that slot is abandoned. If the ratio of M over the number of nodes within the radius R is large, the probability of collision of control packets is small. As long as the control packets are much smaller than the data packets (i.e., the control subframe is much smaller than the data subframe), the network spectral efficiency is dominated by the throughput in the data subframe. This assumption will be our basis for throughput evaluation of D-SAM.

Fig. 3.2 illustrates a snapshot of the concurrent co-channel transmission pairs for a square network, which was determined by D-SAM for data transmission. The radius $\mathrm{R} = d_a$ was chosen, where d_a is the spacing between two nearest neighbors. The number of contention slots was $M = 8$. The full traffic loading condition, i.e., $\zeta = 1$, was assumed.

For D-SAM, we evaluate the network throughput in bits-meter/s/Hz/node as follows:

$$C_{D-SAM} = E\left\{\frac{1}{N}\sum_{n=1}^{N} d_n R_\xi s_n\right\} \tag{3.2}$$

where E denotes expectation, N is the total number of nodes in the network, d_n is the distance between the nth receiving node and its transmitting node, R_ξ is the packet spectral

efficiency as defined before, $s_n \in \{0, 1\}$, and $s_n = 1$ if and only if a packet is intended for the nth node and the corresponding SINR is no less than ξ. In the simulation, the expectation is replaced by the average over many time frames. Each time frame also corresponds to an independent realization of Gaussian random channels. The distance weighting in (3.2) is different from the conversion formulas (from bits-hop/s/Hz/node to bits-meter/s/Hz/node) derived in [19] because the former does not take into account the fact that a typical multi-hop route between source node and destination node is not a straight line due to topology constraint. However, for regular topologies, the weighting used in (3.2) is slightly larger than that used in [19]. For an arbitrary topology, (3.2) represents an upper bound on the throughput in bits-meter/s/Hz/node.

3.2 Throughput Evaluation

In this section, we will illustrate and compare the throughput of O-SAM, D-SAM and ALOHA. The system parameters for O-SAM and ALOHA are the same as those in previous chapter. For D-SAM, we will consider the three regular topologies as well as 20 random topologies. Each random topology consists of 300 nodes positioned by the two-dimensional Poisson random process. We will use $M = 60$ with which the probability of control packet collision is negligible as observed in simulations.

Figure 3.3 compares the throughput of O-SAM, D-SAM and ALOHA versus the traffic load probability ζ. For each ζ, the throughput of O-SAM was maximized over both ξ and θ, and the throughput of D-SAM was maximized over ξ and R (the cooperative range). The square topology as shown in Figure 2.1 and the Gaussian SISO channels

were considered. We see that as long as $\zeta > 10\%$, both O-SAM and D-SAM yield higher throughput than ALOHA. In other words, only when the traffic load is low, does ALOHA yield a higher throughput. As expected, the throughput of D-SAM is lower than that of O-SAM. This is because the concurrent co-channel transmissions for D-SAM are not as ideal as those for O-SAM. This figure shows that the throughput of D-SAM is about two thirds of that of O-SAM in the full load condition.

Figure 3.4 compares the throughput of O-SAM and D-SAM for each of SISO, SIMO and MIMO cases. For O-SAM, the throughput was maximized over ξ and θ. For D-SAM, the throughput was maximized over ξ and R. The square network was considered. This figure illustrates that multiple antennas can significantly improve the network throughput.

Figure 3.5 compares the throughput of O-SAM and D-SAM for each of the three topologies: square, triangle and hexagon. A useful observation is that O-SAM with the hexagonal network has a much higher throughput than all other situations. It is also useful to note here that the optimal subnet partition of the hexagonal network for O-SAM as shown in (2.1) is identical to that for C-SAM as shown in [19]. Hence, for the hexagonal topology, the throughput gain due to the opportunistic transmitter selection is not compromised by any change of subnet partition. This is not the case for the other two topologies. Although the throughput of D-SAM is not as high as that of O-SAM, D-SAM works with any topology.

Figure 3.6 illustrates the ξ-optimized throughput of D-SAM versus the cooperative range R. It is interesting to observe that for all three regular topologies, the optimal cooperative range R^* satisfies $d_a \leq \mathrm{R}^* < d_b$. Here, d_a is the shortest distance between two adjacent nodes, and d_b is the shortest distance between two nodes that are two hops

apart. Clearly, when $\mathrm{R} < d_a$, the throughput for the regular topologies should be zero. We also see that for the regular topologies, the throughput in the interval $d_a \leq \mathrm{R} < d_b$ is essentially constant where the variations due to random subnet partitions and random channel realizations are small and not perceivable from this figure. Under $d_a \leq \mathrm{R} < d_b$, the corresponding optimal target SINR is $\xi^* \approx 4$.

Given $\rho = 1$, we have $d_a = 1$ and $d_b = \sqrt{2}d_a = 1.41$ for square, $d_a = \sqrt{2/\sqrt{3}} = 1.07$ and $d_b = \sqrt{3}d_a = 1.85$ for triangle, and $d_a = \sqrt{4/(3\sqrt{3})} = 0.877$ and $d_b = \sqrt{3}d_a = 1.52$ for hexagonal [19]. We will restrict d_a and d_b to be defined as above only for the regular topologies.

As observed in our simulation, this optimal condition $d_a \leq \mathrm{R}^* < d_b$ also holds for $\alpha = 3$. This observation interestingly supports the two-hop rule adopted in MSH-DSCH of IEEE 802.16. But the corresponding ξ^* decreases as the path loss exponent α decreases. We found that ξ^* is somewhere between 1.5 and 2 when $\alpha = 3$. Note that the spectral efficiency of each packet is governed by the value of ξ, i.e., $R_\xi = \log_2(1 + \xi)$.

Figure 3.6 also shows that for $\mathrm{R} < d_a$, the throughput of the random topologies is nonzero, and furthermore it peaks at $\mathrm{R} = 0.8$. It is important to note that the throughput under $\mathrm{R} < d_a$ is not very meaningful. This is because when $\mathrm{R} < d_a$, the distance between many adjacent nodes is larger than R so that there is no direct link between them. In fact, under $\mathrm{R} = 0.8$, many nodes are not even connected with others, which is illustrated in Figure 3.7. In such a case, the expression defined in (3.2) is only a very loose upper bound on the network throughput.

3.3 Summary

In this chapter, we proposed a distributed media access contron scheme: D-SAM. With D-SAM, the subnet partition within each time frame is decided by the network locally and dynamically. For networks of sufficiently long channel coherence time, the spectral overhead for exchanges of control packets can be affordable or even negligible compared to the exchanges of data packets. In this case, the network throughput is primarily affected by the subnet partition in each time frame. The cooperative radius R has a major effect on the size of each subnet and hence the network throughput. For networks of regular topologies, the optimal value of R has been shown to be anywhere between d_a and d_b where d_a is the shortest distance between two adjacent nodes and d_b is the shortest distance between two nodes that are two hops apart. This result interestingly supports the two-hop rule adopted in MSH-DSCH in IEEE 802.16. For a network of random topology, the cooperative radius seems to be a more effective parameter, than the hop count, for subnet partition or equivalently spacing control between concurrent co-channel transmissions. A detailed study of the implementation issues remains a future task.

Similar as the previous chapter, we compared the throughput of D-SAM with the throughput of ALOHA and O-SAM under a varying probability ζ of traffic load. The same result is presented that ALOHA yields lower throughput than O-SAM and D-SAM unless ζ is small, e.g., less than 10%.

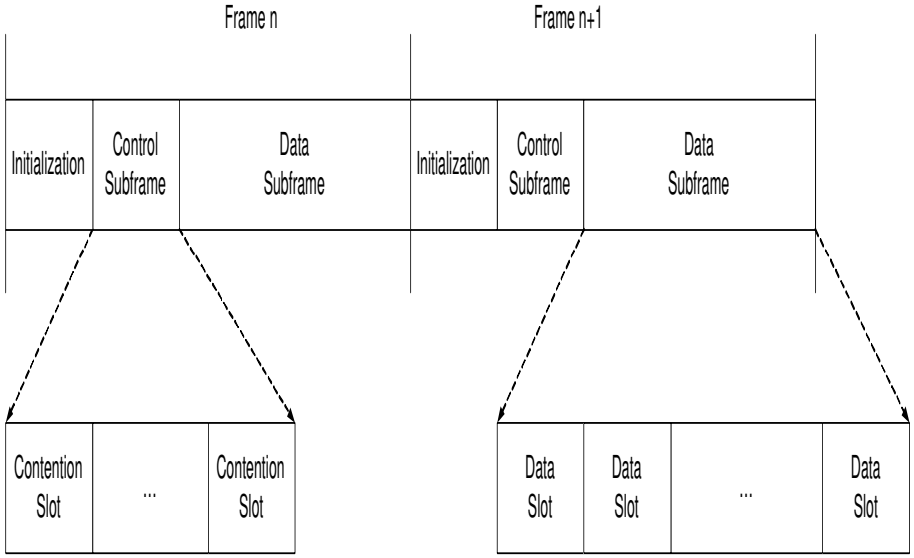

Figure 3.1: Frame structure of the distributed SAM protocol, which resembles that of MSH-DSCH in IEEE 802.16.

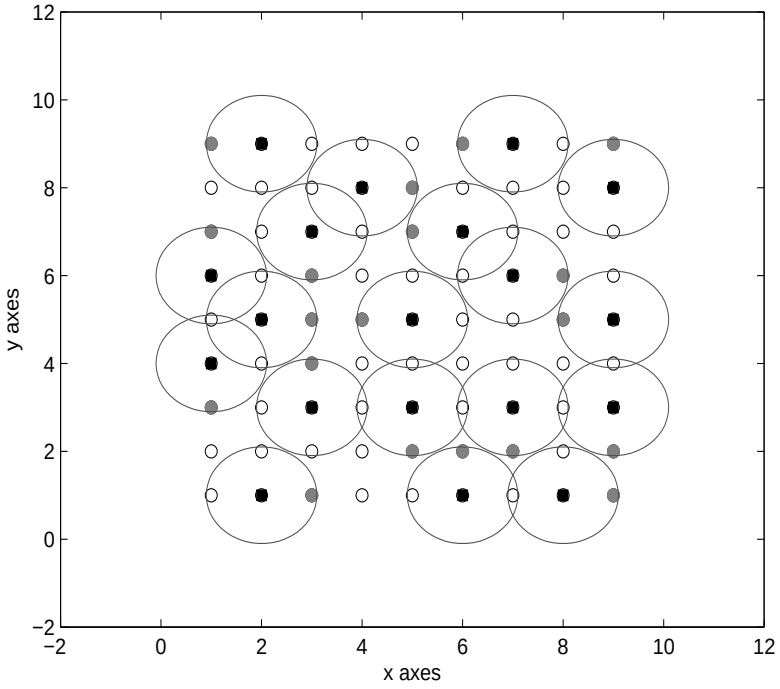

Figure 3.2: A snapshot of concurrent co-channel transmissions determined by the D-SAM protocol for a network in a regular square grid. R = d_a, $M = 8$ and $\zeta = 1$ were used, where d_a is the minimum distance between two adjacent nodes. The black nodes are the receiving nodes, and the grey nodes are the transmitting nodes.

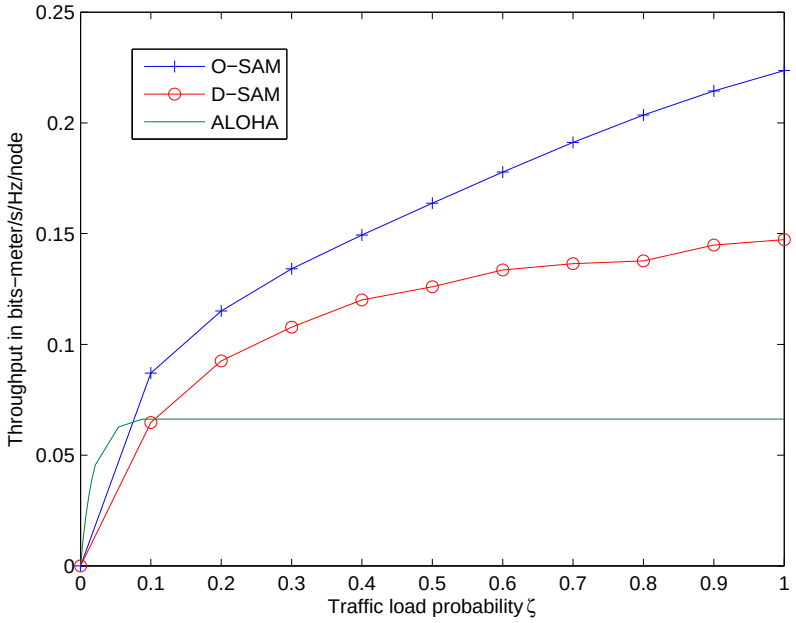

Figure 3.3: Throughput comparison of O-SAM, D-SAM and ALOHA. We used $\rho = 1$, $SNR = 40dB$, square topology, and SISO channels.

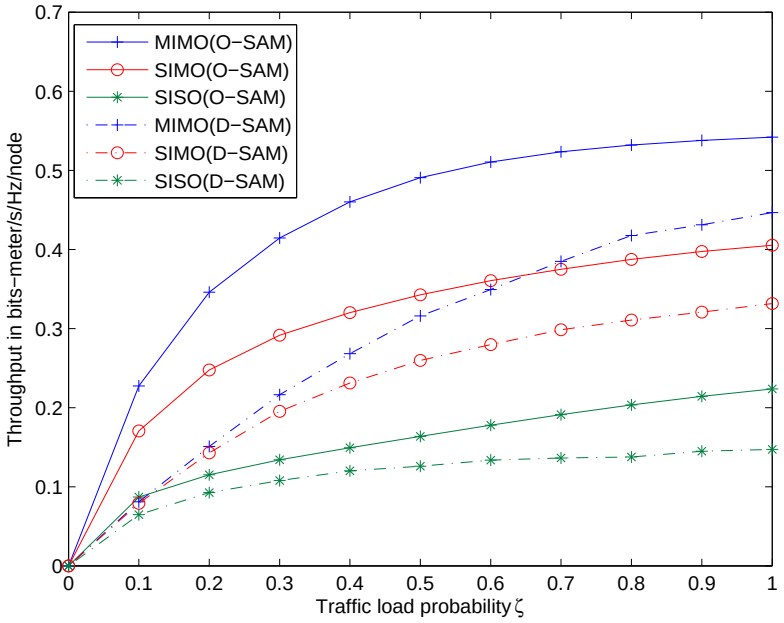

Figure 3.4: Throughput of O-SAM and D-SAM for SISO, SIMO and MIMO channels. We used $\rho = 1$, $SNR = 40dB$, and square topology.

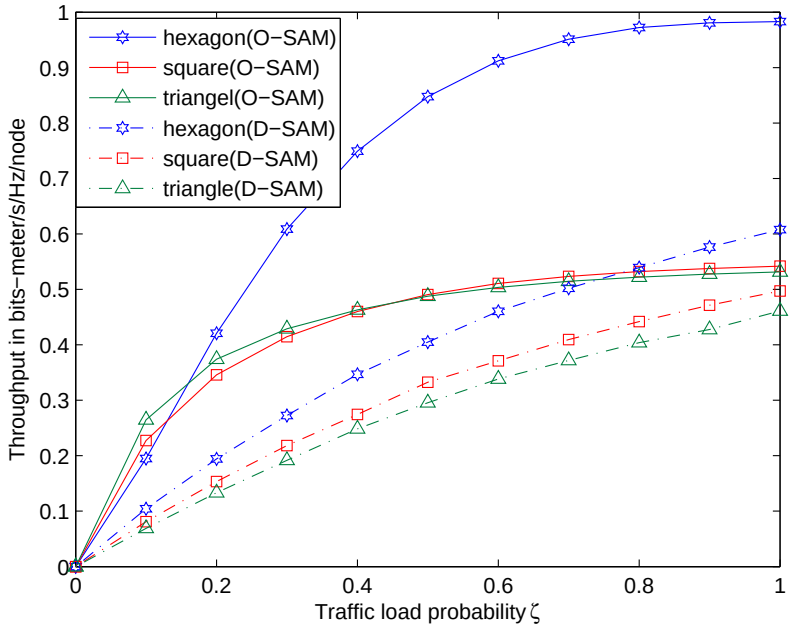

Figure 3.5: Throughput of O-SAM and D-SAM for different network topologies. We used $\rho = 1$, $SNR = 40dB$, and 4×4 MIMO channels.

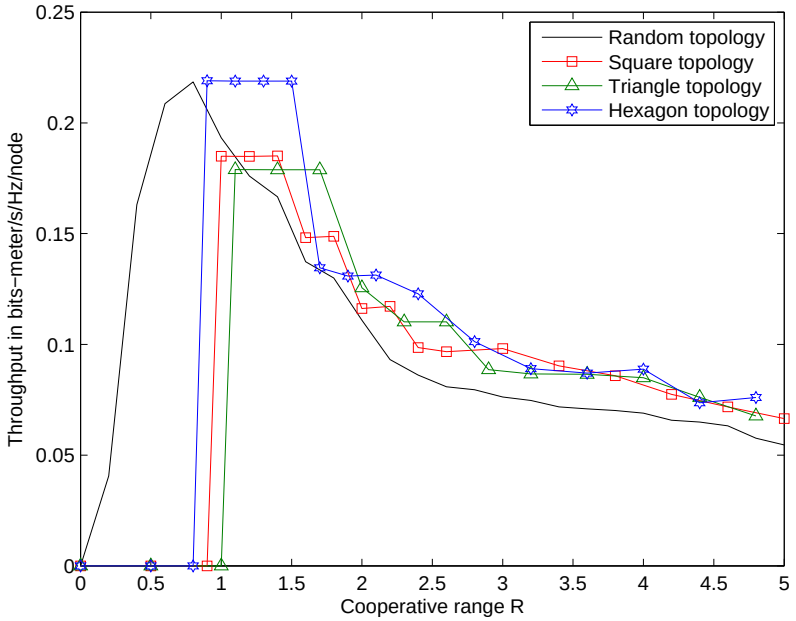

Figure 3.6: Throughput of D-SAM versus the cooperative range R. We used $\rho = 1$, $\zeta = 1$, $SNR = 40dB$, and SISO channels.

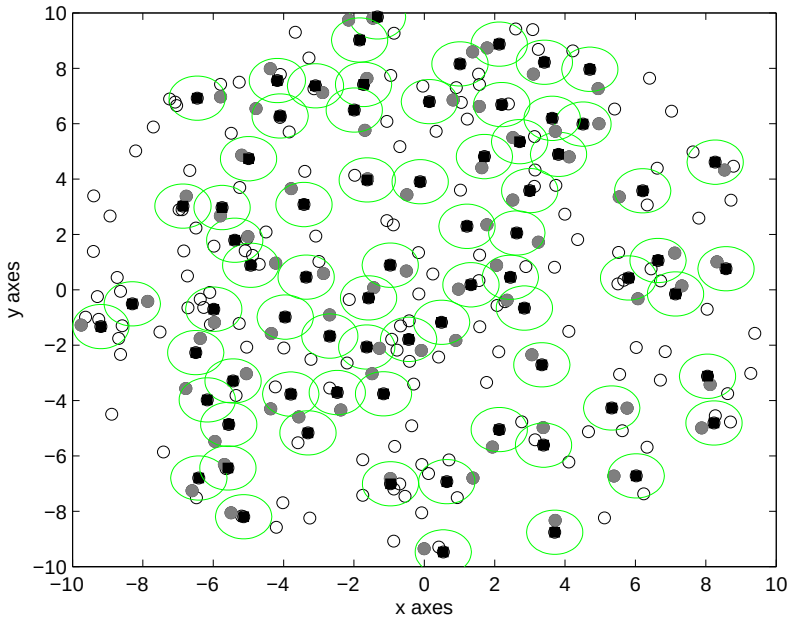

Figure 3.7: A snapshot of subnet partition of a random network by D-SAM with R = 0.8. The black nodes are the receivers, and the grey nodes are the transmitters. We used $\rho = 1$ and $\zeta = 1$. Each circle shown has the radius 0.8.

Chapter 4

Generalized Water-Filling Algorithm

4.1 MIMO Channel Capacity

We first consider the single user MIMO system as illustrated in Fig. 4.1, where $\mathbf{x} \in \mathcal{C}^{M\times 1}$ denotes the signal transmitted from the source equipped with M antennas, and $\mathbf{y} \in \mathcal{C}^{N\times 1}$ the signal received by the receiver equipped with N antennas. Furthermore, $\mathbf{H} \in \mathcal{C}^{N\times M}$ denotes the channel matrix between the source and the destination, and $\mathbf{n}$, is the zero-mean Gaussian noises at receiver.

$$\mathbf{y} \quad = \quad \mathbf{Hx} + \mathbf{n} \tag{4.1}$$

Assume $E[\mathbf{n}\mathbf{n}^H] = I$, that is the noise at different receiving antennas are independent. The transmit power is constraint to be P, i.e.

$$E[\mathbf{x}^H\mathbf{x}] = tr\{E[\mathbf{x}\mathbf{x}^H]\} \leq P \tag{4.2}$$

In this case,the power allocation problem will be

$$\begin{aligned} \max_{\mathbf{Q}} \quad & \mathcal{I}(\mathbf{x};\mathbf{y}) = \max_{\mathbf{Q}} \ \log\det|\mathbf{I} + \mathbf{H}\mathbf{Q}\mathbf{H}^H| \\ s.t. \quad & tr\{\mathbf{Q}\} \leq P \end{aligned} \tag{4.3}$$

This power allocation problem in (4.3) is given by water filling algorithm [23] and easily extended to the weighted constraint scenario. The constraint in (4.3) can be generalized to

$$tr\{\mathbf{B}\mathbf{Q}\mathbf{B}^H\} = tr\{(\mathbf{B}^H\mathbf{B})^{H/2}\mathbf{Q}(\mathbf{B}^H\mathbf{B})^{1/2}\} \leq P \tag{4.4}$$

In fact, the above problem can be transformed to

$$\begin{aligned} \max_{\mathbf{W}} \quad & \log\det|\mathbf{I} + \mathbf{H}(\mathbf{B}^H\mathbf{B})^{-H/2}\mathbf{W}(\mathbf{B}^H\mathbf{B})^{-1/2}\mathbf{H}^H| \\ s.t. \quad & tr\{\mathbf{W}\} \leq P \end{aligned} \tag{4.5}$$

which is the same form as (4.3).

Next section, we develop a generalized water filling (GWF) theorem and the corresponding algorithm to solve (with global optimality) a special type of convex optimization problems. The GWF algorithm is a useful building block for two of the power allocation algorithms proposed in next chapter. Although there are other types of algorithms in the literature also called generalized water filling, they are designed for different problems.

The content of this chapter is partially contained in [68].

4.2 A Generalized Water-Filling Algorithm

Consider the following convex optimization problem:

$$\begin{aligned} \min_{\mathbf{Q}\geq 0} \quad & J \doteq -\log|\mathbf{I}+\mathbf{H}\mathbf{Q}\mathbf{H}^H| \\ s.t. \quad & tr\{\mathbf{B}_i\mathbf{Q}\mathbf{B}_i^H\} \leq P_i, \qquad \forall i \in \{1\dots m\} \end{aligned} \tag{4.6}$$

where $\mathbf{H}$ and $\mathbf{B}_i$ are complex matrices, $\mathbf{Q}$ is a complex positive semi-definite matrix, and P_i are positive numbers. Without its base specified, log has the natural base e. If $m = 1$, the solution to the above problem can be found by a well known water-filling algorithm. Otherwise, one can use a CVX algorithm in Matlab [45] which is designed for any convex optimization problem. We now introduce an algorithm, referred to as generalized water-filling (GWF) algorithm, to solve the problem in (4.6). The GWF algorithm is based on the following GWF theorem:

Theorem 1 *The solution to (4.6) is given by:*

$$\mathbf{Q} = \mathbf{K}^{-H}\mathbf{V}(\mathbf{I}-\mathbf{\Sigma}^{-2})^{+}\mathbf{V}^H\mathbf{K}^{-1} \tag{4.7}$$

where $\mathbf{K} = (\sum_{i=1}^{m}\mu_i\mathbf{B}_i^H\mathbf{B}_i)^{1/2}$ *(assumed to be non-singular),* $\mathbf{V}$ *and* $\mathbf{\Sigma}$ *are determined from the SVD* $\mathbf{H}\mathbf{K}^{-H} = \mathbf{U}\mathbf{\Sigma}\mathbf{V}^H$*,* $(\cdot)^+$ *replaces all negative diagonal elements by zeros and leaves all non-negative diagonal elements unchanged, and* $\boldsymbol{\mu} = (\mu_1, \cdots, \mu_m)$ *are the solution to the following dual problem:*

$$\begin{aligned} \max_{\boldsymbol{\mu}\geq 0} \quad & -\log|\mathbf{I}+\mathbf{H}\mathbf{Q}\mathbf{H}^H| + \sum_{i=1}^{m}\mu_i(tr(\mathbf{B}_i\mathbf{Q}\mathbf{B}_i^H) - P_i) \\ s.t. \quad & \mathbf{Q} = \mathbf{K}^{-H}\mathbf{V}(\mathbf{I}-\mathbf{\Sigma}^{-2})^{+}\mathbf{V}\mathbf{K}^{-1}. \end{aligned} \tag{4.8}$$

Proof. For any $\mathbf{Q} \geq 0$, we can write $\mathbf{Q} = \mathbf{A}\mathbf{A}^H$ where $\mathbf{A}$ is a full column rank matrix. With respect to $\mathbf{A}$, we can write the following Lagrangian function of (4.6):

$$L = -\log\left|I + \mathbf{H}\mathbf{A}\mathbf{A}^H\mathbf{H}^H\right| + \sum_{i=1}^{m} \mu_i \left(tr\left\{\mathbf{B}_i\mathbf{A}\mathbf{A}^H\mathbf{B}_i^H\right\} - P_i\right) \tag{4.9}$$

The gradient of L with respect to $\mathbf{A}$ can be found by using $\partial \log|\mathbf{X}| = tr(\mathbf{X}^{-1}\partial\mathbf{X})$, $\partial(\mathbf{X}\mathbf{X}^H) = (\partial\mathbf{X})\mathbf{X}^H + \mathbf{X}\partial\mathbf{X}^H$ and other basic tools [46]. The result is

$$\begin{aligned}\frac{\partial L}{\partial \mathbf{A}^H} &\doteq \frac{\partial L}{\partial Re(\mathbf{A})^T} - j\frac{\partial L}{\partial Im(\mathbf{A})^T} \\ &= -2\mathbf{A}^H\left(\mathbf{H}^H\left(\mathbf{I} + \mathbf{H}\mathbf{A}\mathbf{A}^H\mathbf{H}^H\right)^{-1}\mathbf{H} - \sum_{i=1}^{m}\mu_i\mathbf{B}_i^H\mathbf{B}_i\right)\end{aligned} \tag{4.10}$$

Then, the complete K.K.T. conditions [47] of the problem (4.6) with respect to $\mathbf{A}$ can be written as

$$-\mathbf{A}^H\left(\mathbf{H}^H\left(\mathbf{I} + \mathbf{H}\mathbf{A}\mathbf{A}^H\mathbf{H}^H\right)^{-1}\mathbf{H} - \sum_{i=1}^{m}\mu_i\mathbf{B}_i^H\mathbf{B}_i\right) = 0 \tag{4.11}$$

$$tr\left\{\mathbf{B}_i\mathbf{A}\mathbf{A}^H\mathbf{B}_i^H\right\} - P_i \leq 0 \tag{4.12}$$

$$\mu_i \geq 0 \tag{4.13}$$

$$\mu_i\left(tr\left\{\mathbf{B}_i\mathbf{A}\mathbf{A}^H\mathbf{B}_i^H\right\} - P_i\right) = 0 \tag{4.14}$$

where $i = 1, \cdots, m$.

Although the problem (4.6) with respect to $\mathbf{A}$ is not convex, we now show that the generalized KKT conditions [47] of the problem (4.6) with respect to $\mathbf{Q} \geq 0$, which is convex, are equivalent to (4.11)-(4.14). Consider L as in (4.9) with $\mathbf{A}\mathbf{A}^H$ replaced by $\mathbf{Q}$. It follows that

$$\frac{\partial L}{\partial \mathbf{Q}} = -\mathbf{H}^H\left(\mathbf{I} + \mathbf{H}\mathbf{Q}\mathbf{H}^H\right)^{-1}\mathbf{H} + \sum_{i=1}^{m}\mu_i\mathbf{B}_i^H\mathbf{B}_i \tag{4.15}$$

We define a vector operator for a complex conjugate symmetric matrix as follows:

$$vec(\mathbf{Q}) \doteq \begin{bmatrix} vec(Re\{\mathbf{Q}\}) \\ vec(Im\{\mathbf{Q}\}) \end{bmatrix}$$

Here, $vec(Re\{\mathbf{Q}\})$ stacks up all elements from $Re\{\mathbf{Q}\}$, and $vec(Im\{\mathbf{Q}\})$ stacks up all elements from $Im\{\mathbf{Q}\}$. Assume $\mathbf{Q} \in \mathcal{C}^{n\times n}$. Then, $vec(\mathbf{Q}) \in \mathcal{R}^{2n^2\times 1}$. Now, based on (5.95) in [47], we have the following sufficient generalized KKT conditions:

$$-vec\left(\mathbf{H}^H\left(\mathbf{I}+\mathbf{H}\mathbf{Q}\mathbf{H}^H\right)^{-1}\mathbf{H}-\sum_{i=1}^{m}\mu_i\mathbf{B}_i^H\mathbf{B}_i\right)-\omega=0 \tag{4.16}$$

$$tr\left\{\mathbf{B}_i\mathbf{Q}\mathbf{B}_i^H\right\}-P_i\leq 0 \tag{4.17}$$

$$\mu_i\geq 0 \tag{4.18}$$

$$\mu_i\left(tr\left\{\mathbf{B}_i\mathbf{Q}\mathbf{B}_i^H\right\}-P_i\right)=0 \tag{4.19}$$

$$\omega^T vec(\mathbf{Q})=0 \tag{4.20}$$

where $i=1,\cdots,m$, $\omega\in\mathcal{R}^{2n^2\times 1}$. Also, $\mathbf{Q}\in\mathcal{K}\doteq\{\mathbf{Q}'\mid\mathbf{Q}'\geq 0\}$, and ω is in the dual cone of $\mathcal{K}$, i.e., $\omega\in\mathcal{K}^D\doteq\{\omega^T vec(\mathbf{Q}')\geq 0|\mathbf{Q}'\geq 0\}$. In fact, the term $-\omega$ in (4.16) is due to the constraint $-\mathbf{Q}\leq 0$ for which we used $\frac{\partial vec^T(\mathbf{Q})}{\partial vec(\mathbf{Q})}=\mathbf{I}$. Note that for two complex conjugate symmetric matrices $\mathbf{A}'$ and $\mathbf{B}'$, $tr(\mathbf{A}'^H\mathbf{B}')$ is always real. And $\mathbf{A}'^H\mathbf{B}'=0\Leftrightarrow tr(\mathbf{A}'^H\mathbf{B}')=0\Leftrightarrow Re\{\mathbf{A}'\}^T Re\{\mathbf{B}'\}+Im\{\mathbf{A}'\}^T Im\{\mathbf{B}'\}=0\Leftrightarrow vec(\mathbf{A}')^T vec(\mathbf{B}')=0$. With this property and $\mathbf{Q}=\mathbf{A}\mathbf{A}^H$, it is easy to verify that if $\mathbf{A}$ satisfies (4.11), (4.16) implies (4.20). Therefore, provided that ω from (4.16) satisfies $\omega\in\mathcal{K}^D$, (4.11)-(4.14) are also *sufficient* KKT conditions for the problem (4.6). Later, we will verify that with a highest rank solution $\mathbf{Q}=\mathbf{A}\mathbf{A}^H$ where $\mathbf{A}$ is constructed from (4.11), (4.16) always yields a $\omega\in\mathcal{K}^D$.

Next, we construct an optimal structure of $\mathbf{Q}$ based on (4.11). Since $\mathbf{K}\mathbf{K}^H = \sum_{i=1}^{m} \mu_i \mathbf{B}_i^H \mathbf{B}_i$ and $\mathbf{K}$ is non-singular, (4.11) is equivalent to

$$-\mathbf{A}^H \mathbf{K} \left(\mathbf{K}^{-1} \mathbf{H}^H \left(\mathbf{I} + \mathbf{H}\mathbf{K}^{-H} \mathbf{K}^H \mathbf{A}\mathbf{A}^H \mathbf{K}\mathbf{K}^{-1} \mathbf{H}^H \right)^{-1} \mathbf{H}\mathbf{K}^{-H} - \mathbf{I} \right) = 0 \tag{4.21}$$

Define the SVD of $\mathbf{H}\mathbf{K}^{-H}$ as

$$\mathbf{H}\mathbf{K}^{-H} = \mathbf{U}\mathbf{\Sigma}\mathbf{V}^H = \mathbf{U} \begin{pmatrix} \mathbf{\Sigma}_1 & \\ & \mathbf{\Sigma}_2 \end{pmatrix} \begin{pmatrix} \mathbf{V}_1 & \mathbf{V}_2 \end{pmatrix}^H \tag{4.22}$$

where $\mathbf{U}$ and $\mathbf{V}$ are square unitary matrices, $\mathbf{\Sigma}_1$ (square) and $\mathbf{\Sigma}_2$ (possibly non-square) are diagonal, all the diagonal elements of $\mathbf{\Sigma}_1$ are larger than one, and all the diagonal elements of $\mathbf{\Sigma}_2$ are less than or equal to one. We now assume that $\mathbf{K}^H \mathbf{A} = \mathbf{V}_1 \mathbf{T}$ where $\mathbf{T}$

is non-singular. Then, (4.21) is equivalent to the following:

$$
\begin{aligned}
& -\mathbf{A}^H\mathbf{K}\left(\mathbf{K}^{-1}\mathbf{H}^H\left(\mathbf{I}+\mathbf{H}\mathbf{K}^{-H}\mathbf{K}^H\mathbf{A}\mathbf{A}^H\mathbf{K}\mathbf{K}^{-1}\mathbf{H}^H\right)^{-1}\mathbf{H}\mathbf{K}^{-H}-\mathbf{I}\right)=0 \\
\overset{(a)}{\Longleftrightarrow}\quad & -\mathbf{T}^H\mathbf{V}_1^H\left(\mathbf{V}\mathbf{\Sigma}^T\mathbf{U}^H\left(\mathbf{I}+\mathbf{U}\mathbf{\Sigma}\mathbf{V}^H\mathbf{V}_1\mathbf{T}\mathbf{T}^H\mathbf{V}_1^H\mathbf{V}\mathbf{\Sigma}^T\mathbf{U}^H\right)^{-1}\mathbf{U}\mathbf{\Sigma}\mathbf{V}^H-\mathbf{I}\right)=0 \\
\overset{(b)}{\Longleftrightarrow}\quad & \mathbf{T}^H\left(\begin{pmatrix}\mathbf{\Sigma}_1 & \mathbf{0}\end{pmatrix}\left(\mathbf{I}+\begin{pmatrix}\mathbf{\Sigma}_1\\ \mathbf{0}\end{pmatrix}\mathbf{T}\mathbf{T}^H\begin{pmatrix}\mathbf{\Sigma}_1 & \mathbf{0}\end{pmatrix}\right)^{-1}\mathbf{\Sigma}-\begin{pmatrix}\mathbf{I} & \mathbf{0}\end{pmatrix}\right)\mathbf{V}^H=0 \\
\overset{(c)}{\Longleftrightarrow}\quad & \mathbf{T}^H\left(\begin{pmatrix}\mathbf{\Sigma}_1 & \mathbf{0}\end{pmatrix}\left(\mathbf{I}-\begin{pmatrix}\mathbf{\Sigma}_1\\ \mathbf{0}\end{pmatrix}\left((\mathbf{T}\mathbf{T}^H)^{-1}+\mathbf{\Sigma}_1^2\right)^{-1}\begin{pmatrix}\mathbf{\Sigma}_1 & \mathbf{0}\end{pmatrix}\right)\mathbf{\Sigma}\right. \\
& \qquad\qquad\qquad\qquad\qquad\qquad\qquad\qquad\qquad\qquad\qquad\qquad\left.-\begin{pmatrix}\mathbf{I} & \mathbf{0}\end{pmatrix}\right)\mathbf{V}^H=0 \\
\overset{(d)}{\Longleftrightarrow}\quad & \mathbf{T}^H\left(\left(\begin{pmatrix}\mathbf{\Sigma}_1^2 & \mathbf{0}\end{pmatrix}-\mathbf{\Sigma}_1^2\left((\mathbf{T}\mathbf{T}^H)^{-1}+\mathbf{\Sigma}_1^2\right)^{-1}\begin{pmatrix}\mathbf{\Sigma}_1^2 & \mathbf{0}\end{pmatrix}\right)-\begin{pmatrix}\mathbf{I} & \mathbf{0}\end{pmatrix}\right)\mathbf{V}^H=0 \\
\overset{(e)}{\Longleftrightarrow}\quad & \mathbf{\Sigma}_1^2-\mathbf{\Sigma}_1^2\left(\left(\mathbf{T}\mathbf{T}^H\right)^{-1}+\mathbf{\Sigma}_1^2\right)^{-1}\mathbf{\Sigma}_1^2-\mathbf{I}=0 \\
\overset{(f)}{\Longleftrightarrow}\quad & \mathbf{\Sigma}_1^2-\mathbf{\Sigma}_1^2\left(\mathbf{\Sigma}_1^{-2}-\mathbf{\Sigma}_1^{-2}\left(\mathbf{T}\mathbf{T}^H+\mathbf{\Sigma}_1^{-2}\right)^{-1}\mathbf{\Sigma}_1^{-2}\right)\mathbf{\Sigma}_1^2-\mathbf{I}=0 \\
\overset{(g)}{\Longleftrightarrow}\quad & \mathbf{T}\mathbf{T}^H=\mathbf{I}-\mathbf{\Sigma}_1^{-2} \qquad (4.23)
\end{aligned}
$$

where for (c) and (f) we used the matrix inverse lemma. We see that since $\mathbf{T}\mathbf{T}^H=\mathbf{I}-\mathbf{\Sigma}_1^{-2}>0$, the above solution for $\mathbf{T}$, and hence the corresponding $\mathbf{A}$, is a valid solution.

The above solution of $\mathbf{K}^H\mathbf{A}$ has the same span as $\mathbf{V}_1$. A simple observation of the above analysis also suggests that as long as the span of $\mathbf{K}^H\mathbf{A}$ belongs to that of $\mathbf{V}_1$, a matrix $\mathbf{T}$ exists such that $\mathbf{K}^H\mathbf{A}=\mathbf{V}_1'\mathbf{T}$ satisfies (4.12) where $\mathbf{V}_1'$ is a sub-matrix of $\mathbf{V}_1$. On the other hand, if the span of $\mathbf{K}^H\mathbf{A}$ contains a vector from $\mathbf{V}_2$, i.e., $\mathbf{K}^H\mathbf{A}=\mathbf{V}_2'\mathbf{T}$ where $\mathbf{V}_2'$ has a column vector from $\mathbf{V}_2$, then there does not exist such a matrix $\mathbf{T}$ for $\mathbf{A}$ to satisfy (4.12), or equivalently the corresponding "solution" $\mathbf{T}\mathbf{T}^H$ would be non-positive

semi-definite which contradicts to the fundamental nature of $\mathbf{T}\mathbf{T}^H$. Therefore, the highest rank solution of $\mathbf{A}$ to satisfy (4.12) is given by $\mathbf{A} = \mathbf{K}^{-H}\mathbf{V}_1\mathbf{T}$ where $\mathbf{T} = \left(\mathbf{I} - \mathbf{\Sigma}_1^{-2}\right)^{1/2}$. Equivalently, the highest rank solution of $\mathbf{Q}$ to satisfy (4.12) is given by

$$\begin{aligned}
\mathbf{Q} &= \mathbf{A}\mathbf{A}^H = \mathbf{K}^{-H}\mathbf{V}_1\mathbf{T}\mathbf{T}^H\mathbf{V}_1^H\mathbf{K}^{-1} \\
&= \mathbf{K}^{-H}\mathbf{V}_1(\mathbf{I} - \mathbf{\Sigma}_1^{-2})\mathbf{V}_1^H\mathbf{K}^{-1} \\
&= \mathbf{K}^{-H}\mathbf{V}(\mathbf{I} - \mathbf{\Sigma}^{-2})^+\mathbf{V}^H\mathbf{K}^{-1} \qquad (4.24)
\end{aligned}$$

where $\mathbf{\Sigma}^{-2} = (\mathbf{\Sigma}^T\mathbf{\Sigma})^{-1}$, the inverse of a zero would be treated as positive infinity, and $(x)^+ \doteq \max(x, 0)$ operates on each diagonal element of the diagonal matrix $\mathbf{I} - \mathbf{\Sigma}^{-2}$.

With (4.24), one can verify that

$$\begin{aligned}
& -\mathbf{H}^H\left(\mathbf{I} + \mathbf{H}\mathbf{Q}\mathbf{H}^H\right)^{-1}\mathbf{H} + \sum_{i=1}^{m}\mu_i\mathbf{B}_i^H\mathbf{B}_i \\
= \;& \mathbf{K}\mathbf{V}\left(\mathbf{I} - \mathbf{\Sigma}^T\left(\mathbf{I} + \mathbf{\Sigma}\left(\mathbf{I} - \mathbf{\Sigma}^{-2}\right)^+\mathbf{\Sigma}^T\right)^{-1}\mathbf{\Sigma}\right)\mathbf{V}^H\mathbf{K}^H \\
\geq \;& 0 \qquad (4.25)
\end{aligned}$$

Note that the ith diagonal element of the diagonal matrix between $\mathbf{V}$ and $\mathbf{V}^H$ in the above, denoted by d_i, is

$$\begin{aligned}
d_i &= 1 - \sigma_i^2\left(1 + \sigma_i^2(1 - \sigma_i^{-2})^+\right)^{-1} \\
&= \begin{cases} 1 - \sigma_i^2 > 0 & \text{if } \sigma_i^2 < 1 \\ 0 & \text{if } \sigma_i^2 \geq 1 \end{cases} \qquad (4.26)
\end{aligned}$$

where σ_i is the ith diagonal element of $\mathbf{\Sigma}$.

Therefore, the corresponding ω from (4.16) belongs to $\mathcal{K}$. Since $\mathcal{K} = \mathcal{K}^D$ for complex conjugate symmetric positive semi-definite matrices, a proof of which is simple and similar to Example 2.24 in [47], ω from (4.16) also belongs to $\mathcal{K}^D$.

If we did not use the highest rank solution for $\mathbf{Q}$ as in (4.24), then there would be a $d_i = 1 - \sigma_i^2 < 0$ associated with a $\sigma_i^2 > 1$ and hence (4.25) would not hold and hence the corresponding $\boldsymbol{\omega}$ from (4.16) would not belong to $\mathcal{K}^D$.

With the optimal $\mathbf{Q}$ given in (4.24), which is a function of $\boldsymbol{\mu} = [\mu_1, \cdots, \mu_m]$, the remaining problem is to find the optimal $\boldsymbol{\mu}$. Since the effective KKT equations for $\boldsymbol{\mu}$ are the same for both (4.11)-(4.14) and (4.16)-(4.20), the optimal $\boldsymbol{\mu}$ can be found by using either the dual problem of (4.6) with respect to $\mathbf{A}$ or the dual problem of (4.6) with respect to $\mathbf{Q}$. Choosing the former, we can find the optimal $\boldsymbol{\mu}$ by solving (4.8). The dual problem of (4.6) with respect to $\mathbf{Q}$ is the same as (4.8) except for the additional term $-vec^T(\mathbf{Q})\boldsymbol{\omega}$ which is however maximized to zero by $\boldsymbol{\omega}$ for any $\boldsymbol{\mu}$. ■

The proof of the theorem is completed. To our knowledge, this theorem is new. As illustrated by a simulation example later 4.4, the GWF algorithm can achieve the same accuracy as CVX, and the former has a much faster speed than the latter when the dimension of $\boldsymbol{\mu}$ is much smaller than that of $\mathbf{Q}$. The GWF algorithm is useful for many applications other than those shown in this thesis. For example, if one wants to design a source covariance matrix to maximize the data rate of a MIMO link and also wants to keep the interference from this source to other neighboring nodes under certain limits, such a problem can be directly formulated as (4.6). In the next section, we show how to find the optimal $\boldsymbol{\mu}$ in more details. For the primal problem (4.6), $\mathbf{Q}$ has $2n^2$ real elements. (Even under the constraint $\mathbf{Q} = \mathbf{Q}^H$, $\mathbf{Q}$ has $\frac{n(n+1)}{2}$ free real-part elements, $\frac{n(n-1)}{2}$ free imaginary-part elements, and hence total n^2 free real elements.) For the dual problem (4.8), there are m real variables in $\boldsymbol{\mu}$. If $m < n^2$, it is reasonable to expect the dual problem to be less costly to solve.

4.3 Computation of the Dual Problem in Theorem 1

Since the dual problem is convex, we can follow the interior-point method [47] and define the following dual function with logarithmic barrier terms:

$$D(\boldsymbol{\mu}) = -\log|\mathbf{I} + \mathbf{H}\mathbf{Q}(\boldsymbol{\mu})\mathbf{H}^H| + \sum_{i=1}^{m} \mu_i (tr(\mathbf{B}_i \mathbf{Q}(\boldsymbol{\mu})\mathbf{B}_i^H) - P_i) + \frac{1}{t}\sum_i \log \mu_i \qquad (4.27)$$

where we use $\mathbf{Q}(\boldsymbol{\mu})$ to stress that $\mathbf{Q}$ is a function of $\boldsymbol{\mu}$. Note that the first two terms in (4.27) equal to $\min_{\mathbf{Q}\geq 0} L$, which we want to maximize subject to $\boldsymbol{\mu} \geq 0$. For each choice of t, we can apply the Newton's method to find the optimal $\boldsymbol{\mu}$, i.e.,

$$\boldsymbol{\mu}^{(k+1)} = \boldsymbol{\mu}^{(k)} + (\nabla^2 D(\boldsymbol{\mu}^{(k)}))^{-1} \nabla D(\boldsymbol{\mu}^{(k)}) \qquad (4.28)$$

where k denotes the iteration index. Upon convergence for each t, we can increase t by a factor $\delta > 1$ and continue a new cycle of the Newton's search. The above process continues until $1/t$ is smaller than a pre-specified number ϵ.

The computation of the gradient vector $\nabla D(\boldsymbol{\mu}^{(k)})$ and the Hessian matrix $\nabla^2 D(\boldsymbol{\mu}^{(k)})$ is straightforward although the detailed expressions are lengthy. Since $\mathbf{Q}(\boldsymbol{\mu})$ depends on the eigenvalue decomposition of $\mathbf{K}^{-1}\mathbf{H}^H\mathbf{H}\mathbf{K}^{-H}$ and the computation of $\mathbf{K} = \left(\sum_{i=1}^{m} \mu_i \mathbf{B}_i^H \mathbf{B}_i\right)^{1/2}$ also needs the eigenvalue decomposition of $\sum_{i=1}^{m} \mu_i \mathbf{B}_i^H \mathbf{B}_i$, we need to use the first-order and second-order differentials of eigenvalues and eigenvectors. The basic formulas for these differentials can be found in [46].

To avoid possible numerical problems in computing the differentials of eigenvectors when there are multiple identical eigenvalues, we added a small random perturbation matrix to $\sum_{i=1}^{m} \mu_i \mathbf{B}_i^H \mathbf{B}_i$ in our program, which proved to be very effective.

4.4 A Comparison of GWF and CVX

To show a comparison of our GWF algorithm with CVX in [45], we ran both algorithms on a desktop with $2.40GHz$ CPU. We chose $P_1 = 1$, $P_2 = 1.5$, $\mathbf{B}_1 = \mathbf{I}$, and used the complex Gaussian distribution with zero mean and unit variance to randomly choose each element in the following matrices:

$$\mathbf{H} = \begin{pmatrix} -0.6705 + 0.3791i & 0.1469 + 0.4499i & -0.2913 - 0.3867i & 0.1568 - 0.0536i \\ 0.2398 - 0.3460i & -0.0702 - 1.0615i & -0.4482 + 0.0759i & -1.0125 + 0.5067i \\ -0.8170 + 0.3401i & -0.5652 + 0.1424i & 0.1243 - 0.1684i & 0.2645 - 0.2377i \\ -0.7213 - 0.5363i & -0.1463 - 0.3667i & -0.7448 + 0.4854i & 0.1717 + 0.0345i \end{pmatrix}$$

$$\mathbf{B}_2 = \begin{pmatrix} 0.1993 + 0.1027i & -0.6859 + 0.4280i & 0.1457 + 0.3800i & 0.2031 + 0.5548i \\ 0.5582 + 0.2944i & -0.3429 - 0.4255i & 0.5535 - 0.8565i & 0.6080 - 0.5549i \\ 0.3102 - 0.1320i & 0.1658 + 0.4059i & 0.1225 + 0.7685i & 0.7242 + 0.1927i \\ -0.1438 + 1.2477i & -0.4989 + 0.3501i & 0.0825 - 0.8049i & -0.5126 + 0.4826i \end{pmatrix}$$

For the GWF algorithm, the initial elements of $\boldsymbol{\mu}^{(0)}$ were randomly chosen between zero and 10^{-2}. We chose $\nabla D(\boldsymbol{\mu})^T(\nabla^2 D(\boldsymbol{\mu}))^{-1}\nabla D(\boldsymbol{\mu}) < 10^{-2}$ as the stopping criterion for the inner loop (for fixed t). We also chose $t^{(1)} = 2$ and $t^{(i+1)} = 2t^{(i)}$, and finally $2/t < 10^{-4}$ as the stopping criterion for the outer loop. We noticed that for each t, the inner loop converged after about 8 iterations.

At the convergence, the following results from the GWF algorithm and the CVX

algorithm were obtained:

$$\mathbf{Q}_{GWF} =$$

$$\begin{pmatrix} 0.3726 & 0.1804 - 0.0634i & 0.0470 - 0.0795i & -0.1740 - 0.0078i \\ 0.1804 + 0.0634i & 0.2722 & -0.0779 - 0.1381i & -0.1265 - 0.1644i \\ 0.0470 + 0.0795i & -0.0779 + 0.1381i & 0.1643 & 0.0893 + 0.0208i \\ -0.1740 + 0.0078i & -0.1265 + 0.1644i & 0.0893 - 0.0208i & 0.1909 \end{pmatrix}$$

$$\mathbf{Q}_{CVX} =$$

$$\begin{pmatrix} 0.3726 & 0.1804 - 0.0634i & 0.0469 - 0.0796i & -0.1739 - 0.0078i \\ 0.1804 + 0.0634i & 0.2722 & -0.0779 - 0.1382i & -0.1265 - 0.1644i \\ 0.0469 + 0.0796i & -0.0779 + 0.1382i & 0.1643 & 0.0894 + 0.0208i \\ -0.1739 + 0.0078i & -0.1265 + 0.1644i & 0.0894 - 0.0208i & 0.1909 \end{pmatrix}$$

These two matrices agree with each other very well. In Table 4.1, we list the computational times used by the two algorithms and the corresponding values of the capacity achieved (i.e., $-J$ in (4.6)). We see that the same capacity is achieved by both algorithms. But the GWF is about four times faster than the CVX.

Figure 4.2 shows how $\boldsymbol{\mu}$ of the GWF converged to the optimal as the outer iterations continued. We see that μ_2 approaches to zero, which means that the second power

Table 4.1: Comparison of GWF with CVX in solving the problem (4.6) where $\mathbf{Q}$ is 4×4 and $m = 2$.

	Time in sec	Capacity in bits/s/Hz
GWF	3.40	2.6139
CVX	14.94	2.6139

constraint is satisfied automatically while the first power constraint is active. Figure 4.3 illustrates the capacity $(-J)$ as function of the barrier constant t.

4.5 Summary

In this chapter, we provide an analytical solution to a general convex optimization problem. This general formulation is useful in many applications, such as MIMO relay system and interference control problem. Although, this problem can be solved by some existing optimization tool, we develop a more efficient algorithm based on the dual principle of convex optimization. The numerical example is studied to illustrate that the new algorithm is much more efficient than those existing software on this specific problem, since the number of variables need to be optimized is the number of constraints instead of the actual matrix variable. In next chapter, this new algorithm is applied to find the optimal source covariance matrix in multiuser MIMO relay system.

4.6 Appendix - The derivatives used in 4.3

The Newton's method needs second order derivative of $D(\boldsymbol{\mu})$. To get the expression of the derivative of $\frac{\partial D(\boldsymbol{\mu})}{\partial \boldsymbol{\mu}}$, we need the following facts: Consider a complex conjugate symmetric matrix $\mathbf{A}$ which depends on a set of parameters $\mu_1, \mu_2, \ldots$. We can write the eigenvalue decomposition as

$$\mathbf{A}\mathbf{x}_i = \lambda_i \mathbf{x}_i \tag{4.29}$$

where the eigenvalues λ_i are real (assumed to be distinct) and the eigenvectors $\mathbf{x}_i$ are complex orthogonal: $\mathbf{x}_i^H \mathbf{x}_i = 1$. Then, we write the first order differentials as follows:

$$\frac{\partial \mathbf{A}}{\partial \mu_m}\mathbf{x}_i + \mathbf{A}\frac{\partial \mathbf{x}_i}{\partial \mu_m} = \frac{\partial \lambda_i}{\partial \mu_m}\mathbf{x}_i + \lambda_i \frac{\partial \mathbf{x}_i}{\mu_m} \tag{4.30}$$

Left multiplying $\mathbf{x}_i^H$ to (4.30), we have

$$\mathbf{x}_i^H \frac{\partial \mathbf{A}}{\partial \mu_m}\mathbf{x}_i + \mathbf{x}_i^H \mathbf{A}\frac{\partial \mathbf{x}_i}{\partial \mu_m} = \mathbf{x}_i^H \frac{\partial \lambda_i}{\partial \mu_m}\mathbf{x}_i + \mathbf{x}_i^H \lambda_i \frac{\partial \mathbf{x}_i}{\mu_m} \tag{4.31}$$

hence, we get

$$\frac{\partial \lambda_i}{\partial \mu_m} = \mathbf{x}_i^H \frac{\partial \mathbf{A}}{\partial \mu_m}\mathbf{x}_i \tag{4.32}$$

bring (4.32) back into (4.30), we can get

$$\frac{\partial \mathbf{x}_i}{\partial \mu_m} = (\mathbf{A} - \lambda_i \mathbf{I})^\dagger (\frac{\partial \lambda_i}{\partial \mu_m}\mathbf{I} - \frac{\partial \mathbf{A}}{\partial \mu_m})\mathbf{x}_i \tag{4.33}$$

where $\mathbf{A}^\dagger$ denotes the pseudoinverse of $\mathbf{A}$, which ignores the component of $\frac{\partial \mathbf{x}_i}{\partial \mu_m}$ in the direction of $\mathbf{x}_i$ while keeping all the components orthogonal to $\mathbf{x}_i$, i.e. $(\mathbf{A}-\lambda_i\mathbf{I})^\dagger = \sum_{j\neq i}(\lambda_j - \lambda_i)^{-1}\mathbf{x}_j\mathbf{x}_j^H$. Because of the pseudoinverse used in (4.33), we have ingored a component of $\frac{\partial \mathbf{x}_i}{\partial \mu_m}$ in the direction of $\mathbf{x}_i$ but have kept all components orthogonal to $\mathbf{x}_i$.

Now apply the second derivative of (4.30) with respect to another parameter and again multiplied by $\mathbf{x}_i^H$, we have

$$\frac{\partial^2 \lambda_i}{\partial \mu_m \partial \mu_n} = \mathbf{x}_i^H \frac{\partial^2 \mathbf{A}}{\partial \mu_m \partial \mu_n} \mathbf{x}_i + \mathbf{x}_i^H (\frac{\partial \mathbf{A}}{\partial \mu_m} - \frac{\partial \lambda_i}{\partial \mu_m} \mathbf{I}) \frac{\partial \mathbf{x}_i}{\partial \mu_n} + \mathbf{x}_i^H (\frac{\partial \mathbf{A}}{\partial \mu_n} - \frac{\partial \lambda_i}{\partial \mu_n} \mathbf{I}) \frac{\partial \mathbf{x}_i}{\partial \mu_m} \tag{4.34}$$

and

$$\frac{\partial^2 \mathbf{x}_i}{\partial \mu_m \partial \mu_n} = (\mathbf{A} - \lambda_i \mathbf{I})^\dagger (\frac{\partial^2 \lambda_i}{\partial \mu_m \partial \mu_n} \mathbf{x}_i - \frac{\partial^2 \mathbf{A}}{\partial \mu_m \partial \mu_n} + \frac{\partial \lambda_i}{\partial \mu_m} \frac{\partial \mathbf{x}_i}{\partial \mu_n} - \frac{\partial \mathbf{A}}{\partial \mu_m} \frac{\partial \mathbf{x}_i}{\partial \mu_n} \tag{4.35}$$

$$+ \frac{\partial \lambda_i}{\partial \mu_n} \frac{\partial \mathbf{x}_i}{\partial \mu_m} - \frac{\partial \mathbf{A}}{\partial \mu_n} \frac{\partial \mathbf{x}_i}{\partial \mu_m}) \tag{4.36}$$

All the first and second order derivatives are listed below:

$$\frac{\partial D(\boldsymbol{\mu})}{\partial \mu_i} = -tr\{(\mathbf{I} + \mathbf{H}\mathbf{Q}\mathbf{H}^H)^{-1} \mathbf{H} \frac{\partial \mathbf{Q}}{\partial \mu_i} \mathbf{H}^H\} + tr\{\mathbf{B}_i \mathbf{Q} \mathbf{B}_i^H\} - P_i + \sum_{j=0}^{m} (\mu_j (tr\{\mathbf{B}_j \frac{\partial \mathbf{Q}}{\partial \mu_i} \mathbf{B}_j^H\}) + \frac{1}{t} \frac{1}{\mu_j}) \tag{4.37}$$

$$\begin{aligned} \frac{\partial \mathbf{Q}}{\partial \mu_i} &= \frac{\partial}{\partial \mu_i} [\mathbf{K}^{-H} \mathbf{V}_1 (\mathbf{I} - \boldsymbol{\Lambda}_1) \mathbf{V}_1^H \mathbf{K}^{-1}] \\ &= \frac{\partial \mathbf{K}^{-1}}{\partial \mu_i} \mathbf{V}_1 (\mathbf{I} - \boldsymbol{\Lambda}_1^{-1}) \mathbf{V}_1^H \mathbf{K}^{-1} + \mathbf{K}^{-1} \frac{\partial [\mathbf{V}_1 (\mathbf{I} - \boldsymbol{\Lambda}_1^{-1}) \mathbf{V}_1^H]}{\partial \mu_i} \mathbf{K}^{-1} \\ &\quad + \mathbf{K}^{-1} \mathbf{V}_1 (\mathbf{I} - \boldsymbol{\Lambda}_1^{-1}) \mathbf{V}_1^H \frac{\partial \mathbf{K}^{-1}}{\partial \mu_i} \end{aligned} \tag{4.38}$$

$$\frac{\partial [\mathbf{V}_1 (\mathbf{I} - \boldsymbol{\Lambda}_1^{-1}) \mathbf{V}_1^H]}{\partial \mu_i} = \frac{\partial \mathbf{V}_1}{\partial \mu_i} (\mathbf{I} - \boldsymbol{\Lambda}_1^{-1}) \mathbf{V}_1^H + \mathbf{V}_1 \boldsymbol{\Lambda}_1^{-2} \frac{\partial \boldsymbol{\Lambda}_1}{\partial \mu_i} \mathbf{V}_1^H + \mathbf{V}_1 (\mathbf{I} - \boldsymbol{\Lambda}_1^{-1}) \frac{\partial \mathbf{V}_1^H}{\partial \mu_i} \tag{4.39}$$

$$\begin{aligned} \frac{\partial \mathbf{v}_n}{\partial \mu_i} &= -(\mathbf{K}^{-1} \mathbf{H}^H \mathbf{H} \mathbf{K}^{-1} - \lambda_n \mathbf{I})^\dagger (\frac{\partial \mathbf{K}^{-1}}{\partial \mu_i} \mathbf{H}^H \mathbf{H} \mathbf{K}^{-1} + \mathbf{K}^{-1} \mathbf{H}^H \mathbf{H} \frac{\partial \mathbf{K}^{-1}}{\partial \mu_i} - \frac{\partial \lambda_n}{\partial \mu_i} \mathbf{I}) \mathbf{v}_n \\ &= -(\sum_{j \neq i} (\lambda_j - \lambda_i)^{-1} \mathbf{v}_j \mathbf{v}_j^H) (\frac{\partial \mathbf{K}^{-1}}{\partial \mu_i} \mathbf{H}^H \mathbf{H} \mathbf{K}^{-1} + \mathbf{K}^{-1} \mathbf{H}^H \mathbf{H} \frac{\partial \mathbf{K}^{-1}}{\partial \mu_i}) \mathbf{v}_n \end{aligned} \tag{4.40}$$

$$\frac{\partial \lambda_n}{\partial \mu_i} = \mathbf{v}_n^H (\frac{\partial \mathbf{K}^{-1}}{\partial \mu_i} \mathbf{H}^H \mathbf{H} \mathbf{K}^{-1} + \mathbf{K}^{-1} \mathbf{H}^H \mathbf{H} \frac{\partial \mathbf{K}^{-1}}{\partial \mu_i}) \mathbf{v}_n \tag{4.41}$$

$$\frac{\partial \mathbf{K}^{-1}}{\partial \mu_i} = \frac{\partial}{\partial \mu_i} [\mathbf{E} \mathbf{\Phi}^{-1/2} \mathbf{E}^H] = \frac{\partial \mathbf{E}}{\partial \mu_i} \mathbf{\Phi}^{-1/2} \mathbf{E}^H - \frac{1}{2} \mathbf{E} \mathbf{\Phi}^{-3/2} \frac{\partial \mathbf{\Phi}}{\partial \mu_i} \mathbf{E}^H + \mathbf{E} \mathbf{\Phi}^{-1/2} \frac{\partial \mathbf{E}^H}{\partial \mu_i} \tag{4.42}$$

$$\begin{aligned} \frac{\partial \mathbf{e}_n}{\partial \mu_i} &= -(\sum_{i=0}^{m} \mu_i \mathbf{B}_i \mathbf{B}_i^H - \phi_n \mathbf{I})^\dagger (\mathbf{B}_i \mathbf{B}_i^H - \frac{\partial \phi_n}{\partial \mu_i} \mathbf{I}) \mathbf{e}_n \\ &= -(\sum_{j \neq i} (\phi_j - \phi_i)^{-1} \mathbf{e}_j \mathbf{e}_j^H)(\mathbf{B}_i \mathbf{B}_i^H - \frac{\partial \phi_n}{\partial \mu_i} \mathbf{I}) \mathbf{e}_n \\ &= -(\sum_{j \neq i} (\phi_j - \phi_i)^{-1} \mathbf{e}_j \mathbf{e}_j^H) \mathbf{B}_i \mathbf{B}_i^H \mathbf{e}_n \end{aligned} \tag{4.43}$$

$$\frac{\partial \phi_n}{\partial \mu_i} = \mathbf{e}_n^H \mathbf{B}_i \mathbf{B}_i^H \mathbf{e}_n \tag{4.44}$$

$$\begin{aligned} \frac{\partial^2 D(\boldsymbol{\mu})}{\partial \mu_i \partial \mu_j} &= tr\{(\mathbf{I} + \mathbf{H}\mathbf{Q}\mathbf{H}^H)^{-1} \mathbf{H} \frac{\partial \mathbf{Q}}{\partial \mu_i} \mathbf{H}^H (\mathbf{I} + \mathbf{H}\mathbf{Q}\mathbf{H}^H)^{-1} \mathbf{H} \frac{\partial \mathbf{Q}}{\partial \mu_j} \mathbf{H}^H\} \\ &\quad - tr\{(\mathbf{I} + \mathbf{H}\mathbf{Q}\mathbf{H}^H)^{-1} \mathbf{H} \frac{\partial^2 \mathbf{Q}}{\partial \mu_i \partial \mu_j} \mathbf{H}^H\} + tr\{\mathbf{B}_j \frac{\partial \mathbf{Q}}{\partial \mu_i} \mathbf{B}_j^H\} + tr\{\mathbf{B}_i \frac{\partial \mathbf{Q}}{\partial \mu_j} \mathbf{B}_i^H\} \\ &\quad + \sum_{k=1}^{m} \mu_k tr\{\mathbf{B}_k \frac{\partial^2 \mathbf{Q}}{\partial \mu_i \partial \mu_j} \mathbf{B}_k^H\} + \frac{1}{t} \frac{\partial 1/\mu_i}{\partial \mu_j} \end{aligned} \tag{4.45}$$

$$\frac{\partial^2 \mathbf{Q}}{\partial \mu_i \partial \mu_j} = \frac{\partial^2 \mathbf{K}^{-1}}{\partial \mu_i \partial \mu_j}\mathbf{V}_1(\mathbf{I}-\mathbf{\Lambda}_1^{-1})\mathbf{V}_1^H\mathbf{K}^{-1} + \frac{\partial \mathbf{K}^{-1}}{\partial \mu_j}\frac{\partial[\mathbf{V}_1(\mathbf{I}-\mathbf{\Lambda}_1^{-1})\mathbf{V}_1^H]}{\partial \mu_i}\mathbf{K}^{-1}$$
$$+\frac{\partial \mathbf{K}^{-1}}{\partial \mu_j}\mathbf{V}_1(\mathbf{I}-\mathbf{\Lambda}_1^{-1})\mathbf{V}_1^H\frac{\partial \mathbf{K}^{-1}}{\partial \mu_i} + \frac{\partial \mathbf{K}^{-1}}{\partial \mu_i}\frac{\partial[\mathbf{V}_1(\mathbf{I}-\mathbf{\Lambda}_1^{-1})\mathbf{V}_1^H]}{\partial \mu_j}\mathbf{K}^{-1}$$
$$+\mathbf{K}^{-1}\frac{\partial^2[\mathbf{V}_1(\mathbf{I}-\mathbf{\Lambda}_1^{-1})\mathbf{V}_1^H]}{\partial \mu_i \partial \mu_j}\mathbf{K}^{-1} + \mathbf{K}^{-1}\frac{\partial[\mathbf{V}_1(\mathbf{I}-\mathbf{\Lambda}_1^{-1})\mathbf{V}_1^H]}{\partial \mu_j}\frac{\partial \mathbf{K}^{-1}}{\partial \mu_i}$$
$$+\frac{\partial \mathbf{K}^{-1}}{\partial \mu_i}\mathbf{V}_1(\mathbf{I}-\mathbf{\Lambda}_1^{-1})\mathbf{V}_1^H\frac{\partial \mathbf{K}^{-1}}{\partial \mu_j} + \mathbf{K}^{-1}\frac{\partial[\mathbf{V}_1(\mathbf{I}-\mathbf{\Lambda}_1^{-1})\mathbf{V}_1^H]}{\partial \mu_i}\frac{\partial \mathbf{K}^{-1}}{\partial \mu_j}$$
$$+\mathbf{K}^{-1}\mathbf{V}_1(\mathbf{I}-\mathbf{\Lambda}_1^{-1})\mathbf{V}_1^H\frac{\partial^2 \mathbf{K}^{-1}}{\partial \mu_i \partial \mu_j} \tag{4.46}$$

$$\frac{\partial^2[\mathbf{V}_1(\mathbf{I}-\mathbf{\Lambda}_1^{-1})\mathbf{V}_1^H]}{\partial \mu_i \partial \mu_j} = \frac{\partial^2 \mathbf{V}_1}{\partial \mu_i \partial \mu_j}(\mathbf{I}-\mathbf{\Lambda}_1^{-1})\mathbf{V}_1^H + \frac{\partial \mathbf{V}_1}{\partial \mu_j}\mathbf{\Lambda}_1^{-2}\frac{\partial \mathbf{\Lambda}_1}{\partial \mu_i}\mathbf{V}_1^H$$
$$+\frac{\partial \mathbf{V}_1}{\partial \mu_j}(\mathbf{I}-\mathbf{\Lambda}_1^{-1})\frac{\partial \mathbf{V}_1^H}{\partial \mu_i} + \frac{\partial \mathbf{V}_1}{\partial \mu_i}\mathbf{\Lambda}_1^{-2}\frac{\partial \mathbf{\Lambda}_1}{\partial \mu_j}\mathbf{V}_1^H$$
$$-2\mathbf{V}_1\mathbf{\Lambda}_1^{-3}\frac{\partial \mathbf{\Lambda}_1}{\partial \mu_i}\frac{\partial \mathbf{\Lambda}_1}{\partial \mu_j}\mathbf{V}_1^H + \mathbf{V}_1\mathbf{\Lambda}_1^{-2}\frac{\partial^2 \mathbf{\Lambda}_1}{\partial \mu_i \partial \mu_j}\mathbf{V}_1^H$$
$$+\mathbf{V}_1\mathbf{\Lambda}_1^{-2}\frac{\partial \mathbf{\Lambda}_1}{\partial \mu_j}\frac{\partial \mathbf{V}_1^H}{\partial \mu_i} + \frac{\partial \mathbf{V}_1}{\partial \mu_i}(\mathbf{I}-\mathbf{\Lambda}_1^{-1})\frac{\partial \mathbf{V}_1^H}{\partial \mu_j}$$
$$+\mathbf{V}_1\mathbf{\Lambda}_1^{-2}\frac{\partial \mathbf{\Lambda}_1}{\partial \mu_i}\frac{\partial \mathbf{V}_1^H}{\partial \mu_j} + \mathbf{V}_1(\mathbf{I}-\mathbf{\Lambda}_1^{-1})\frac{\partial^2 \mathbf{V}_1^H}{\partial \mu_i \partial \mu_j} \tag{4.47}$$

$$\frac{\partial^2 \mathbf{K}^{-1}\mathbf{H}^H\mathbf{H}\mathbf{K}^{-1}}{\partial \mu_i \partial \mu_j} = \frac{\partial^2 \mathbf{K}^{-1}}{\partial \mu_i \partial \mu_j}\mathbf{H}^H\mathbf{H}\mathbf{K}^{-1} + \frac{\partial \mathbf{K}^{-1}}{\partial \mu_i}\mathbf{H}^H\mathbf{H}\frac{\partial \mathbf{K}^{-1}}{\partial \mu_j}$$
$$+\frac{\partial \mathbf{K}^{-1}}{\partial \mu_j}\mathbf{H}^H\mathbf{H}\frac{\partial \mathbf{K}^{-1}}{\partial \mu_i} + \mathbf{K}^{-1}\mathbf{H}^H\mathbf{H}\frac{\partial^2 \mathbf{K}^{-1}}{\partial \mu_j \partial \mu_i} \tag{4.48}$$

$$\frac{\partial^2 \mathbf{K}^{-1}}{\partial \mu_i \partial \mu_j} = \frac{\partial^2 \mathbf{E}}{\partial \mu_i \partial \mu_j}\mathbf{\Phi}^{-1/2}\mathbf{E}^H - \frac{1}{2}\frac{\partial \mathbf{E}}{\partial \mu_i}\mathbf{\Phi}^{-3/2}\frac{\partial \mathbf{\Phi}}{\partial \mu_j}\mathbf{E}^H + \frac{\partial \mathbf{E}}{\partial \mu_i}\mathbf{\Phi}^{-1/2}\frac{\partial \mathbf{E}^H}{\partial \mu_j}$$
$$-\frac{1}{2}\frac{\partial \mathbf{E}}{\partial \mu_j}\mathbf{\Phi}^{-3/2}\frac{\partial \mathbf{\Phi}}{\partial \mu_i}\mathbf{E}^H + \frac{3}{4}\mathbf{E}\mathbf{\Phi}^{-5/2}\frac{\partial \mathbf{\Phi}}{\partial \mu_i}\frac{\partial \mathbf{\Phi}}{\partial \mu_j}\mathbf{E}^H - \frac{1}{2}\mathbf{E}\mathbf{\Phi}^{-3/2}\frac{\partial^2 \mathbf{\Phi}}{\partial \mu_i \partial \mu_j}\mathbf{E}^H$$
$$-\frac{1}{2}\mathbf{E}\mathbf{\Phi}^{-3/2}\frac{\partial \mathbf{\Phi}}{\partial \mu_j}\frac{\partial \mathbf{E}^H}{\partial \mu_i} + \frac{\partial \mathbf{E}}{\partial \mu_j}\mathbf{\Phi}^{-1/2}\frac{\partial \mathbf{E}^H}{\partial \mu_i} - \frac{1}{2}\mathbf{E}\mathbf{\Phi}^{-3/2}\frac{\partial \mathbf{\Phi}}{\partial \mu_i}\frac{\partial \mathbf{E}^H}{\partial \mu_j}$$
$$+\mathbf{E}\mathbf{\Phi}^{-1/2}\frac{\partial^2 \mathbf{E}^H}{\partial \mu_i \partial \mu_j} \tag{4.49}$$

$$\frac{\partial^2 \mathbf{v}_n}{\partial \mu_i \partial \mu_j} = (\mathbf{K}^{-1}\mathbf{H}^H\mathbf{H}\mathbf{K}^{-1} - \lambda_n \mathbf{I})^\dagger(-\frac{\partial^2 \mathbf{K}^{-1}\mathbf{H}^H\mathbf{H}\mathbf{K}^{-1}}{\partial \mu_i \partial \mu_j}\mathbf{v}_n + \frac{\partial \lambda_n}{\partial \mu_i}\frac{\partial \mathbf{v}_n}{\partial \mu_j}$$
$$-\frac{\partial \mathbf{K}^{-1}\mathbf{H}^H\mathbf{H}\mathbf{K}^{-1}}{\partial \mu_i}\frac{\partial \mathbf{v}_n}{\partial \mu_j} - \frac{\partial \mathbf{K}^{-1}\mathbf{H}^H\mathbf{H}\mathbf{K}^{-1}}{\partial \mu_j}\frac{\partial \mathbf{v}_n}{\partial \mu_i} + \frac{\partial \lambda_n}{\partial \mu_j}\frac{\partial \mathbf{v}_n}{\partial \mu_i}) \tag{4.50}$$

$$\frac{\partial^2 \lambda_n}{\partial \mu_i \partial \mu_j} = \mathbf{v}_n\frac{\partial^2 \mathbf{K}^{-1}\mathbf{H}^H\mathbf{H}\mathbf{K}^{-1}}{\partial \mu_i \partial \mu_j}\mathbf{v}_n^H + \mathbf{v}_n^H(\frac{\partial \mathbf{K}^{-1}\mathbf{H}^H\mathbf{H}\mathbf{K}^{-1}}{\partial \mu_i} - \frac{\partial \lambda_n}{\partial \mu_i}\mathbf{I})\frac{\partial \mathbf{v}_n}{\partial \mu_j}$$
$$+\mathbf{v}_n^H(\frac{\partial \mathbf{K}^{-1}\mathbf{H}^H\mathbf{H}\mathbf{K}^{-1}}{\partial \mu_j} - \frac{\partial \lambda_n}{\partial \mu_j}\mathbf{I})\frac{\partial \mathbf{v}_n}{\partial \mu_i} \tag{4.51}$$

$$\frac{\partial^2 \mathbf{e}_n}{\partial \mu_i \partial \mu_j} = (\sum_{i=0}^{m}\mu_i \mathbf{B}_i\mathbf{B}_i^H - \phi_n \mathbf{I})^\dagger(\frac{\partial \phi_n}{\partial \mu_i}\frac{\partial \mathbf{e}_n}{\partial \mu_j} + \frac{\partial \phi_n}{\partial \mu_j}\frac{\partial \mathbf{e}_n}{\partial \mu_i} - \mathbf{B}_i^H\mathbf{B}_i\frac{\partial \mathbf{e}_n}{\partial \mu_j} - \mathbf{B}_j^H\mathbf{B}_j\frac{\partial \mathbf{e}_n}{\partial \mu_i}) \tag{4.52}$$

$$\frac{\partial^2 \phi_n}{\partial \mu_i \partial \mu_j} = \mathbf{e}_n^H(\mathbf{B}_i^H\mathbf{B}_i - \frac{\partial \phi_n}{\partial \mu_i}\mathbf{I})\frac{\partial \mathbf{e}_n}{\partial \mu_j} + \mathbf{e}_n^H(\mathbf{B}_j^H\mathbf{B}_j - \frac{\partial \phi_n}{\partial \mu_j}\mathbf{I})\frac{\partial \mathbf{e}_n}{\partial \mu_i} \tag{4.53}$$

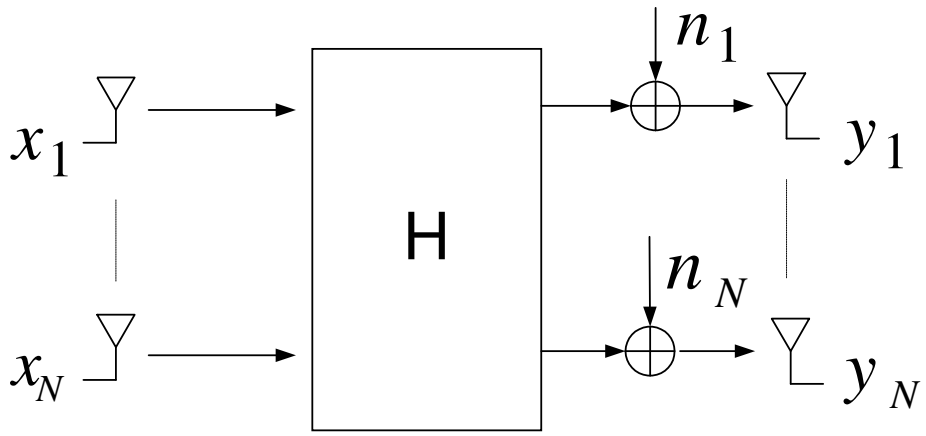

Figure 4.1: A diagram of single user MIMO system. The transmitter and the receiver are equipped with N antennas

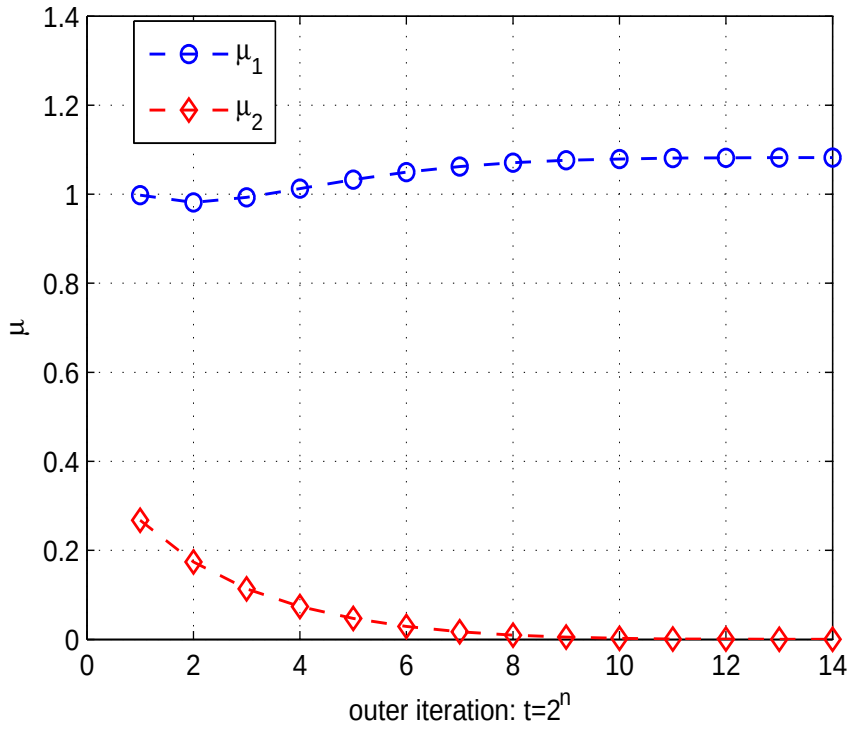

Figure 4.2: Optimal values of μ_1 and μ_2 as function of the outer loop index n in $t = 2^n$.

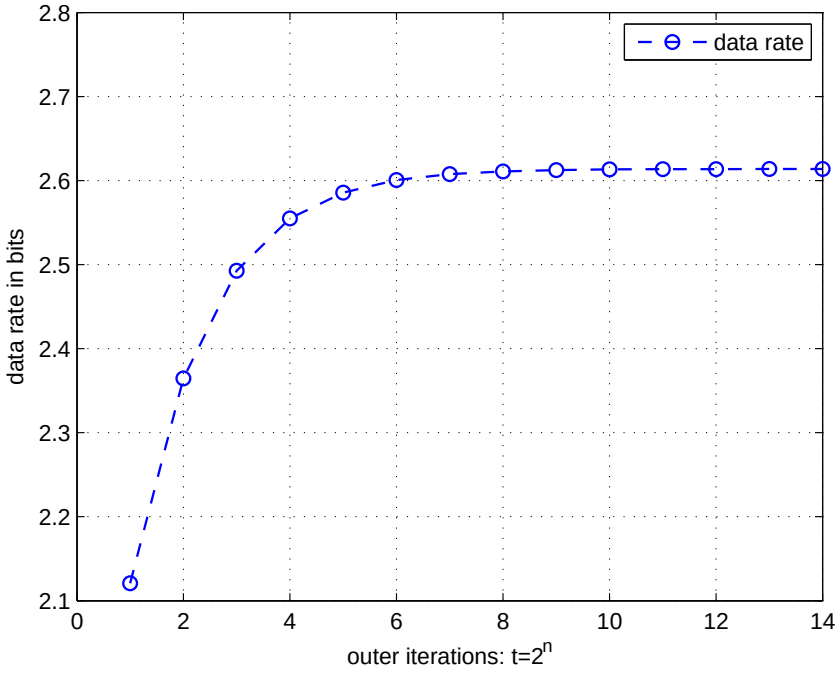

Figure 4.3: Optimal value of $-J$ (capacity) as function of the outer loop index n in $t = 2^n$.

Chapter 5

Power Allocation for a MIMO Relay System with Multiple-Antenna Users

In this chapter, we study power allocation for a multiuser MIMO wireless relay network where there is a non-regenerative relay between one access point and multiple users. Each node in the system is equipped with multiple antennas. In order to determine the source covariance matrices and the relay transformation matrix to minimize the total power consumption or maximize the total throughput of the system, the central problem is non-convex and there is no simple solution. In this chapter, we present a number of computational strategies and investigate their performances. Both uplink and downlink cases are considered. The use of multiple carriers is also discussed.

The content of this chapter is partially contained in [68].

For this problem with multiuser MIMO relay system, the diagonal structure as shown in [26], [28], [27] and [48] is no longer optimal, and the uplink-downlink duality property shown in [34] and [49] no longer applies. In order to maximize the system throughput or minimize the system power consumption, the nature of this problem is non-convex. In this chapter, we present a number of computational strategies for throughput maximization or power consumption minimization. These algorithms are summarized in Table 5.1 5.2and discussed in details in this paper. These algorithms can solve problems that are more general than those treated in [26], [28], [27], [30], [50] and [33]. In particular, for a problem as treated in [33], our approach can yield much better performance. We assume that all channel matrices are known to a central scheduler and to the transmitters and receivers if needed. Also note that except for Algorithm 1, all other algorithms in Table 5.1 5.2 are not mathematically proven to yield globally optimal results of their corresponding problems. However, Algorithm 1 solves a convex problem which is an approximation of the original problem. Because of the approximation used in the problem reformulation, there is a penalty to the performance of Algorithm 1 as shown later in Section 5.4.

In Section 5.1, we treat a multiuser MIMO relay downlink system. We present power allocation algorithms for maximizing the system throughput (i.e., sum rate) under a power constraint, and minimizing the system power consumption under individual user rate constraints. In Section 5.2, we deal with similar issues for the uplink case. In Section 5.3, we show how to apply our algorithms for multicarrier power allocation. In Section 5.4, simulations results are presented to illustrate the performances of our algorithms.

5.1 Multiuser MIMO Downlink Relay

We first consider the multiuser MIMO downlink relay system as illustrated in Fig. 5.1, where $\mathbf{x} \in \mathcal{C}^{M\times 1}$ denotes the signal transmitted from the source equipped with M antennas, $\mathbf{F} \in \mathcal{C}^{M\times M}$ the transformation matrix performed by the non-regenerative relay also equipped with M antennas, and $\mathbf{y}_i \in \mathcal{C}^{N\times 1}$ the signal received by the user i equipped with N antennas. Furthermore, $\mathbf{H} \in \mathcal{C}^{M\times M}$ denotes the channel matrix between the source and the relay, $\mathbf{H}_i \in \mathcal{C}^{N\times M}$ is the channel matrix between the relay and the user i, and $\mathbf{n}$, $\mathbf{n}_1$, $\cdots$, $\mathbf{n}_K$ are the zero-mean Gaussian noises at the relay and the K users. Here, we assume that all the users are equipped with the same number of antennas. The transmission from the source to the relay is assumed to be orthogonal (in time and/or frequency) to the transmission from the relay to all users. We also assume that the direct link between the source and any of the users is very weak and negligible.

Note that if the actual numbers of antennas at the users, relay or source are different from what is described above, we can always add imaginary dummy antennas to make up the number M or N. The effective $\mathbf{H} \in \mathcal{C}^{M\times M}$ or $\mathbf{H}_i \in \mathcal{C}^{N\times M}$ may have zero rows or zero columns, which however do not affect the expressions of our results.

The signal $\mathbf{y}$ received at the relay, the signal $\mathbf{r}$ transmitted from the relay, and the signal $\mathbf{y}_i$ received by the user i can be expressed as follows:

$$\mathbf{y} = \mathbf{H}\mathbf{x} + \mathbf{n} \tag{5.1}$$

$$\mathbf{r} = \mathbf{F}\mathbf{y} = \mathbf{F}\mathbf{H}\mathbf{x} + \mathbf{F}\mathbf{n} \tag{5.2}$$

$$\mathbf{y}_i = \mathbf{H}_i\mathbf{r} + \mathbf{n}_i = \mathbf{H}_i\mathbf{F}\mathbf{H}\mathbf{x} + \mathbf{H}_i\mathbf{F}\mathbf{n} + \mathbf{n}_i \tag{5.3}$$

Note that if $\mathbf{n}$ has a covariance matrix $\mathbf{C}_n$, we can write $\mathbf{C}_n^{-1/2}\mathbf{y} = \mathbf{C}_n^{-1/2}\mathbf{H}\mathbf{x} + \mathbf{C}_n^{-1/2}\mathbf{n}$ where the noise term $\mathbf{C}_n^{-1/2}\mathbf{n}$ has the covariance matrix equal to the identity matrix. So, provided that the noise covariance matrices of $\mathbf{n}$ and $\mathbf{n}_i$ are known, we can assume for convenience that they are the identity matrices. We now define $\mathbf{H}_c^H = [\mathbf{H}_1^H, \ldots, \mathbf{H}_K^H]$, $\mathbf{y}_c^H = [\mathbf{y}_1^H, \ldots, \mathbf{y}_K^H]$ and $\mathbf{n}_c^H = [\mathbf{n}_1^H, \ldots, \mathbf{n}_K^H]$. Then, using (5.3) for all i, we have

$$\mathbf{y}_c = \mathbf{H}_c\mathbf{F}\mathbf{H}\mathbf{x} + \mathbf{H}_c\mathbf{F}\mathbf{n} + \mathbf{n}_c \tag{5.4}$$

This is an effective channel model between the source and all users.

5.1.1 Maximization of Sum Rate under Power Constraint and ZFDPC (Algorithms 1-2)

The problem of maximizing the sum rate for all users under a power constraint for the downlink case was considered in [33] where each user has a single antenna. They also assume the use of zero forcing dirty paper coding (ZFDPC) [51] which is suboptimal compared to the exact DPC. We now extend the approach in [33] to users with multiple antennas.

Define the QR decomposition of the $KN \times M$ matrix $\mathbf{H}_c$ as $\mathbf{H}_c = \mathbf{R}\mathbf{Q}$, where $\mathbf{Q}$ is an $M \times M$ unitary matrix (which is not the same $\mathbf{Q}$ in section 4.2) and $\mathbf{R}$ is a $KN \times M$ lower triangular matrix. Define the SVD of the channel matrix $\mathbf{H}$ as $\mathbf{H} = \mathbf{U}_h\mathbf{\Sigma}_h\mathbf{V}_h^H$ where $\mathbf{\Sigma}_h = \mathbf{\Lambda}_h^{1/2} = diag(\lambda_{h,1}, \lambda_{h,2}, \ldots, \lambda_{h,N})^{1/2}$ with descending diagonal elements, and $\mathbf{U}_h$ and $\mathbf{V}_h$ are unitary.

We assume that the source precoder generates $\mathbf{x} = \mathbf{A}_x\mathbf{s}$ where $\mathbf{s}$ contains i.i.d. symbols of unit variance and $\mathbf{A}_x$ is such that the source covariance matrix is $\mathbf{\Pi}_x = E\{\mathbf{x}\mathbf{x}^H\} =$

$\mathbf{A}_x\mathbf{A}_x^H = \mathbf{V}_h\mathbf{\Lambda}_x\mathbf{V}_h^H$ with $\mathbf{\Lambda}_x = diag(\lambda_{x,1}, \lambda_{x,2}, \cdots, \lambda_{x,M})$. We also assume that the relay matrix is constructed as

$$\mathbf{F} = \mathbf{Q}^H\mathbf{\Sigma}_f\mathbf{U}_a^H, \qquad \mathbf{\Sigma}_f = \mathbf{\Lambda}_f^{1/2} = diag(\lambda_{f,1}, \lambda_{f,2}, \ldots, \lambda_{f,N})^{1/2} \tag{5.5}$$

Here, the source covariance matrix is matched to the right singular vectors of the channel matrix $\mathbf{H}$, the optimality of which for a single user relay system is shown in [27]. The relay matrix here is matched to the left singular vectors of $\mathbf{H}$ and the unitary matrix $\mathbf{Q}$ of $\mathbf{H}_c$, which is adopted only heuristically without proof of optimality. As mentioned in [33], the matrix $\mathbf{Q}$ is also affected by column permutations of $\mathbf{H}_c$, which can be further optimized. With the above structures of the precoder $\mathbf{A}_x$ and the relay matrix $\mathbf{F}$, (5.4) becomes

$$\mathbf{y}_c = \mathbf{R}\mathbf{\Sigma}_f\mathbf{\Sigma}_a\mathbf{s} + (\mathbf{R}\mathbf{\Sigma}_f\tilde{\mathbf{n}} + \mathbf{n}_c) \tag{5.6}$$

where $\tilde{\mathbf{n}} = \mathbf{U}_a^H\mathbf{n}$. Note that each element of $\mathbf{s}$ represents a scalar stream of data. Since $\mathbf{R}$ is lower triangular, it is clear from the first term of (5.6) that the interference from stream j to stream i for $j > i$ is now absent. To remove the interference from stream j to stream i for $j < i$, we can use the dirty paper coding (DPC) starting from the first stream. Then, signal to noise ratio for the ith data stream is

$$SNR_i = \frac{|R_{i,i}|^2\lambda_{f,i}\lambda_{h,i}\lambda_{x,i}}{\sum_{j=1}^{i}|R_{i,j}|^2\lambda_{f,j} + 1} \tag{5.7}$$

where $R_{i,j}$ is the (i,j)th element of $\mathbf{R}$. The above interference cancellation method based on the QR decomposition and the DPC is known as zero forcing dirty paper coding (ZFDPC) [51].

The problem of maximizing the sum rate of this downlink relay system under

ZFDPC can now be formulated as

$$\max_{\mathbf{\Lambda}_f, \mathbf{\Lambda}_x} \quad R'_{sum,d} \doteq \sum_{i}^{KN} \log_2(1 + SNR_i) \tag{5.8}$$

$$s.t. \quad tr\{\mathbf{\Lambda}_x\} \leq P_x \tag{5.9}$$

$$tr\{\mathbf{\Lambda}_f(\mathbf{\Lambda}_h\mathbf{\Lambda}_x + \mathbf{I})\} \leq P_f \tag{5.10}$$

where the power constraint (5.9) is for the source, and the power constraint (5.10) is for the relay. In [33], the problem (5.8) is solved by a geometric programming under a high SNR approximation, which will be referred to as Algorithm 1.

Next, we present an algorithm without the high-SNR assumption, referred to as Algorithm 2. We will search for $\mathbf{\Lambda}_f$ and $\mathbf{\Lambda}_x$ in an alternate fashion, where each cycle of the alternation is as follows.

Source optimization with fixed $\mathbf{\Lambda}_f$

It is easy to verify that with any fixed $\mathbf{\Lambda}_f$, the problem (5.8) is a special case of the problem (4.6) shown in Section 4.2, and hence the optimal $\mathbf{\Lambda}_x$ can be found by the GWF algorithm.

Relay optimization with fixed $\mathbf{\Lambda}_x$

With any fixed $\mathbf{\Lambda}_x$, the optimal $\mathbf{\Lambda}_f$ can be found by maximizing the following penalized function of (5.8):

$$L_1\left(\mathbf{\Lambda}_f\right) \doteq \sum_{i}^{KN} \log_2\left(1 + \frac{|R_{i,i}|^2\lambda_{f,i}\lambda_{h,i}\lambda_{x,i}}{\sum_{j=1}^{i}|R_{i,j}|^2\lambda_{f,j} + 1}\right) + \frac{1}{t}\left[\log\left(P_f - \sum_{i}\lambda_{f,i}(\lambda_{h,i}\lambda_{x,i} + 1)\right)\right] \tag{5.11}$$

where the second term is the logarithmic barrier function [47] associated with the constraint (5.10). For convenience, we will also write $L_1(\mathbf{\Lambda}_f) = L_1(\boldsymbol{\lambda}_f)$ where $\mathbf{\Lambda}_f = diag(\boldsymbol{\lambda}_f)$. The gradient of $L_1(\boldsymbol{\lambda}_f)$ with respect to $\boldsymbol{\lambda}_f$, denoted by $\nabla L_1(\boldsymbol{\lambda}_f)$, is easy to derive, which is omitted. Following the Armijo's rule [52], the search algorithm for $\boldsymbol{\lambda}_f$ is as follows:

$$\boldsymbol{\lambda}_f^{(k+1)} = \boldsymbol{\lambda}_f^{(k)} + \beta^m \nabla L_1(\boldsymbol{\lambda}_f^{(k)}) \tag{5.12}$$

where m is the smallest integer satisfying

$$L_1\left(\boldsymbol{\lambda}_f^{(k+1)}\right) - L_1\left(\boldsymbol{\lambda}_f^{(k)}\right) > \sigma\beta^m \left\|\nabla L_1(\boldsymbol{\lambda}_f^{(k)})\right\|^2 \tag{5.13}$$

$$P_f - \sum_i \lambda_{f,i}^{k+1}(\lambda_{h,i}\lambda_{x,i} + 1) > 0 \tag{5.14}$$

and $0 < \sigma < 1$ and $0 < \beta < 1$. After convergence of the above search for a fixed t, a new search is started with an increased t. When $1/t$ becomes small enough, the search for $\mathbf{\Lambda}_f$ is considered completed for the given $\mathbf{\Lambda}_x$.

5.1.2 Maximization of Sum Rate under Power Constraint and DPC (Algorithm 3)

Instead of using ZFDPC, one can use DPC [34] which is more general than ZFDPC. Given that the K users receive independent messages from the source, we can write the transmitted vector from the source as $\mathbf{x} = \mathbf{x}_1 + \cdots + \mathbf{x}_K$ and its (source) covariance matrix as $\mathbf{\Pi}_x = \mathbf{\Pi}_1 + \cdots + \mathbf{\Pi}_K$ where $\mathbf{\Pi}_i$ is the covariance matrix of the signal $\mathbf{x}_i$ meant for user i. Assuming the use of the DPC in the descending order starting from user K, i.e., the interference from user j to user i for $j > i$ is virtually absent, the achievable data rate for

user i in bits/s/Hz is given by

$$I_{d,i} = \log_2 \frac{\left|\mathbf{H}_i\mathbf{F}\mathbf{H}\left(\sum_{j=1}^{i}\mathbf{\Pi}_j\right)\mathbf{H}^H\mathbf{F}^H\mathbf{H}_i^H + \mathbf{H}_i\mathbf{F}\mathbf{F}^H\mathbf{H}_i^H + \mathbf{I}\right|}{\left|\mathbf{H}_i\mathbf{F}\mathbf{H}\left(\sum_{j=1}^{i-1}\mathbf{\Pi}_j\right)\mathbf{H}^H\mathbf{F}^H\mathbf{H}_i^H + \mathbf{H}_i\mathbf{F}\mathbf{F}^H\mathbf{H}_i^H + \mathbf{I}\right|} \tag{5.15}$$

It is useful to remark that the "precoding matrix" at the source is simply any (since it is not unique) square root of the source covariance matrix $\mathbf{\Pi}_x$. And the "postcoding" matrix at each user needs not to be explicitly given here. However, assuming Gaussian noise and Gaussian source symbols, the optimal "postcoding" matrix at each user to achieve the date rate shown in (5.15) is given by the (standard) linear minimum mean square error (LMMSE) estimation of the desired source symbols. The structure of the LMMSE estimation is not affected by DPC or SIC at the digital coding level.

Note that in the absence of total power constraint, the maximum possible data rate for user i is independent of $\mathbf{\Pi}_j$ for $j > i$ because of the DPC. We can formulate the following problem:

$$\max_{\mathbf{\Lambda}_f, \mathbf{\Lambda}_x} \qquad R_{sum,d} \doteq \sum_{i}^{KN} I_{d,i} \tag{5.16}$$

$$s.t. \qquad tr\{\mathbf{\Pi}_x\} \leq P_x \tag{5.17}$$

$$tr\{\mathbf{F}(\mathbf{H}\mathbf{\Pi}_x\mathbf{H}^H + \mathbf{I})\mathbf{F}^H\} \leq P_f \tag{5.18}$$

A joint gradient search of $\mathbf{F}$, $\mathbf{\Pi}_1$, $\cdots$, $\mathbf{\Pi}_K$ can be performed directly to maximize the following penalized function of (5.16):

$$L_2(\mathbf{F}, \mathbf{A}_1, \cdots, \mathbf{A}_K) \doteq \sum_{i}^{KN} I_{d,i} + \frac{1}{t_1}\log\left(P_x - tr\{\mathbf{\Pi}_x\}\right) + \frac{1}{t_2}\log\left(P_f - tr\{\mathbf{F}(\mathbf{H}\mathbf{\Pi}_x\mathbf{H}^H + \mathbf{I})\mathbf{F}^H\}\right) \tag{5.19}$$

where $\mathbf{A}_i$ is such that $\mathbf{\Pi}_i = \mathbf{A}_i\mathbf{A}_i^H$. We can denote all parameters in $\mathbf{F}, \mathbf{A}_1, \cdots, \mathbf{A}_K$ by a single vector $\mathbf{p}$, and the gradient of L_2 with respect to $\mathbf{p}$ by $\nabla L_2(\mathbf{p})$. Similar to the case of

(5.11), there are two loops in the search. The inner loop is for a fixed pair of (t_1, t_2) where the Armijo gradient search is conducted until the norm of $\nabla L_2(\mathbf{p})$ is small enough. The outer loop corresponds to the increase of (t_1, t_2) until they are large enough.

To show an explicit expression of $\nabla L_2(\mathbf{p})$, it suffices to derive explicit expressions of $\frac{\partial L_2}{\partial \mathbf{F}}$ and $\frac{\partial L_2}{\partial \mathbf{A}_i}$ as follows. Following the rules of matrix differentials [46], we can show

$$\frac{\partial L_2}{\partial \mathbf{F}} = \sum_i^{KN} \frac{\partial I_{d,i}}{\partial \mathbf{F}} - \frac{2}{t_2} \frac{\mathbf{F}(\mathbf{H}\mathbf{\Pi}_x\mathbf{H}^H + \mathbf{I})}{P_f - tr\{\mathbf{F}(\mathbf{H}\mathbf{\Pi}_x\mathbf{H}^H + \mathbf{I})\mathbf{F}^H\}} \tag{5.20}$$

$$\frac{\partial L_2}{\partial \mathbf{A}_i} = \sum_i^{KN} \frac{\partial I_{d,i}}{\partial \mathbf{A}_j} - \frac{2}{t_1} \frac{\mathbf{A}_j}{P_x - tr\{\mathbf{\Pi}_x\}} - \frac{2}{t_2} \frac{\mathbf{H}^H\mathbf{F}^H\mathbf{F}\mathbf{H}\mathbf{A}_j}{P_f - tr\{\mathbf{F}(\mathbf{H}\mathbf{\Pi}_x\mathbf{H}^H + \mathbf{I})\mathbf{F}^H\}} \tag{5.21}$$

where the derivative of L_2 with respect to the complex matrix $\mathbf{F}$ is defined as $\frac{\partial L_2}{\partial \mathbf{F}} = \frac{\partial L_2}{\partial Re\{\mathbf{F}\}} + j\frac{\partial L_2}{\partial Im\{\mathbf{F}\}}$, and the same applies to $\frac{\partial L_2}{\partial \mathbf{A}_j}$. To derive $\frac{\partial I_{d,i}}{\partial \mathbf{F}}$ and $\frac{\partial I_{d,i}}{\partial \mathbf{A}_j}$, we first define $\mathbf{X}_i$ and $\mathbf{Y}_i$ according to (5.15) such that $I_{d,i} = \log_2 \frac{|\mathbf{X}_i|}{|\mathbf{Y}_i|}$. Then, using $\partial \log |\mathbf{X}| = tr\{\mathbf{X}^{-1}\partial\mathbf{X}\}$ [46], we have $\partial I_{d,i} = (\log_2 e) tr\left\{\mathbf{X}_i^{-1}\partial\mathbf{X}_i - \mathbf{Y}_i^{-1}\partial\mathbf{Y}_i\right\}$. Furthermore, it follows that

$$\partial I_{d,i} = 2(\log_2 e) Re\left(tr\left\{\mathbf{H}_i^H\mathbf{X}_i^{-1}\mathbf{M}_i\partial\mathbf{F}^H - \mathbf{H}_i^H\mathbf{Y}_i^{-1}\mathbf{N}_i\partial\mathbf{F}^H\right\}\right) \tag{5.22}$$

where $\mathbf{M}_i = \mathbf{H}_i\mathbf{F}\mathbf{H}\left(\sum_{j=1}^{i}\mathbf{\Pi}_j\right)\mathbf{H}^H + \mathbf{H}_i\mathbf{F}$ and $\mathbf{N}_i = \mathbf{H}_i\mathbf{F}\mathbf{H}\left(\sum_{j=1}^{i-1}\mathbf{\Pi}_j\right)\mathbf{H}^H + \mathbf{H}_i\mathbf{F}$, and therefore

$$\frac{\partial I_{d,i}}{\partial \mathbf{F}} = 2(\log_2 e)\left(\mathbf{H}_i^H\mathbf{X}_i^{-1}\mathbf{M}_i - \mathbf{H}_i^H\mathbf{Y}_i^{-1}\mathbf{N}_i\right) \tag{5.23}$$

Similarly, one can verify that for $j \leq i-1$,

$$\frac{\partial I_{d,i}}{\partial \mathbf{A}_j} = 2(\log_2 e)\left(\mathbf{H}^H\mathbf{F}^H\mathbf{H}_i^H\left(\mathbf{X}_i^{-1} - \mathbf{Y}_i^{-1}\right)\mathbf{H}_i\mathbf{F}\mathbf{H}\mathbf{A}_j\right) \tag{5.24}$$

and for $j = i$, $\frac{\partial I_{d,i}}{\partial \mathbf{A}_j} = 2(\log_2 e)\left(\mathbf{H}^H\mathbf{F}^H\mathbf{H}_i^H\mathbf{X}_i^{-1}\mathbf{H}_i\mathbf{F}\mathbf{H}\mathbf{A}_j\right)$, and for $j > i$, $\frac{\partial I_{d,i}}{\partial \mathbf{A}_j} = 0$. The above algorithm is referred to as Algorithm 3.

5.1.3 Minimization of Power under Rate Constraint (Algorithms 4-5)

We now address minimization of power under rate constraint. The total power consumed by the source and the relay is

$$P_d \doteq tr\{\mathbf{\Pi}_x\} + tr\left\{\mathbf{F}\left(\mathbf{H}\mathbf{\Pi}_x\mathbf{H}^H + \mathbf{I}\right)\mathbf{F}^H\right\} \tag{5.25}$$

Our problem now is to minimize the total power consumption subject to rate constraints:

$$\min_{\mathbf{F},\mathbf{\Pi}_1,\cdots,\mathbf{\Pi}_K} P_d \tag{5.26}$$

$$\text{subject to} \qquad I_{d,i} \geq R_i \ \forall i \in \{1, 2, \cdots, K\} \tag{5.27}$$

where R_i is a desired data rate for user i in bits/s/Hz. To solve this problem, we can search for the optimal relay matrix $\mathbf{F}$ and the optimal source covariance matrices $\mathbf{\Pi}_1, \cdots, \mathbf{\Pi}_K$ in an alternate fashion, where each cycle of the alternation is shown below.

Source optimization with fixed F

We now assume a fixed $\mathbf{F}$ and present an algorithm for computing the optimal $\mathbf{\Pi}_1, \cdots, \mathbf{\Pi}_K$. We will use the property that $I_{d,i}$ is independent of $\mathbf{\Pi}_{i+1}, \cdots, \mathbf{\Pi}_K$ and is a concave function of $\mathbf{\Pi}_i$, and P is a linear function of $\mathbf{\Pi}_1, \cdots, \mathbf{\Pi}_K$. It follows from (5.25) that

$$P_d = \sum_{i=1}^{K} tr\{\mathbf{Q}_i\} + tr\left\{\mathbf{F}\mathbf{F}^H\right\} \tag{5.28}$$

where $\mathbf{Q}_i = (\mathbf{I} + \mathbf{H}^H\mathbf{F}^H\mathbf{F}\mathbf{H})^{H/2}\mathbf{\Pi}_i(\mathbf{I} + \mathbf{H}^H\mathbf{F}^H\mathbf{F}\mathbf{H})^{1/2}$, and we have applied $tr(\mathbf{AB}) = tr(\mathbf{BA})$. Clearly, $\mathbf{Q}_i$ and $\mathbf{\Pi}_i$ are one-to-one mappings of each other. We now define

$$\mathbf{G}_i = \mathbf{H}_i\mathbf{F}\mathbf{H}\left(\mathbf{I} + \mathbf{H}^H\mathbf{F}^H\mathbf{F}\mathbf{H}\right)^{-H/2} \tag{5.29}$$

$$\mathbf{S}_i = \mathbf{G}_i^H\left(\mathbf{G}_i\sum_{j=1}^{i-1}\mathbf{Q}_j\mathbf{G}_i^H + \mathbf{H}_i\mathbf{F}\mathbf{F}^H\mathbf{H}_i^H + \mathbf{I}\right)^{-1}\mathbf{G}_i \tag{5.30}$$

where $\mathbf{S}_i$ depends on $\mathbf{Q}_1, \cdots, \mathbf{Q}_{i-1}$ but not any of $\mathbf{Q}_i, \cdots, \mathbf{Q}_K$. Then, it follows from (5.15) that

$$I_{d,i} = \log_2|\mathbf{S}_i\mathbf{Q}_i + \mathbf{I}| \tag{5.31}$$

where we have applied $\log|\mathbf{AB} + \mathbf{I}| = \log|\mathbf{BA} + \mathbf{I}|$ with $\mathbf{AB}$ being conjugate symmetric.

Based on (5.28) and (5.31), the optimal solution to the problem (5.26) for $\mathbf{Q}_i$, conditional upon $\mathbf{F}, \mathbf{Q}_1, \cdots, \mathbf{Q}_{i-1}$, is given by the standard water filling solution. Namely, if the eigenvalue decomposition of $\mathbf{S}_i$ is denoted by $\mathbf{S}_i = \sum_{l=1}^{r}\lambda_{i,l}\mathbf{u}_{i,l}\mathbf{u}_{i,l}^H$ where $\lambda_{i,l} > 0$, then the optimal choice of $\mathbf{Q}_i$ is $\mathbf{Q}_i = \sum_{l=1}^{r}(v_i - \frac{1}{\lambda_{i,l}})^+\mathbf{u}_{i,l}\mathbf{u}_{i,l}^H$ where $(x)^+ = \max(x, 0)$ and v_i is such that $I_{d,i} = R_i$. (Note: In order to keep the solution inside the interior feasible region to ensure a good convergence behavior, we should choose $I_{d,i}$ slightly larger than R_i.) Furthermore, with a fixed $\mathbf{F}$, the optimal solution for $\mathbf{Q}_1, \cdots, \mathbf{Q}_K$ (and hence $\mathbf{\Pi}_1, \cdots, \mathbf{\Pi}_K$) can be obtained one at a time sequentially by starting with $\mathbf{\Pi}_1$.

Relay optimization with fixed $\mathbf{\Pi}_1, \cdots, \mathbf{\Pi}_K$

We now assume that $\mathbf{\Pi}_1, \cdots, \mathbf{\Pi}_K$ are fixed. To find the optimal $\mathbf{F}$, we can use the gradient method to minimize the following penalized cost of (5.26):

$$L_3 = P_d - \frac{1}{t}\sum_i \log(I_{d,i} - R_i) \tag{5.32}$$

where the second term is the barrier, and both P_d and $I_{d,i}$ are functions of $\mathbf{F}$. With the gradient $\frac{\partial L_3}{\partial \mathbf{F}}$, also denoted by $\nabla L_3(\mathbf{F})$, the Armijo search algorithm for the optimal $\mathbf{F}$ is $\mathbf{F}^{(k+1)} = \mathbf{F}^{(k)} - \beta^m \nabla L_3(\mathbf{F}^k)$ where m is the smallest integer such that $L_3(\mathbf{F}^{(k)}) - L_3\left(\mathbf{F}^{(k+1)}\right) > \sigma\beta^m \|\nabla L_3(\mathbf{F}^k)\|^2$ and $I_{d,i}\left(\mathbf{F}^{(k+1)}\right) - R_i > 0$, $\forall i \in \{1, \ldots, K\}$ where $0 < \beta < 1$ and $0 < \sigma < 1$. Note that the second condition $I_{d,i}\left(\mathbf{F}^{(k+1)}\right) - R_i > 0$ is important to ensure that none of the rate constraints is violated. In fact, for good convergence behavior, for both the source optimization and the relay optimization, we need to keep $\mathbf{F}, \mathbf{\Pi}_1, \cdots, \mathbf{\Pi}_K$ strictly inside the interior feasible region of the problem.

The above algorithm for power minimization is referred to as Algorithm 4. Alternatively, we can solve the problem (5.26) by a joint gradient search similar to Algorithm 3, which will be referred to as Algorithm 5.

5.2 Multiuser MIMO Uplink Relay

A multiuser MIMO uplink relay system is illustrated in Fig. 5.2, where we denote by $\mathbf{H}_i^H \in \mathcal{C}^{M \times N}$ the channel matrix from user i to the relay, and by $\mathbf{H}^H \in \mathcal{C}^{M \times M}$ the channel matrix from the relay to the access point. Then, we write the received signal at relay as

$$\mathbf{y}_r = \sum_{i=1}^{K} \mathbf{H}_i^H \mathbf{x}_i + \mathbf{n}_r \tag{5.33}$$

where $\mathbf{x}_i$ is the signal transmitted from user i, and $\mathbf{n}_r$ is the white Gaussian noise at the relay. The signal transmitted from the relay is

$$\mathbf{r} = \mathbf{F}^H \mathbf{y}_r \tag{5.34}$$

where $\mathbf{F}^H$ is the relay matrix. The signal received at the access point is

$$\begin{aligned} \mathbf{y}_u &= \mathbf{H}^H\mathbf{r} + \mathbf{n}_u \\ &= \mathbf{H}^H\mathbf{F}^H \sum_{i=1}^{K} \mathbf{H}_i^H \mathbf{x}_i + \mathbf{H}^H\mathbf{F}^H\mathbf{n}_r + \mathbf{n}_u \end{aligned} \tag{5.35}$$

where $\mathbf{n}_u$ is the white Gaussian noise at the access point. We assume the use of successive interference cancellation (SIC) at the access point, starting from user K. This means that the interference from user i to user k for $i > k$ is virtually absent, and hence the achievable data rate for user k is

$$I_{u,k} = \log_2 \frac{\left|\mathbf{H}^H\mathbf{F}^H \left(\sum_{i=1}^{k} \mathbf{H}_i^H \mathbf{\Pi}_i \mathbf{H}_i\right) \mathbf{F}\mathbf{H} + \mathbf{H}^H\mathbf{F}^H\mathbf{F}\mathbf{H} + \mathbf{I}\right|}{\left|\mathbf{H}^H\mathbf{F}^H \left(\sum_{i=1}^{k-1} \mathbf{H}_i^H \mathbf{\Pi}_i \mathbf{H}_i\right) \mathbf{F}\mathbf{H} + \mathbf{H}^H\mathbf{F}^H\mathbf{F}\mathbf{H} + \mathbf{I}\right|} \tag{5.36}$$

where $\mathbf{\Pi}_i = E\{\mathbf{x}_i\mathbf{x}_i^H\}$.

5.2.1 Maximization of Sum Rate under Power Constraint (Algorithms 6-7)

The problem of maximizing the sum rate from all users under power constraints is formulated as follows:

$$\max_{\mathbf{F},\mathbf{\Pi}_1,\cdots,\mathbf{\Pi}_K} \quad R_{sum,u} = \sum_{i=1}^{K} I_{u,i} = \log_2 \frac{\left|\mathbf{H}^H\mathbf{F}^H \left(\sum_{i=1}^{K} \mathbf{H}_i^H \mathbf{\Pi}_i \mathbf{H}_i\right) \mathbf{F}\mathbf{H} + \mathbf{H}^H\mathbf{F}^H\mathbf{F}\mathbf{H} + \mathbf{I}\right|}{|\mathbf{H}^H\mathbf{F}^H\mathbf{F}\mathbf{H} + \mathbf{I}|} \tag{5.37}$$

$$s.t. \quad tr\{\mathbf{\Pi}_i\} \le P_i, \forall i \in \{1, 2, \cdots, K\} \tag{5.38}$$

$$tr\left\{\mathbf{F}^H \left(\sum_{i=1}^{K} \mathbf{H}_i^H \mathbf{\Pi}_i \mathbf{H}_i + \mathbf{I}\right) \mathbf{F}\right\} \le P_f \tag{5.39}$$

Note that the sum rate of the uplink case is independent of the order of SIC, which is unlike the sum rate of the downlink case with DPC. To solve this problem, we can optimize each of $\mathbf{F}, \mathbf{\Pi}_1, \cdots, \mathbf{\Pi}_K$ in a cyclic fashion. The basic components in each cycle are shown below.

Source optimization with fixed relay and other sources

If all $\mathbf{F}, \mathbf{\Pi}_1, \cdots, \mathbf{\Pi}_K$, but $\mathbf{\Pi}_i$, are fixed, we can define $c = \log_2 |\mathbf{H}^H \mathbf{F}^H \mathbf{F} \mathbf{H} + \mathbf{I}|$ and

$$\mathbf{G}_i = \mathbf{H}^H \mathbf{F}^H \left(\sum_{j=1, j \neq i}^{K} \mathbf{H}_j^H \mathbf{\Pi}_j \mathbf{H}_j \right) \mathbf{F} \mathbf{H} + \mathbf{H}^H \mathbf{F}^H \mathbf{F} \mathbf{H} + \mathbf{I}$$

which are independent of $\mathbf{\Pi}_i$. Then, we can write

$$\begin{aligned} R_{sum,u} &= \log_2 \left| \mathbf{G}_i + \mathbf{H}^H \mathbf{F}^H \mathbf{H}_i^H \mathbf{\Pi}_i \mathbf{H}_i \mathbf{F} \mathbf{H} \right| - c \\ &= \log_2 \left| \mathbf{I} + \mathbf{G}_i^{-1/2} \mathbf{H}^H \mathbf{F}^H \mathbf{H}_i^H \mathbf{\Pi}_i \mathbf{H}_i \mathbf{F} \mathbf{H} \mathbf{G}_i^{-H/2} \right| + \log_2 |\mathbf{G}_i| - c \end{aligned} \tag{5.40}$$

The power constraint (5.39) is equivalent to

$$tr \left\{ \mathbf{F}^H \mathbf{H}_i^H \mathbf{\Pi}_i \mathbf{H}_i \mathbf{F} \right\} \leq P_f - tr \left\{ \mathbf{F}^H \left(\sum_{j=1, j \neq i}^{K} \mathbf{H}_j^H \mathbf{\Pi}_j \mathbf{H}_j + \mathbf{I} \right) \mathbf{F} \right\}$$

It should be clear now that with respect to $\mathbf{\Pi}_i$ alone, the problem (5.37) is equivalent to the convex problem (4.6) which is solvable by the GWF algorithm.

Relay optimization with fixed sources

If $\mathbf{\Pi}_1, \cdots, \mathbf{\Pi}_K$ are fixed, then the problem (5.37) with respect to $\mathbf{F}$ alone is similar to a problem solved in [27], the solution of which is stated below. Define the SVD of $\mathbf{H}$ as $\mathbf{H} = \mathbf{U}_h \mathbf{\Sigma}_h \mathbf{V}_h^H$ where $\mathbf{\Sigma}_h = diag(\sigma_1, \cdots, \sigma_M)$ with descending diagonal order, and the EVD of $\mathbf{R} = \sum_{i=1}^{K} \mathbf{H}_i^H \mathbf{\Pi}_i \mathbf{H}_i$ as $\mathbf{R} = \mathbf{E}_r \mathbf{\Lambda}_r \mathbf{E}_r^H$ where $\mathbf{\Lambda}_r = diag(\lambda_1, \cdots, \lambda_M)$ with descending diagonal order. Then, the optimal structure of $\mathbf{F}$ is given by

$$\mathbf{F} = \mathbf{E}_r \mathbf{\Sigma}_f \mathbf{U}_h^H \tag{5.41}$$

where $\mathbf{\Sigma}_f = diag(f_1, \ldots, f_M)^{1/2} \geq 0$ which are to be determined. With (5.41), the problem (5.37) becomes

$$\begin{aligned} \max_{f_1,\cdots,f_M} \quad & R_{sum,u} = \sum_{i=1}^{M} \log_2 \frac{\sigma_i^2 \lambda_i f_i + \sigma_i^2 f_i + 1}{\sigma_i^2 f_i + 1} \\ s.t. \quad & \sum_{i=1}^{M} (\lambda_i + 1) f_i \leq P_f \text{ and } f_i \geq 0 \ \forall i \end{aligned} \tag{5.42}$$

Then, by the KKT method [47], we have

$$f_i = \frac{1}{2\sigma_i^2(1+\lambda_i)} \left[\sqrt{\lambda_i^2 + 4\lambda_i \sigma_i^2 \mu} - \lambda_i - 2 \right]^+ \tag{5.43}$$

where μ is such that

$$\sum_{i=1}^{M} \frac{1}{2\sigma_i^2} \left[\sqrt{\lambda_i^2 + 4\lambda_i \sigma_i^2 \mu} - \lambda_i - 2 \right]^+ = P_f.$$

The above algorithm that searches for $\mathbf{F}, \mathbf{\Pi}_1, \cdots, \mathbf{\Pi}_K$ in a cyclic fashion is referred to as Algorithm 6. Note that each component in Algorithm 6 is a convex optimization. Alternatively, we can solve the problem (5.37) by a joint gradient search over $\mathbf{F}, \mathbf{\Pi}_1, \cdots, \mathbf{\Pi}_K$ simultaneously, which will be referred to as Algorithm 7. The details of Algorithm 7 are omitted because of its similarity to other joint gradient search algorithms.

5.2.2 Minimization of Power under Rate Constraint (Algorithms 8-9)

The total power consumption for the uplink case is:

$$P_u = \sum_{i=1}^{K} tr\{\mathbf{\Pi}_i\} + tr\left\{ \mathbf{F}^H \left(\sum_{i=1}^{K} \mathbf{H}_i^H \mathbf{\Pi}_i \mathbf{H}_i + \mathbf{I} \right) \mathbf{F} \right\} \tag{5.44}$$

With the assumption of SIC, the individual rate $I_{u,i}$ for user i is given by (5.36). Hence, the problem is formulated as:

$$\min_{\mathbf{F},\mathbf{\Pi}_1,\cdots,\mathbf{\Pi}_K} P_u \tag{5.45}$$

$$s.t. \qquad I_{u,i} \geq R_i, \qquad \forall i \in \{1,2,\ldots K\} \tag{5.46}$$

The problem (5.45) can be solved by a joint gradient search algorithm (Algorithm 9) which is omitted, or an alternate optimization algorithm (Algorithm 8) as shown below.

Source optimization with fixed relay

Since the order of the SIC is from K to 1, $I_{u,i}$ is independent of $\mathbf{\Pi}_{i+1},\ldots,\mathbf{\Pi}_K$, which is a property also shared in the downlink case. With fixed $\mathbf{F},\mathbf{\Pi}_1,\cdots,\mathbf{\Pi}_{i-1}$, the optimal $\mathbf{\Pi}_i$ can be found by a convex optimization same as in section 5.1.3.

Relay optimization with fixed sources

Given $\mathbf{\Pi}_1,\cdots,\mathbf{\Pi}_K$, the optimal $\mathbf{F}$ can be found by the following gradient method. Define the following cost with a barrier:

$$L_4 = tr\left\{\mathbf{F}^H\left(\sum_{i=1}^{K}\mathbf{H}_i^H\mathbf{\Pi}_i\mathbf{H}_i+\mathbf{I}\right)\mathbf{F}\right\} - \frac{1}{t}\sum_i \log(I_{u,i}-R_i) \tag{5.47}$$

It follows that

$$\frac{\partial L_4}{\partial \mathbf{F}} = 2\left(\sum_{i=1}^{K}\mathbf{H}_i^H\mathbf{\Pi}_i\mathbf{H}_i+\mathbf{I}\right)\mathbf{F} - \frac{1}{t}\sum_i \frac{1}{I_{u,i}-R_i}\frac{\partial I_{u,i}}{\partial \mathbf{F}} \tag{5.48}$$

To derive $\frac{\partial I_{u,i}}{\partial \mathbf{F}}$, we first rewrite (5.36) as $I_{u,i} = \log_2 \frac{|\mathbf{W}_i|}{|\mathbf{W}_{i-1}|}$. Similar to the derivation of (5.23), it can be shown that

$$\frac{\partial I_{u,i}}{\partial \mathbf{F}} = 2(\log_2 e)\left(\mathbf{C}_i\mathbf{W}_i^{-1}\mathbf{H}^H - \mathbf{C}_{i-1}\mathbf{W}_{i-1}^{-1}\mathbf{H}^H\right) \tag{5.49}$$

where $\mathbf{C}_i = \left(\mathbf{I} + \sum_{j=1}^{k} \mathbf{H}_j^H \mathbf{\Pi}_j \mathbf{H}_j\right) \mathbf{FH}$. The rest of the algorithm is the same as in section 5.1.3.

5.3 Multi-Carrier Extensions

In the previous sections, we have assumed that there is a single carrier for power allocation. If one wants to use M_c (orthogonal) carriers for joint power allocation, the previously shown algorithms are also applicable after the following changes of notations are adopted.

For the downlink case, the signal models shown in (5.1)-(5.3) hold except that

$$\mathbf{x} = [\mathbf{x}(1)^T, \cdots, \mathbf{x}(M_c)^T]^T \in \mathcal{C}^{MM_c \times 1} \tag{5.50}$$

$$\mathbf{y} = [\mathbf{y}(1)^T, \cdots, \mathbf{y}(M_c)^T]^T \in \mathcal{C}^{MM_c \times 1} \tag{5.51}$$

$$\mathbf{n} = [\mathbf{n}(1)^T, \cdots, \mathbf{n}(M_c)^T]^T \in \mathcal{C}^{MM_c \times 1} \tag{5.52}$$

$$\mathbf{H} = diag[\mathbf{H}(1), \cdots, \mathbf{H}(M_c)] \in \mathcal{C}^{MM_c \times MM_c} \tag{5.53}$$

$$\mathbf{r} = [\mathbf{r}(1)^T, \cdots, \mathbf{r}(M_c)^T]^T \in \mathcal{C}^{MM_c \times 1} \tag{5.54}$$

$$\mathbf{y}_i = [\mathbf{y}_i(1)^T, \cdots, \mathbf{y}_i(M_c)^T]^T \in \mathcal{C}^{NM_c \times 1} \tag{5.55}$$

$$\mathbf{n}_i = [\mathbf{n}_i(1)^T, \cdots, \mathbf{n}_i(M_c)^T]^T \in \mathcal{C}^{NM_c \times 1} \tag{5.56}$$

$$\mathbf{H}_i = diag[\mathbf{H}_i(1), \cdots, \mathbf{H}_i(M_c)] \in \mathcal{C}^{NM_c \times MM_c} \tag{5.57}$$

and $\mathbf{F} \in \mathcal{C}^{MM_c \times MM_c}$, where for example $\mathbf{x}(m)$ denotes the signal transmitted from the access point on the mth carrier. Note that the optimal $\mathbf{F}$ is not necessarily block diagonal. In other words, the relay may use a different carrier to forward a stream of data that was received by the relay on another carrier [50]. Good (if not globally optimal) choices of $\mathbf{F}$

along with the source covariance matrices at all carriers can be determined by any of the power allocation algorithms. For the uplink case, the signal models shown in (5.33)-(5.35) also hold after a similar change of definitions of the notations.

These notational changes do not affect any of the algorithms shown in this chapter as long as the power of interest is a sum over all carriers and the rate of interest is also a sum over all carriers. However, the complexity of these algorithms will increase because of the increased dimensions.

5.4 Simulation Results

For convenience of reference, all algorithms presented in Sections 5.1 and 5.2 are summarized in Table 5.1,5.2. For the simulation examples shown below, a sample set of computational times of all algorithms for a random channel realization and a random initialization are listed in the last line in Table 5.1,5.2. All algorithms have roughly the same speed except Algorithm 1 which uses CVX and is much slower than others for a single run. Algorithm 1 uses geometric programming as proposed in [33], for which the GWF is not applicable. However, unlike other algorithms, Algorithm 1 is globally convergent and needs no multiple runs associated with multiple initializations. When multiple runs are considered for other algorithms, they may become effectively slower than Algorithm 1. However, one can use the result from Algorithm 1 (for down link only) as an initialization for Algorithm 2 for a new research, which will be further discussed later.

Next, we show simulation examples to compare these algorithms. We assume that there are two users $K = 2$, each user is equipped with two antennas $N = 2$, the relay and the

Table 5.1: Summary of power scheduling algorithms for a multiuser MIMO relay system

	Alg. 1	Alg. 2	Alg. 3	Alg. 4	Alg. 5
Section No.	5.1.1	5.1.1	5.1.2	5.1.3	5.1.3
Downlink	✓	✓	✓	✓	✓
Uplink					
Max Rate	✓	✓	✓		
Min Power				✓	✓
ZFDPC	✓	✓			
DPC			✓	✓	✓
SIC					
Cyclic Search		✓		✓	
Joint Search	✓		✓		✓
Use of GWF		✓			
Sample Run Time in Sec	17.10	5.12	4.38	7.44	6.32

Table 5.2: Summary of power scheduling algorithms for a multiuser MIMO relay system

	Alg. 6	Alg. 7	Alg. 8	Alg. 9
Section No.	5.2.1	5.2.1	5.2.2	5.2.2
Downlink				
Uplink	✓	✓	✓	✓
Max Rate	✓	✓		
Min Power			✓	✓
ZFDPC				
DPC				
SIC	✓	✓	✓	✓
Cyclic Search	✓		✓	
Joint Search		✓		✓
Use of GWF	✓			
Sample Run Time in Sec	8.15	6.91	4.18	3.92

access point are both equipped with four antennas $M = 4$. A single carrier is assumed. Each of the channel parameters is realized independently using a complex Gaussian distribution with zero mean and unit variance. As assumed throughout this paper, every entry of the noise vectors has zero mean and unit variance. The performance in terms of either the sum rate or the total power is based on an average over 50 channel realizations. Unless mentioned otherwise, the search conducted by each algorithm (except Algorithm 1 which is globally convergent) was initialized randomly, 20 random initializations were chosen for each realization of channel matrices, and the best result from the 20 initializations were selected for computing the performance. We have found that the performance difference between the "best" and "worst" from 20 initializations can be up to 20%. In general, the more initializations are used, the better is the chance the optimal solution is found. But the computational cost increases as the number of initialization increases.

Figure 5.3 compares the averaged sum rates achieved by the downlink Algorithms 1-3 versus the relay power P_f. The power at the source is fixed at $P_x = 1$. Algorithm 1 is based on the geometric programming proposed in [33]. Both Algorithms 1-2 are based on ZFDPC while Algorithm 3 is based on DPC. For Algorithm 2, there are two curves in this figure. For the lower curve, we used the results from Algorithm 1 as initializations for Algorithm 2. For the upper curve, we used random initializations. We see that except for the region of small relay power, Algorithm 1 yielded the least sum rate among the three algorithms while Algorithm 3 yielded the largest sum rate. In theory, Algorithm 3 should yield the largest sum rate for the entire region of relay power if a global optimum (including the optimal ordering of the DPC) is achieved. This figure suggests that in the small relay

power region, Algorithm 3 was trapped in unfavorable local minima. Since ZFDPC and DPC are different coding schemes, the results from Algorithms 1-2 cannot unfortunately be used as good initializations for Algorithm 3. The complexity of DPC is much more complex than that of ZFDPC.

Figure 5.4 compares the averaged total power consumptions required by the downlink Algorithms 4-5 versus individual rate constraint. Also shown in this figure is the power consumption based on the identity relay matrix, i.e., $\mathbf{F} = \mathbf{I}$, while the source covariance matrix is optimized by the source optimization subroutine in Algorithm 4. Algorithm 4 uses cyclic search while Algorithm 5 uses joint gradient search. The search directions for cyclic search are more limited than the joint gradient search. We see that when the date rate is high, the difference of power consumptions is very large. The power consumption from Algorithm 5 is the least, i.e., the best.

Figure 5.5 compares the averaged sum rates achieved by the uplink Algorithms 6-7 versus the power constraint at the relay. The source power is fixed at $P_i = 1$ for all i. It turns out that the two algorithms yield the same results. The relay optimization and the source optimization in Algorithm 6 (which is cyclic) are both convex, and Algorithm 7 uses the joint gradient search. The lower curve in this figure is based on the identity relay matrix, i.e., $\mathbf{F} = \mathbf{I}$, while the source covariance matrices of all users are optimized by the source optimization subroutine in Algorithm 6.

Figure 5.6 compares the averaged total power consumptions required by the uplink Algorithms 8-9 versus a common data rate of all users. Also shown in this figure is a curve based on the identify relay matrix, i.e., $\mathbf{F} = \mathbf{I}$, while the source covariance matrices of all

users are optimized by the source optimization subroutine in Algorithm 8. In this case, the joint gradient search by Algorithm 9 yields better results than the cyclic search by Algorithm 8.

Finally, Figure 5.7 illustrates an effect of joint multi-carrier power allocation. Here, the relay system is for downlink, there are two users $K = 2$ each with two antennas $N = 2$, there are four antennas $M = 4$ at the relay and the access point, and there are two carriers $M_c = 2$. For each of the two carriers, an independent channel realization was made. The first top curve is the sum rate over two users and two carriers, which was obtained by the joint multi-carrier power allocation. The second top curve is the sum rate over two users and two carriers, which was obtained by two separate single-carrier power allocations. The bottom two curves are the sum rates each summed over the two users for carrier 1 and carrier 2, respectively. The total power for the two carriers used for the first curve is twice that for each carrier used for the other curves. The power per carrier is the same for all curves. We see that there is an improvement of the sum rate by using joint multi-carrier power allocation, which is expected. However, the improvement is not large. It is known that the distribution of the singular values of a matrix of independent Gaussian random variables hardens (becomes invariant) as the dimension of the matrix increases. Hence, if the number of antennas at each node becomes large, the improvement from the joint multi-carrier power allocation is expected to disappear.

5.5 Summary

In this chapter, we have developed several computational strategies for a multiuser MIMO relay system where each node can be equipped with multiple antennas. The complexities of these algorithms are about the same, but their performances can be very much different. Although the central problem is non-convex, the joint gradient search for the relay matrix and the source covariance matrices, with multiple random initializations, has consistently yielded the best result. The use of logarithmic barrier functions, which is a key approach of the interior-point optimization methods, has been very effective for constrained optimizations. For one case, the cyclic (or alternating) search for the relay matrix and the source covariance matrices yielded similar results as the joint gradient search. For applications with realistic coding methods, the rate-versus-power model of each link may need to be revised with simple penalty factors while the power allocation algorithms shown in this paper are still applicable.

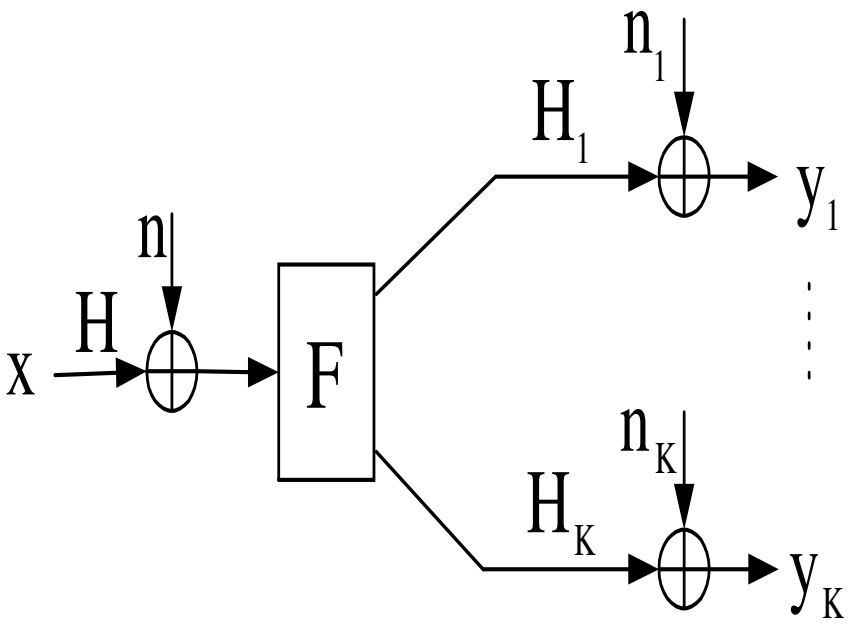

Figure 5.1: Diagram of a multiuser MIMO relay downlink system.

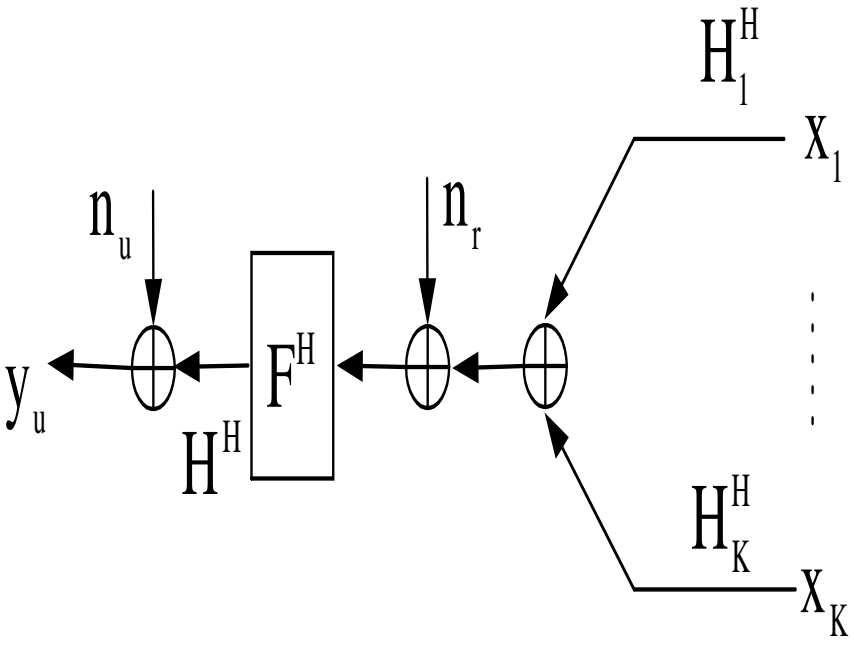

Figure 5.2: Diagram of a multiuser MIMO relay uplink system.

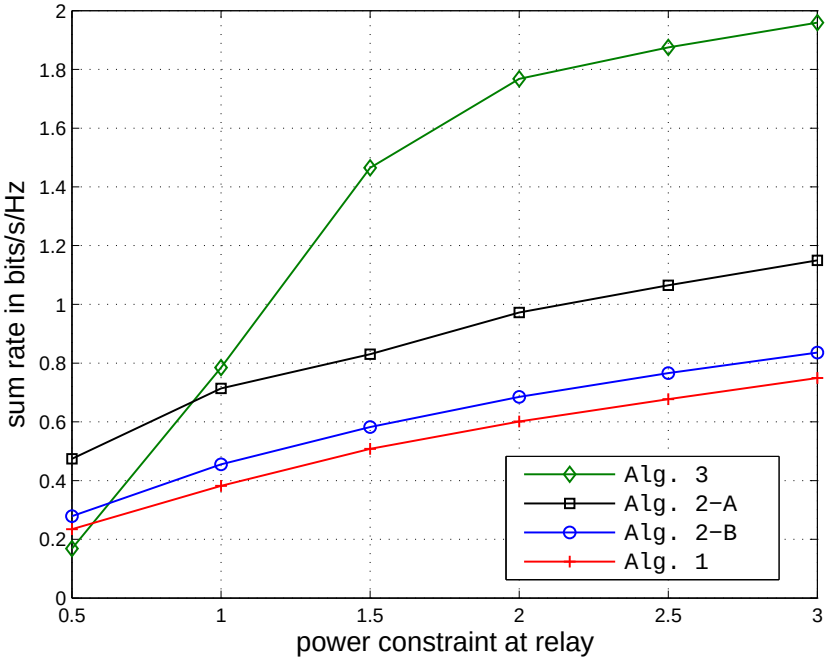

Figure 5.3: Comparison of downlink Algorithms 1-3: Averaged sum rate versus power constraint at relay. Alg. 2-A is Algorithm 2 using the best out of 20 random initializations. Alg. 2-B is Algorithm 2 using the results from Algorithm 1 as initializations.

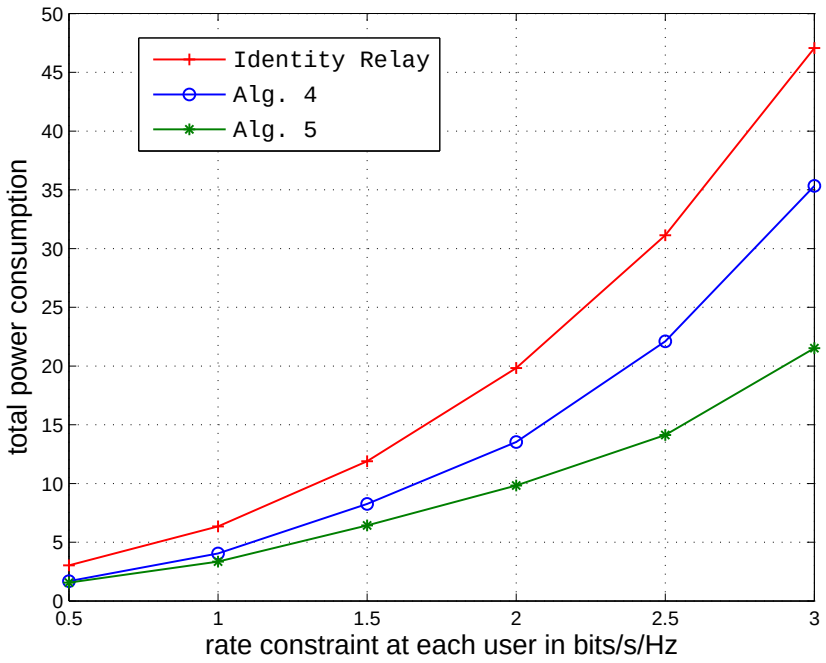

Figure 5.4: Comparison of downlink Algorithms 4-5: Averaged total power consumptions versus individual rate constraint. The curve on the top is for the identity relay matrix.

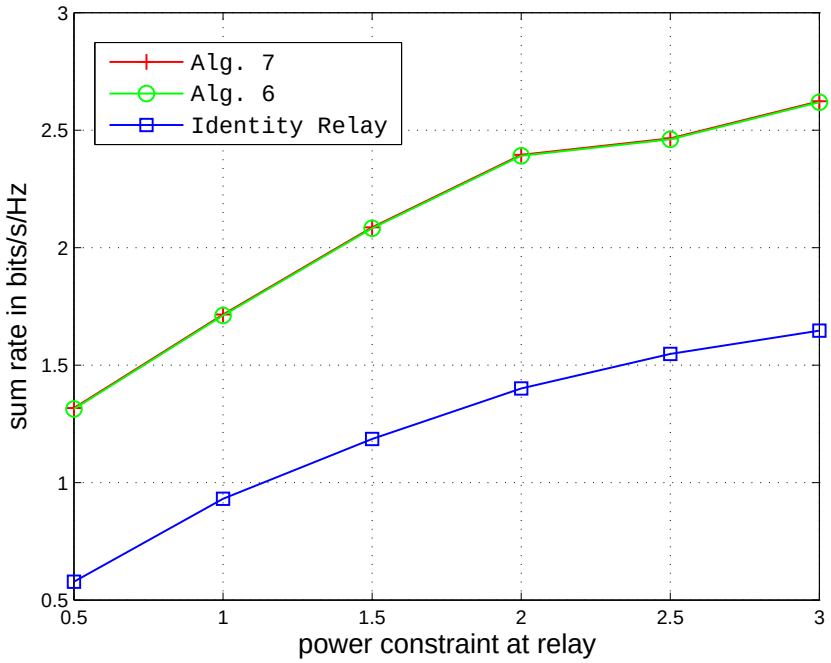

Figure 5.5: Comparison of uplink Algorithms 6-7: Averaged sum rate versus relay power constraint. The curves for Algorithms 6-7 are identical. The lower curve is for the identity relay matrix.

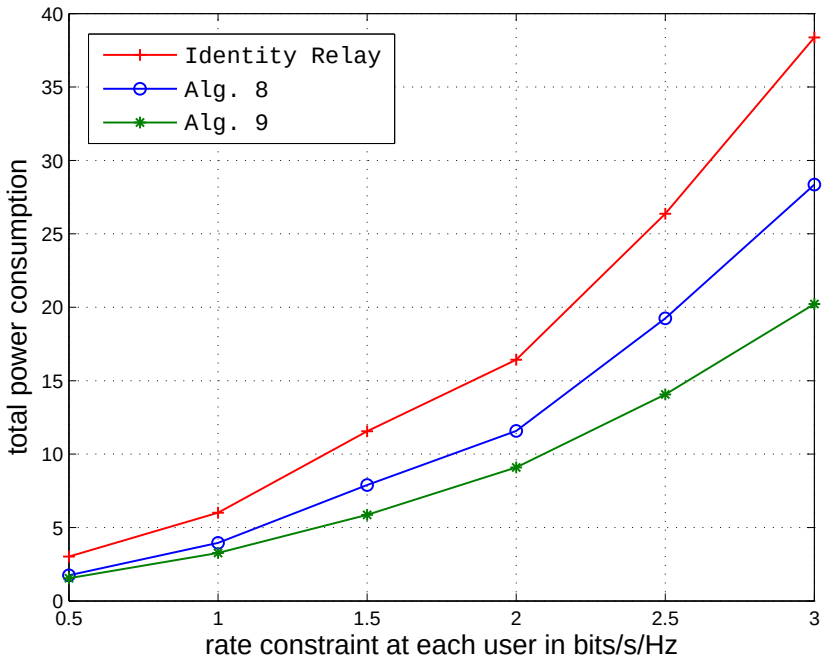

Figure 5.6: Comparison of uplink Algorithms 8-9: Averaged total power consumptions versus individual rate constraint. The curve on the top is for the identity relay matrix.

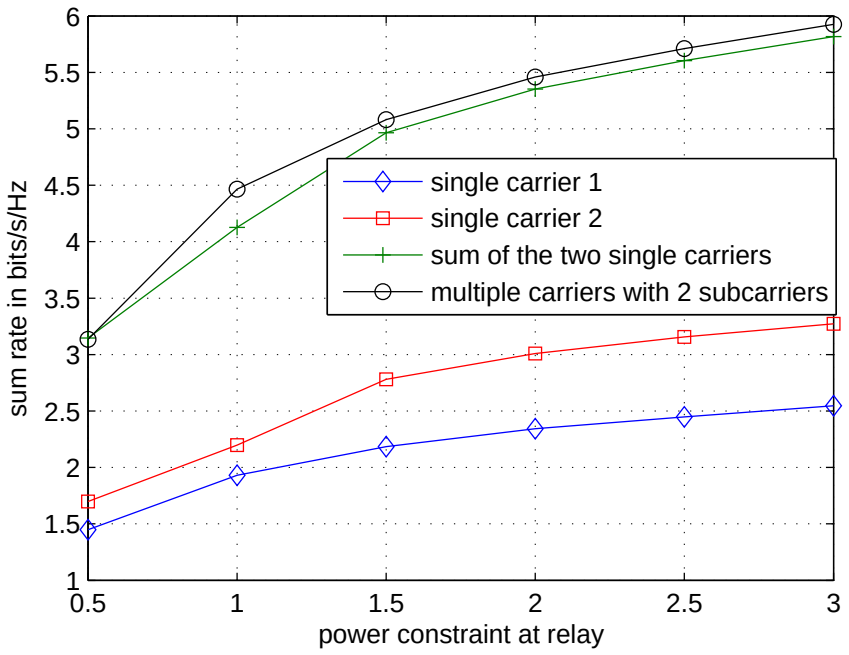

Figure 5.7: An example of joint multi-carrier power allocation for downlink multi-user MIMO relay system where $K = 2$, $N = 2$, $M = 4$ and $M_c = 2$. Algorithm 3 was applied with 20 random initializations. The rates shown are based on a single channel realization for each of the two carriers.

Chapter 6

Conclusion

In this chapter, a summary of the contributions of the Ph.D. research work is presented.

- The throughput of O-SAM has been evaluated. We have presented a relationship between the network throughput and the traffic load condition characterized by a probability variable ζ. The throughput of O-SAM has been evaluated under different topologies: triangle, square and hexagon. Under different topologies, the throughput of O-SAM is compared fairly using the unit $bits - meters/s/Hz/node$ and assuming the unit node density. The impact of multiple antennas has also been investigated. The performance of O-SAM is also compared to that of slotted ALOHA.A distributed synchronous array method (D-SAM) has also been proposed. The performance of D-SAM has been evaluated. D-SAM can be applied to any random topology and a key factor referred to as cooperation range has been shown to be critical to the throughput.

- A generalized water filling(GWF) theorem has been established for the source covariance matrix design in MIMO channel with multiple power constraints. The corresponding GWF algorithm is a faster solution than the CVX package to solve a class of convex optimization problems. The numerical example has shown that GWF algorithm can be as accurate as CVX which uses the Sedumi as optimization engine.

- In the last part of the thesis, the power allocation problem in the multiuser MIMO relay network has been investigated. Multiple antennas are assumed on all the nodes in the network. Both uplink and downlink cases have been studied. We have considered two problems for each case: to minimize total power under rate constraint and to maximize sum rate under power constraint. Although the central problem is non-convex, the joint gradient search for the relay matrix and the source covariance matrices has consistently yielded the best result. The use of logarithmic barrier functions, which is a key approach of the interior-point optimization methods, has been very effective for the constrained optimizations.

In the thesis, perfect channel state information is assumed. In the future work, the channel estimation error, quantization error and limited feedback should be considered.

Bibliography

[1] Y. Hua, Y. Huang, and J. J. Garcia-Luna-Aceves, "Maximizing the throughput of large ad hoc wireless networks," *IEEE Signal Processing Magazine*, vol. 23, pp. 84–94, Sept. 2006.

[2] "GSM - Wikipedia, the free encyclopedia," 2009, `http://en.wikipedia.org/wiki/GSM`.

[3] "IEEE standard for wireless LAN medium access control (MAC) and physical layer (PHY) specifications," Nov. 1997.

[4] "IEEE 802.15 Wireless Personal Area Networks," 2005, `http://standards.ieee.org/getieee802/802.15.html` .

[5] "IEEE standard for local and metropolitan area networks - IEEE 802.16," Oct 2004.

[6] "LTE Advanced relay," 2009, `http://www.nokiasiemensnetworksevents.com` .

[7] P. Gupta and P. R. Kumar, "The capacity of wireless networks," *IEEE Trans. Inform. Theory*, vol. 46, pp. 388–404, Mar. 2000.

[8] U. C. Kozat and L. Tassiulas, "Throughput capacity of random ad hoc networks with infrastructure support," in *Mobicom*, 2003, pp. 55–65.

[9] B. Liu, Z. Liu, and D. Towsley, "On the capacity of hybrid wireless networks," in *Infocom*, 2003, pp. 1543–1542.

[10] A. Agarwal and P. R. Kumar, "Capacity bounds for ad hoc and hybrid wireless networks," in *ACM SIGCOMM Computer Communications Review*, 2004, pp. 71–82.

[11] S. Toumpis, "Capacity bounds for three classes of wireless networks: asymmetric, cluster, and hybrid," in *Mobihoc*, 2004, pp. 133–144.

[12] S. Yi, Y. Pei, and S. Kalyanaraman, "On the capacity improvement of ad hoc wireless networks using directional antennas," in *Mobihoc*, 2003, pp. 108–116.

[13] R. Negi and A. Rajeswaran, "Capacity of power constrained ad-hoc network," in *IEEE Proc of INFOCOM*, 2004.

[14] X. Tang and Y. Hua, "Capacity of ultra-wide-band power-constrained ad hoc networks," *IEEE Transactions on Information Theory*, vol. 54, no. 2, pp. 916–920, Feb 2008.

[15] O. Levegue, A. Ozgur, and D. Tse, "How does the information capactiy of ad hoc networks scale," *Allerton Conference*, Sept. 2006.

[16] *IEEE Trans. Information Theory, Special Issue on Random-Access Communications*, vol. 31, Mar 1985.

[17] "Carrier sense multiple access with collision detection (CSMA/CD) access method and physical layer specification.," 2002, `http://standards.ieee.org/getieee802/download/802.3-2002.pdf` .

[18] X. Liu and M. Haenggi, "Throughput analysis of fading sensor networks with regular and random topologies," *EURASIP Journal on Wireless Communications and Networking*, vol. 2005, pp. 554–564, 2005.

[19] K. Hong and Y. Hua, "Throughput analysis of large wireless networks with regular topologies," *EURASIP Journal on Wireless Communications and Networking*, 2007, Article ID 26760, 11 pages.

[20] B. Zhao and Y. Hua, "A distributed medium access control scheme for a large network of wireless routers," *IEEE Transactions on Wireless Communications*, vol. 7, pp. 1614–1622, May 2008.

[21] S. Adireddy and L. Tong, "Exploiting decentralized channel state information for random access," *IEEE Trans. Inform. Theory*, vol. 51, pp. 537–561, Feb. 2005.

[22] B. Zhao and Y. Hua, "Distributed medium access for a large wireless mesh network with multiple antenna elements on each node," in *IEEE ICASSP*, Honolulu, Hawaii, April 2007.

[23] D. Tse and P. Viswanath, *Fundamentals of wireless commmunication*, Cambridge University Press, 2004.

[24] T. S. Rappaport, *Wireless Communications Principle and Practice*, Prentice-Hall, 2001.

[25] A. Goldsmith, *Wireless Communications*, Cambridge University Press, 2005.

[26] X. Tang and Y. Hua, "Optimal design of non-regenerative MIMO wireless relay," *IEEE Transactions on Wireless Communications*, vol. 6, pp. 1398–1407, Apr. 2007.

[27] Z. Fang, Y. Hua, and J. Koshy, "Joint source and relay optimization for a non-regenerative MIMO relay," in *IEEE Workshop on Sensor Array and Multi-channel Processing*, Waltham, MA, Jul. 2006.

[28] O. Munoz-Medina, J. Vidal, and A. Agustin, "Linear transceiver design in nonregenerative relays with channel state information," *IEEE Transactions on Signal Processing*, vol. 55, no. 6, pp. 2593–2604, June 2007.

[29] W. Guan and H. Luo, "Joint MMSE transceiver design in non-regenerative MIMO relay systems," *IEEE Communication Letters*, vol. 12, pp. 517–519, 2008.

[30] Y. Fan and J. Thompson, "MIMO configurations for relay channels: Theory and practice," *IEEE Transactions on Wireless Communications*, vol. 6, pp. 1774–1786, May 2007.

[31] A. S. Behbahani, R. Merched, and A. M. Eltawil, "Optimizations of a MIMO relay network," *IEEE Trans. on Signal Processing*, vol. 56, pp. 5062–5073, 2008.

[32] H. Shi, T. Abe, T. Asai, and H. Yoshino, "Relaying schemes using matrix triangularization for MIMO wireless networks," *IEEE Transactions on Communications*, vol. 55, pp. 1683–1688, Setptember 2007.

[33] C. Chae, T. Tang, R. Heath, and S. Cho, "MIMO relaying with linear processing for multiuser transmission in fixed relay networks," *IEEE Transactions on Signal Processing*, vol. 56, pp. 727–738, Feb. 2008.

[34] S. Jafar, K. Gomadam, and C. Huang, "Duality and rate optimization for multiple access and broadcast channels with amplify-and-forward relays," *IEEE Transactions on Information Theory*, vol. 53, pp. 3350– 3370, Oct. 2007.

[35] R. Zhang, C. C. Chai, and Y. Liang, "Joint beamforming and power control for multiantenna relay broadcast channel with QoS constraints," *IEEE Trans. on Signal Processing*, vol. 57, pp. 726–737, 2009.

[36] B. K. Chalise and L. Vandendorpe, "MIMO relay design for multi-point to multi-point communications with imperfect channel state information," *IEEE Trans. on Signal Processing*, to appear.

[37] S. W. Peters and R. W. Heath, "Nonregenerative MIMO relaying with optimal transmit antenna selection," *IEEE Signal Processing Letters*, vol. 15, pp. 421–424, 2008.

[38] I. Lee and D. Kim, "Outage probability of multi-hop MIMO relaying with transmit antenna selection and ideal relay gain over Rayleigh fading channels," *IEEE Trans. on Communications*, vol. 57, pp. 357–360, 2009.

[39] Y. Yu, Y. Huang, B. Zhao, and Y. Hua, "Throughput analysis of wireless mesh networks," in *IEEE ICASSP*, Las Vegas, April 2008.

[40] Y. Yu, Y. Huang, B. Zhao, and Y. Hua, "Further development of Synchronous Array Method for Ad Hoc wireless networks," *EURASIP Journal on Advances in Signal Processing*, 2009, Article ID 873202, 14 pages.

[41] A. Shah and A. M. Haimovich, "Performance analysis of maximal ratio combining and comparison with optimum combining for mobile radio commnications with cochannel interference," *IEEE Trans. on Vehicular Technology*, pp. 1454–1463, Jul. 2000.

[42] M. Kang and M.-S. Alouini, "Largest eigenvalue of complex wishart matrices and performance analysis of MIMO MRC systems," *IEEE Journal on Selected Areas in Communications*, pp. 418–426, APR. 2003.

[43] M. Cao, W. Ma, Q. Zhang, and X. Wang, "Analysis of IEEE 802.16 mesh mode scheduler performance," *IEEE Transactions on Wireless Communications*, vol. 6, no. 4, pp. 1455–1464, April 2007.

[44] K. Hong, Y. Hua, and A. Swami, "Distributed and cooperative link scheduling for large-scale multi-hop wireless networks," *EURASIP Journal on Wireless Communications and Networking*, 2007, Article ID 34716, 9 pages.

[45] M. Grant and S. Boyd, *CVX: Matlab software for disciplined convex programming*, http://stanford.edu/ boyd/cvx, 2008.

[46] J. Magnus and H. Neudecker, *Matrix Differential Calculus with Applications in Statistics and Econometrics*, JOHN WILEY&SONS, 1999.

[47] S. Boyd and L. Vandenberghe, *Convex Optimization*, Cambridge University Press, 2004.

[48] Y. Rong, X. Tang, and Y. Hua, "A unified framework for optimizing linear non-regenerative multicarrier MIMO relay communication systems," *IEEE Transactions on Signal Processing*, to appear.

[49] S. Vishwanath, M. Jindal, and A. Goldsmith, "Duality, achievable rates and sum-rate capacity of Gaussian MIMO broadcast channels," *IEEE Transactions on Information Theory*, vol. 49, pp. 2658– 2668, Oct. 2003.

[50] W. Zhang and U. Mitra, "Channel-adaptive frequency-domain relay processing in multicarrier multihop transmission," in *ICASSP 2008*, Apr. 2008, Las Vegas, NV.

[51] H. Weingarten, Y. Steinberg, and S. Shamai, "The capacity region of the Gaussian multiple-input multiple-output broadcast channel," *IEEE Transactions on Information Theory*, vol. 52, pp. 3936– 3964, Sept. 2006.

[52] D. Bertsekas, *Nonlinear Programming*, Athena Scientific, second edition, 1995.

[53] C. S. R. Murthy and B. S. Manoj, *Ad Hoc Wireless Networks - Architectures and Protocols*, Prentice-Hall, 2005.

[54] L.-L. Xie and P. R. Kumar, "A network information theory for wireless communications: Scaling laws and optimal operation," *IEEE Trans. Inform. Theory*, vol. 50, pp. 748–767, May. 2004.

[55] F. Xue and P. R. Kumar, "The transport capacity of wireless networks over fading channels," *IEEE Trans. Inform. Theory*, vol. 51, pp. 834–847, Mar. 2005.

[56] G. Mergen and L. Tong, "Maximum asymptotic stable throughput of opportunistic slotted aloha and applications to cdma networks," *IEEE Trans. on Wireless Communications*, vol. 6, pp. 1159–1163, Apr. 2007.

[57] P. K. Appani, J. L. Hammond, D. L. Noneaker, and H. B. Russell, "An adaptive transmission-scheduling protocol for mobile ad hoc networks," *Ad Hoc Networks*, pp. 254–271, Dec. 2005.

[58] B. Yi, S. Wang, and S. Kwon, "On MIMO relay with finite-rate feedback and imperfect channel estimation," in *IEEE GLOBECOM*, 2007.

[59] J. Chen, X. Yu, and C. Kuo, "V-BLAST receiver for MIMO relay networks with imperfect CSI," in *IEEE GLOBECOM*, 2007.

[60] A. Coso and C. Ibars, "The amplify-based multiple-relay multiple-access channel: Capacity region and MAC-BC duality," in *Information Theory for Wireless Networks, 2007 IEEE Information Theory Workshop on*, 2007.

[61] V. Havary-Nassab, S. Shahbazpanahi, A. Grami, and Zh. Luo, "Distributed beamforming for relay networks based on seconde-order statistics of the channel state information," *IEEE Transactions on Signal Processing*, vol. 56, pp. 4306– 4316, Sept. 2008.

[62] Y. Li, B. Vucetic, Zh. Zhou, and M. Dohler, "Distributed adaptive power allocation for wireless relay networks," *IEEE Transactions on Wireless Communications*, vol. 6, pp. 948– 958, Mar. 2007.

[63] J. Cai, X. Shen, J. Mark, and A. Alfa, "Semi-distributed user relaying algorithm for amplify-and-forward wireless relay networks," *IEEE Transactions on Wireless Communications*, vol. 7, pp. 1348– 1357, Apr. 2008.

[64] L. Weng and R. Murch, "Multi-user MIMO relay system with self-interference cancellation," in *IEEE WCNC,*, 2007.

[65] W. Yu, W. Rhee, S. Boyd, and J. M. Cioffi, "Iterative water-filling for Gaussian vector multiple access channels," *IEEE Transactions on Information Theory*, vol. 50, pp. 145–152, 2004.

[66] Gene H. Golub and Charles F. Van Loan, *Matrix Computations (3rd ed.)*, Johns Hopkins University Press, Baltimore, MD, USA, 1996.

[67] S. Berger, M. Kuhn, A. Wittneben, T. Unger, and A. Klein, "Recent advances in amplify-and-forward two-hop relaying," *IEEE Communications Magazine*, pp. 50–56, July 2009.

[68] Y. Yu and Y. Hua, "Power allocation for a MIMO relay system with multiple-antenna users," *IEEE Trans. on Signal Processing*, submitted.